Contract No. NAS7-758
Report No. IITRI-B6102-13

INVESTIGATION OF REFRACTORY COMPOSITES FOR LIQUID ROCKET ENGINES

V. L. Hill and M. J. Malatesta

IIT Research Institute
10 West 35 Street
Chicago, Illinois 60616

30 November 1970

Final Report for Period 1 October 1969 - 31 October 1970

Prepared for

LIQUID PROPULSION TECHNOLOGY PROGRAM
Chemical Propulsion Division
NASA Headquarters, Code RPL
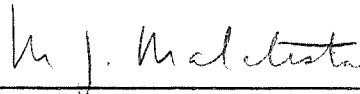Washington, D.C. 20546

FOREWORD

This is the final report, IITRI-B6102-13, of IITRI Project B6102, on Contract NAS7-758, entitled "Investigation of Refractory Composites for Liquid Rocket Engines." This Report covers work performed during the period 1 October 1969 to 31 October 1970.

Personnel contributing to this program were V. L. Hill, Manager, Coatings Research, IITRI Project Manager, and M. J. Malatesta, Assistant Metallurgist, responsible for fluorine corrosion studies and composite fabrication. The Program Manager on this program is Mr. G. Heidenreich of the Jet Propulsion Laboratory.
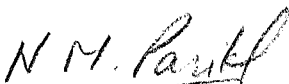
Data are recorded in IITRI Logbooks C19718 and C19719.

M. J. Malatesta
Assistant Metallurgist

V. L. Hill, Manager
Coatings Research

N. M. Parikh, Director
Metals Research Division

IIT RESEARCH INSTITUTE

INVESTIGATION OF REFRACTORY COMPOSITES
FOR LIQUID ROCKET ENGINES

ABSTRACT

The objective of this program was to identify and
evaluate potential composite systems for use in exhaust atmo-
spheres containing fluorine-oxygen in liquid rocket engines.

A literature search was conducted to define potential
matrix-additive combinations for composite systems. The basis
for selection of materials for composites was a minimum melting
point of 4000°F, oxidation-corrosion resistance in fluorine-
oxygen, high-temperature stability, and fabricability. Iridium
and iridium-rich alloys were the most oxidation-corrosion resist-
ant in fluorine-oxygen atmospheres. Data in the literature
indicated that boron in combination with fluorine-oxygen would
further limit the potential materials available for rocket noz-
zles and chambers.

Oxidation-corrosion studies were conducted on W-Re-Ir,
Re-Ir, $TaIr_3$ and $HfIr_3$ in fluorine, oxygen, hydrogen fluoride,
and their combinations, at 3000°-4500°F. Tests were also con-
ducted on these materials, tungsten, and ATJ graphite in boron-
containing atmospheres. Re-Ir and iridium intermetallics had
good oxidation-corrosion resistance in fluorine-oxygen, but
exhibited surface melting in boron-containing atmospheres at
3000°-4000°F. W-Re-Ir alloys had higher surface recession rates
than iridium-rich systems. A discussion of oxidation-corrosion
mechanisms is included.

High-temperature interaction studies of iridium-rich
alloys in combination with borides, carbides, and graphite
revealed that the highest melting systems were $TaIr_3$ in combina-
tion with TaC and ATJ graphite. Rhenium was also shown to be
stable in contact with HfC-graphite composites.

IIT RESEARCH INSTITUTE

TABLE OF CONTENTS

IIT RESEARCH INSTITUTE

LIST OF FIGURES

IIT RESEARCH INSTITUTE

LIST OF TABLES

INVESTIGATION OF REFRACTORY COMPOSITES
FOR LIQUID ROCKET ENGINES

I.   INTRODUCTION

The development of materials for liquid rocket engines
to date has concentrated on hydrocarbon-fueled engines in which
oxygen is the major corrosive species. Higher specific impulse
can be obtained with liquid propellant systems in which fluorine
or OF_2 is the oxidizer, such as a diborane-oxygen difluoride sys-
tem. The exhaust products of these propellants, however, require
more corrosion-resistant and probably higher melting materials
than hydrocarbon-fueled engines. Fluorine is as corrosive as ox-
ygen at high temperatures for many materials. Furthermore, many
materials which are suitable for oxygen are not resistant to
fluorine. It was shown on Contract NAS7-431[1] that nozzle and
thrust chamber materials must generally be resistant to both oxy-
gen and fluorine in order to survive combined fluoride-oxygen en-
vironments. Thus, nozzle materials which have been developed for
hydrocarbon-fueled engines are not necessarily applicable to
fluorine-containing propellant systems.

A single material with the requisite combination of
high melting point, high-temperature strength, and corrosion re-
sistance for rocket nozzles and thrust chambers of fluorine en-
gines may not exist. Composite systems offer a means of obtain-
ing optimum properties in materials for these engine components.
Promising composite materials beyond those currently available
need investigation, for their development would enable the full
potential of fluorine-containing propellants to be realized.

This program constituted one of the initial efforts to-
ward development of nonablative composite materials specifically
for rocket engine combustion products containing both fluorides
and oxygen. (Ablative nozzle materials were not included in the

IIT RESEARCH INSTITUTE

IITRI-B6102-13
(Report Final)

scope of this work.) Accordingly, the first portion of the program consisted of a literature survey to define potential combinations of refractory materials for these composites. Composite systems could then be fabricated by appropriate methods. Finally, selected systems were evaluated in fluorine, oxygen, hydrogen fluoride, boron trifluoride and combinations of these gases at 3000°-5500°F.

II. EXPERIMENTAL PROCEDURE AND RESULTS

A. Literature Survey

Considerable data exist in the literature on the high-temperature stability, reactivity, and melting points of most of the refractory materials. This information combined with the fluorine-oxygen corrosion information generated on Contract NAS7-431 was required to select potential combinations of material for composite systems.

Nominally, the composites considered in this program differ somewhat from those of most composite developments. These composites did not necessarily consist of fibers and/or a dispersion of a second phase in a matrix whose primary objective is to improve the mechanical properties of the system. Rather, the primary purpose of the second phase incorporated in a suitable matrix was to improve the resistance of the composite to oxidation-corrosion in rocket engine combustion products. This additional latitude in the selection of combinations of materials for composite systems was necessary because a single low-cost material did not exist for the very severe operating conditions of fluorine-containing rocket engines.

Accordingly, a literature search was initiated to summarize existing literature data on high-temperature properties of refractory materials. In general, the search was limited to materials with melting points above 4000°F, excluding oxides.

The properties examined included:

1. Melting points;
2. Resistance to F_2, O_2, HF, and their combinations;

IIT RESEARCH INSTITUTE

3. High temperature interactions (melting points) with other refractory materials; and

4. Thermal stability above 4000°F.

In addition, amenability to fabrication into composite structures was considered, although the fabrication procedures were secondary to the oxidation-corrosion requirements.

The unclassified literature from 1962 to the present was examined as abstracted in: Scientific and Technical Aerospace Reports, International Aerospace Abstracts, Review of Metal Literature, Metals Abstracts, Metallurgical Abstracts, and Technical Abstracts Bulletin. In addition, pertinent data previous to 1962 cited in these reports were also obtained for review. A total of over 75 technical reports were accumulated for examination. It was found that some amount of additional materials information probably exists in classified literature. Examination of classified literature and ablative materials was not included in this survey.

The materials data are summarized in Tables I through V. The magnitude of this effort is indicated in the fact that, excluding oxides, at least 110 known metals, nitrides, borides, carbides, silicides, sulfides, and intermetallics have melting points above 4000°F (2200°C). However, little is known about the high-temperature properties of most of the lesser known materials and, therefore, all potential systems could not be treated in detail.

It was found that the most comprehensive evaluation of refractory materials in fluorine and hydrogen fluoride was the work conducted on NAS7-431 (IITRI-B6058-40).[1] Consequently, these data were the basis for determining the compatibility of materials in these environments. Since most of the classes of refractory materials, excluding oxides and ablators, were evaluated under NAS7-431, a general comparison of the corrosion behavior of most refractory materials was possible in addition to the specific materials evaluated in fluorine and hydrogen fluoride.

IIT RESEARCH INSTITUTE

IITRI-B6102-13
(Final Report)

A summary of the minimum melting points and supplemental data for the elemental combinations with melting points above 400°F is presented in Table I. The elements, in order of decreasing melting point, include carbon (sublimes ~6700°F), tungsten (6100°F), rhenium (5720°F), osmium (5480°F), tantalum (5430°F), molybdenum (4750°F), columbium (4470°F), iridium (4450°F), ruthenium (4130°F), and hafnium (4030°F). Interactions with boron (3950°-4040°F) are not included in Table I, but are considered in subsequent tables.

The metallic elements represent five basic groups; the body-centered cubic elements molybdenum and tungsten (Group VIB), the body-centered cubic elements tantalum and columbium (Group VB), the platinum group metals osmium, iridium, and ruthenium (Group VIII), hexagonal rhenium (Group VIIB), and hexagonal→BCC hafnium (Group IVB). Platinum group metals represent both hexagonal (osmium and ruthenium) and face-centered cubic (iridium) crystal structures. Because of these differences in crystal structures, complete solid solubility occurs only in combinations of Groups VB and VIB elements and in the systems Re-Os and Re-Ru. Here, the melting point of any binary alloy is related directly to the concentration of the lowest melting element. The solidus in the binary systems generally represents a straight line joining the melting points of the two constituents.

Binary systems of metallic elements with different crystal structures results in lower melting eutectics, peritectics, and intermetallic compounds. These interactions are indicated in Table I wherever data exist. Obviously, the highest melting series of binary metallic alloys exist in the systems W-Ta (5400°-6100°F) and W-Mo (4750°-6100°F). However, Table I does indicate that the highest melting nonmetallics are the carbides TaC (6910°F) and HfC (6920°F), and of course graphite (sublimes ~6700°F). Melting points of the MC carbides of the lighter corresponding elements CbC and ZrC are 6300°F and 6180°F, respectively, although zirconium metal melts at about 3360°F.

TABLE I

SUMMARY OF BINARY SYSTEMS OF ELEMENTS

WITH MELTING TEMPERATURES IN EXCESS OF 4000°F

System	Minimum Solidus Temperature		Remarks	High Melting Compounds	Ref.
	°C	°F			
Carbon-W	2710	4910	Eutectic (25% C)		2
-Re	2500	4532	Eutectic (17% C)		2
-Ta	2825	5117	Eutectic (11% C)	TaC (6920°F)	2
-Os	2732	4950	Eutectic (Os rich)		3
-Mo	2200	3992	Eutectic (17% C)		2
-Cb	2335	4235	Eutectic (11% C)	CbC (6300°F)	3
-Ir	2303	4177	Eutectic (7% C)		4
-Ru	1942	3528	Eutectic (Ru rich)		3
-Hf	2210	4010	Eutectic (10% C)	HfC (6925°F)	2
Tungsten-Re	2825	5117	Eutectic (26% W)	Re_3W_2 (>5430°F)	3
-Ta	2998	5426	Isomorphous Ta M.P.		3
-Os	2725	4937	Eutectic (60% W)		3
-Mo	2621	4750	Isomorphous Mo M.P.		3
-Cb	2468	4470	Isomorphous Cb M.P.		2
-Ir	2305	4181	Eutectic (22% W)		2
-Ru	2205	4001	Eutectic (55% W)		3
-Hf	1930	3506	Eutectic (22% W)	W_2Hf (4170°F)	3
Rhenium-Ta	2690	4874	Eutectic (50% Re)		3
-Os	3027	5481	Isomorphous Os M.P.		2
-Mo	2440	4424	Eutectic (50% Re)	Re_3Mo_2 (4530°F)	3
-Cb	2435	4415	Eutectic (48% Re)		3
-Ir	2443	4430	Peritectic Ir M.P.		2
-Ru	2280	4136	Isomorphous Ru M.P.		2
-Hf	1840	3344	Eutectic (24% Re)	$HfRe_2$ (4720°F)	2

TABLE I (cont.)

System	Minimum Solidus Temperature		Remarks	High Melting Compounds	Ref.
	°C	°F			
Tantalum-Os	2400	4352	Eutectic (53% Ta)		3
-Mo	2615	4739	Isomorphous Mo M.P.		5
-Cb	2468	4474	Isomorphous Cb M.P.		3
-Ir	1950	3542	Eutectic (56% Ta)	TaIr$_3$ (4440°F)	2
-Ru	1970	3578	Eutectic (29% Ta)		3
-Hf	2110	3830	Minimum (20% Ta)		2
Osmium-Mo	2380	4316	Eutectic (20% Os)		2
-Cb	--				
-Ir	2443	4430	Peritectic Ir M.P.		2
-Ru	2280	4136	Isomorphous Ru M.P.		2
-Hf	--		No Data Available		
Molybdenum-Cb	2290	4154	Minimum (35% Mo)		2
-Ir	2080	3776	Eutectic (69% Mo)		2
-Ru	1945	3533	Eutectic (58% Mo)		3
-Hf	1930	3506	Eutectic (42% Mo)	Mo$_2$Hf (4170°F)	3
Columbium-Ir	1840	3344	Eutectic (55% Cb)		2
-Ru	1774	3225	Eutectic (35% Cb)		2
-Hf	2100	3812	Minimum (~25% Cb)		2
Iridium-Ru	2280	4136	Peritectic Ru M.P.		2
-Hf	1430	2606	Eutectic (17% Ir)	HfIr$_3$ (4470°F)	2
Ruthenium-Hf	--		No Data Available		

Unfortunately, all of the high-melting elements, with the exception of iridium, have poor oxidation resistance at high temperatures. Only tantalum or hafnium develop oxides which melt above 3000°F. The remaining elements form oxides which melt or volatilize below 3000°F. This is true also of iridium, but the rate of reaction is relatively slow to the melting point. At 4000°F, ranking of the elements which form volatile oxides (linear oxidation rates) in decreasing order of oxidation resistance would be iridium, ruthenium, rhenium, osmium, tungsten, molybdenum, and carbon. Oxidation of iridium would be about one-fifth that of ruthenium, and about an order of magnitude less than rhenium. Ranking of tantalum and hafnium in this group would be dependent on the testing method, since their oxidation rate would be nonlinear and could be controlled by spalling or flow of the oxides formed. A more detailed examination of oxidation-corrosion of these materials will be presented later.

A summary of nonmetallic materials with melting points above 4000°F, excluding oxides, is presented in Table II. Over 110 known borides, carbides, nitrides, silicides, sulfides, phosphides and intermetallics are included. In many cases, particularly for the lesser known materials, the reported melting points vary widely. No attempt has been made to resolve these differences in Table II. The majority of these materials are carbides and borides, although very high melting nitrides (TaN, HfN), silicides (Hf$_2$Si), and intermetallics (HfRe$_2$) also exist. The remaining materials, sulfides, phosphides, and low-melting silicides do not appear to provide any potential in this program. A more detailed analysis of these materials is contained in Table V.

The materials in Table II of interest to this program include:

Borides: HfB$_2$, ZrB$_2$, TaB$_2$
Carbides: HfC, TaC, ZrC, CbC
Nitrides: TaN, HfN, BN
Intermetallics: HfRe$_3$, HfIr$_3$, TaIr$_3$

IIT RESEARCH INSTITUTE

TABLE II

SUMMARY OF MATERIALS
WITH MELTING, SUBLIMATION, OR DECOMPOSITION
TEMPERATURES ABOVE 4000°F (2204°C)

Material	Melting Temperature °C	°F	References
	Borides		
HfB_2	3240-3380	5864-6110	6, 7-12
TaB_2	3035-3200	5495-5792	7-10, 12
ZrB_2	2995-3095	5423-5603	6-8, 11, 12
ZrB (a)	2996		8
CbB_2	2900-3050	5252-5522	7-10, 12
TiB_2	2870-3225	5198-5837	7-10, 12
β-WB (a)	2665-2920	4829-5288	7-10
HfB	2899	5250	7
Ta_3B_4	2620-3030	4748-5486	7-10, 12
TaB	2400-3090	4352-5594	7, 9, 10
Cb_3B_4	2195-2935	3983-5315	7-10, 12
CbB	2260-2920	4100-5288	7, 9, 10
YB_4 (a)	2800	5072	8
W_2B	2670-2770	4838-5018	7-10, 12
ZrB_{12} (a)	2250-2680	4082-4856	7, 8, 10, 12
MoB	2080-2600	3776-4712	7-10
NdB_6	2540	4604	7, 8
SmB_6	2400-2540	4352-4604	7, 8
ThB_4	2480-2500	4496-4532	7-9
LaB_6	2150-2530	3902-4586	7, 8
UB_4	2482	4500	7
MoB_2	2100-2475	3812-4487	7, 9, 10
VB_2	2400-2430	4352-4406	7, 8, 12
Ta_2B	1800-2420	3272-4388	7, 9, 10
α-WB (d)	1950-2400	3542-4352	7-10, 12
UB_2	2365-2370	4289-4298	7, 8
W_2B_5	2300-2365	4172-4289	7-10, 12
ScB_2	2250-2360	4082-4280	7, 8

TABLE II (cont.)

Material	Melting Temperature		References
	°C	°F	
YB_6	2300	4172	7, 8
BeB_6	2300	4172	8
VB	2250-2300	4082-4172	7-10, 12
V_3B_4	2275-2280	4127-4136	7, 8, 12
Mo_2B	2280	4135	7
BaB_6	2265-2270	4109-4118	7, 8
Ti_2B (a)	2204-2250	4000-4082	7-9
Mo_3B_2 (a)	2070-2280	3758-4136	7-10
CaB_6	2230-2235	4046-4055	7, 8
UB_{12}	2200-2235	3992-4055	7-9
WB_2	2200	3992	8
	Carbides		
HfC	3890-3950	7034-7142	7, 8, 10, 12, 13
TaC	3880-4000	7016-7232	7, 8, 10, 12, 13
CbC	3480-3615	6300-6542	7, 8, 10, 12, 13
ZrC	3420-3540	6100-6400	7, 8, 10, 12, 13
Ta_2C (d)	3400	6152	8, 12
TiC	3066-3147	5050-5700	7, 8, 10, 12, 13
Cb_2C	3088	5590	7
WC	2720-2870	4928-5198	7, 8, 10, 12, 13
VC	2648-2810	4800-5144	7, 8. 10, 12, 13
Al_4C_3	2700-2800	4890-5070	7, 8
W_2C	2730-2776	4946-5028	7, 10, 12
MoC	2580-2700	4676-4890	7, 8, 10, 12, 13
SiC	2538-2700	4600-4890	7, 8
Mo_2C	2410-2690	4370-4870	8, 10, 12
ThC	2625-2670	4757-4838	7, 8, 13
ThC_2	2655	4810	7, 8
CeC_2	2500-2538	4532-4600	7, 8
PrC_2	2532	4590	7, 8

TABLE II (cont.)

Material	Melting Temperature		References
	°C	°F	
UC_2 [a]	2482	4500	7
B_4C	2427-2450	4400-4442	7, 8
UC	2371-2450	4300-4442	7, 8, 13
CaC_2	2160-2300	3920-4172	7, 8
Co_3C	2300	4172	8
VC_2	2300	4172	7, 8
GdC_2	2200	3992	7, 8
SmC_2	2200	3992	7, 8
	Nitrides		
TaN	3090-3360	5595-6080	7-9, 12
HfN	2980-3310	4855-5990	7-9, 12
BN	2704-3000	4900-5432	7, 8
Ta_2N	2050-2982	3722-5400	7, 12
ZrN	2980	5396	7-9
TiN	2930-3205	5306-5800	7-9, 12
YN	2670	4840	7, 8
ScN	2650	4800	7, 8
UN	2630-2904	4766-5260	7-9
CbN	2050-2573	3722-4660	7-9, 12
ThN	2570-2788	4658-5410	7-9
AcN	2500	4532	8
Cb_2N	2316-2420	4200-4388	7, 9, 12
Th_2N_3	2360	4280	8
VN	2050-2360	3722-4280	7-9, 12
AlN	2230-2289	4045-4150	7, 8
Be_3N_4	2205	4000	8
Be_3N_2	2200	3992	8
Ba_3N_2	2200	3992	8

TABLE II (cont.)

Material	Melting Temperature		References
	°C	°F	
Silicides			
Hf_2Si	2999	5430	7
B_3Si	2765	5010	8
Cb_4Si	1950-2580	3542-4676	8, 9, 12
Ta_9Si_2	2510	4550	8, 9, 12
Ta_5Si_3	2482-2500	4500-4532	7-9
Cb_5Si_3	2480	4496	7-9, 12
Ta_2Si	2450-2499	4442-4512	7-9, 12
W_5Si_3	2315-2350	4200-4262	7-9
Hf_5Si_3	2300-2438	4172-4420	7, 8
Zr_4Si_3	2225	4037	8
Zr_5Si_3	2250	4082	7, 8, 12
Zr_3Si_2 (d)	2210	4010	8
Zr_2Si	2200-2221	3992-4030	7-9, 12
$TaSi_2$	2200	3992	7, 9, 12
Sulfides			
CeS	2450	4442	8, 17
CaS	2400	4352	8
Th_2S	~2300	~4172	8
PrS	2230	4046	8
ThS	2220	4028	8
BaS	>2200	>3992	17
Phosphides			
Ba_3P_2	3200	5792	8
Pa_3P_2	~3200	~5792	8

TABLE II (cont.)

Material	Melting Temperature		References
	°C	°F	
Intermetallics			
$HfRe_2$	3160	5720	2
Re_3W_2	>3000	>5432	8
Re_3Mo_2	2500	4532	8
$HfIr_3$	2465	4469	2
RePt	2450	4442	8
$TaIr_3$	2450	4442	2
HfIr	2400	4352	2
Mo_2Hf	2300	4172	8
W_2Hf	2300	4172	8
$GeZr_2$	<2280	<4136	8

(a)High temperature phase.

(d)Decomposes.

With the exception of the intermetallics, selected materials representing each group were evaluated in fluorine and/or hydrogen fluoride on Contract NAS7-431. The only other exception is BN, which represents a departure from the reactive metal nitrides (HfN, TaN) that were evaluated in fluorine atmospheres. The results with unmodified hafnium and tantalum borides and nitrides demonstrated poor resistance to both fluorine and hydrogen fluoride. Consequently, the potential of BN is, at present, questionable. Limited evaluation of this material in fluorine was conducted in this program to resolve this lack of information on fluorine compatibility.

Intermetallics may be of interest as secondary additions to improve the corrosion resistance of other materials. The rhenium and iridium intermetallics are of primary interest because of the low fluorine corrosion rate of iridium above 3000°F and rhenium above 4000°F. Furthermore, the high iridium concentration of these intermetallics also provides potentially good oxidation resistance as discussed previously. This potential is the basis for examining the fluorine and hydrogen fluoride corrosion resistance of W-Re-Ir alloys in this program.

A summary of the existing data on the compatibility of refractory materials at high temperature is presented in Table III. Again, most of the data are associated with refractory borides and carbides, since these materials provide the highest interaction temperatures. Eutectics in the carbon-carbide systems are generally high, varying from about 4700°F (C-WC) to about 5970°F (C-TaC).[14] These high melting temperatures provide the basis for the development of carbide-graphite composites in which the graphite is added to improve the thermal shock resistance.

On the other hand, boron is incompatible with high melting MC carbides at the melting point of boron (~4000°F) because reactions occur producing borides and B_4C. According to Rudy,[21] the reactions are:

$$B + TaC \rightleftharpoons TaB_2 + C \text{ or } B_4C$$
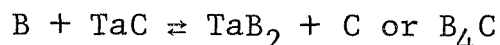
IIT RESEARCH INSTITUTE

TABLE III

SUMMARY OF MINIMUM MELTING POINTS OF REFRACTORY MATERIALS

System	Minimum Melting Point		Remarks	Reference
	°C	°F		
Carbon-TaC	3450	6240	Eutectic	14
-CbC	>3000	>5432	Eutectic	14
-TiC	2900	5250	Eutectic	14
-HfC	3150	5105	Eutectic	14
-WC	2600	4710	Eutectic	14
Boron-Mo	2050	3720	Eutectic (~20% B)	2
-Hf	1880	3415	Eutectic (13% B)	3
-Ta	~1750-2140	~3180-3704	Eutectic (20% B)	3
-Re	>1750	>3300	-	41
-Cb	~1600	~2910	Eutectic (15% B)	3
-Ru	1420	2590	Eutectic (44% B)	2
-Ir	1050, 1240	1920, 2265	Eutectic (66% B)	3, 15
-Pt	830	1525	Eutectic (40% B)	3
-HfC	2030	3686	Incompatible at M.P. of Boron	21
-ZrC	2030	3686	Incompatible at M.P. of Boron	21
-TaC	1600	2912	Incompatible at 1600°C $B + TaC \rightarrow TaB_2 + C$ or B_4C	21
Tungsten-HfC	2710-2800	4910-5070	Interaction temperature probably depends on heating rate; i.e. $HfC + W \rightarrow HfC_{1-x} + W_2C$ on heating. Minimum interfacial melting temperature then 4910°F. ($W-W_2C$ eutectic)	14, 19, 20, 23, 23

TABLE III (cont.)

System	Minimum Melting Point		Remarks	Reference
	°C	°F		
Tungsten-ZrC	2640-2850	4780-5160	Interaction temperature probably depends on heating rate; i.e. $HfC + W \rightarrow HfC_{1-x} + W_2C$ on heating. Minimum interfacial melting temperature then 4910°F. ($W-W_2C$ eutectic)	14, 17, 18, 20
-TaC	2740-2850	4960-5160	Interaction temperature probably depends on heating rate; i.e. $HfC + W \rightarrow HfC_{1-x} + W_2C$ on heating. Minimum interfacial melting temperature then 4910°F. ($W-W_2C$ eutectic)	14, 18, 19, 21, 22, 24
-TiC	~2550	~4640	Lump samples reacted, powder samples did not-- H_2 atmosphere.	17
-CbC	2200-2680	4000-4850	Lump samples reacted, powder samples did not-- H_2 atmosphere.	17, 22
-HfN	2500-2990	4530-5400	HfN unstable in H_2 (4720°F)	16, 17, 18
-TaN	2615	4760	Compatible, TaN unstable in H_2 (4570°F)	17
-ZrN	2760-2950	5000-5240	ZrN unstable in H_2 (5070°F)	17, 18
-TiN	2800	5070	TiN unstable in H_2 (4370°F) compatible at 4500°F.	
Tantalum-TaC	2843	5150	Ta-βTa$_2$C eutectic	20
-HfC	2450	4445	Liquid formation	20
-ZrC	2375	4310	Liquid formation	20

TABLE III (cont.)

System	Minimum Melting Point		Remarks	References
	°C	°F		
Tantalum-HfB_2	2220	4028	Liquid formation	20
-ZrB_2	2160	3920	Liquid formation	20
Rhenium-HfC	2500	4530	No reaction	18
-TaC	2500	4530	No reaction	18
-NbC	2500	4530	No reaction	18
-ZrC	2500	4530	No reaction	18
-HfN	2500	4530	No reaction	18
-TaB_2	2000	3632	No reaction	18
-TaB_2	2350	4262	Reaction occurs	18
-NbB_2	2250	4082	Reaction occurs	18
Iridium-HfC	1450, 1900	2642, 3450	$Ir + HfC \rightarrow Ir_3Hf + C$	26, 25
-ZrC	1400, 1900	2552, 3450	$Ir + ZrC \rightarrow Ir_3Zr + C$	26, 25
-ThC	1450	2642	$Ir + ThC \rightarrow Ir_3Th + C$	26
-HfN	~1800	~3275	Ir decomposes HfN	25
-ZrN	~1800	~3275	Ir decomposes ZrN	25
-HfB_2	~1370	~2500	$Ir + HfB_2 \rightarrow Ir_3Hf + B$	26
-ZrB_2	~1370	~2500	$Ir + ZrB_2 \rightarrow Ir_3Zr + B$	26
-ThB_2	~1370	~2500	$Ir + ThB_2 \rightarrow Ir_3Th + B$	26
Ruthenium-ZrC	1900	3450	Ru decomposes ZrC	25
-ZrN	~1900	3450	Ru decomposes ZrN	25
Platinum-ZrC	1540	2800	Pt decomposes ZrC	25
-HfC	1540	2800	Pt decomposes HfC	25

Data on minimum melting points of boron in contact with selected refractory metals are included in Table III. Very low melting eutectics occur for boron in combination with platinum group metals and rhenium. Thus, problems with the use of iridium and rhenium are likely if the rocket nozzle exhaust contains appreciable boron. These data are the basis for questioning the use of iridium on rhenium-base alloys in atmospheres containing boron, as presented in subsequent data tables, and for the corrosion tests in BF_3 conducted in this program.

Tungsten is compatible with MC carbides to at least 4710°F. Here the minimum melting point is determined by the heating rate.[22] If the heating rate is slow, tungsten is carburized by partial decomposition of the carbide as follows:

$$W + MC \rightleftarrows MC_{1-x} + W_xC_y,$$
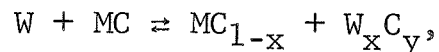
where W_xC_y is probably W_2C. Melting then occurs at the interface between W and the carbide at the $W-W_2C$ eutectic (4910°F) or at W_2C-MC_{1-x} eutectic. The dependence of the observed melting temperature on the heating rate explains the variation in melting points reported for tungsten in contact with carbides.

Tungsten is also stable in contact with high-melting nitrides such as HfN and TaN. Here the problem is instability of the nitrides, as reported by May,[17] although HfN has been evaluated as a short-time barrier for the W-C reaction at 5400°F.[16] In the event of decomposition of the nitride, the minimum melting temperature is predictable from the interaction temperatures for the metals given in Table I. For example, if decomposition of the nitrides occurs, the minimum melting point for W-HfN is the W-Hf eutectic (3510°F) and for W-TaN is the solidus of the W-Ta solid solution (~5750°F at 50% W). Thus, it is clear that the minimum interaction temperatures in the tungsten-nitride systems may also be dependent on the exposure time.

Tantalum exhibits a high-melting eutectic only with TaC; the melting temperature for the system is the $Ta-Ta_2C$ eutectic at

IIT RESEARCH INSTITUTE

5150°F.[20]   On the other hand, melting occurs at 4000°-4400°F
when tantalum is in contact with high-melting carbides and borides
of hafnium and zirconium. Again, this is probably due to reac-
tions producing mixed borides and carbides and should therefore
be time dependent.

Rhenium has been reported to be stable in contact with
high-melting carbides and nitrides at 4500°F, probably because
rhenium does not form stable carbides or nitrides.[18] Converse-
ly, reaction (melting) occurs at much lower temperatures (3600°-
4000°F) when rhenium is in contact with borides. This is not
surprising since the minimum melting eutectic in the Re-B system
is about 3330°F.[41]   In comparison, the Re-C eutectic occurs at
4530°F.

Interaction studies of platinum group metals with car-
bides, borides, and nitrides show interesting results. Iridium,
ruthenium, and platinum decompose even the most stable carbides
at temperatures as low as 2500°F.[25,26] Most of the existing
data are for iridium, but platinum and ruthenium have also been
examined. The reactions with iridium generally proceed as fol-
lows:

$$Ir + MC \rightleftharpoons MIr_3 + C$$

$$Ir + MB_2 \rightleftharpoons MIr_3 + B$$
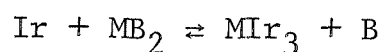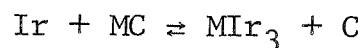
Obviously, the final reaction products can vary depend-
ing on the relative concentration of reactants.

The results do show that MIr_3 intermetallics have a
high thermodynamic stability; i.e., greater than that of the most
stable carbides and borides. These results suggest that MIr_3 in-
termetallics should be stable in contact with carbides and borides
to the melting points of the MIr_3 compounds. Composites of the
type HfB_2-HfIr_3, $HfC-HfIr_3$, $TaC-HfIr_3$ with melting points of at
least about 4500°F appear feasible from an interaction standpoint.
However, the MIr_3 intermetallics may not be suitable for addition
to graphites because of the Ir-C eutectic that occurs at 4180°F.

Re-Ir type additions may be more suitable for additions to graphite because the Re-C eutectic occurs at 4530°F.

A summary of the corrosion data for refractory materials in oxygen, fluorine, hydrogen fluoride, F_2-O_2, and HF-O_2 conducted at IITRI on Contract NAS7-431 is presented in Table IV. In addition, estimates of the compatibility of these materials with boron-containing atmospheres are included, although no testing with boron was conducted. In general, the data represent corrosion measurements to the melting point of each material except for carbides and graphite, which were tested to only 5000°F. Wherever experimental data were not available, estimates were made based on other information, and by extrapolation of low-temperature data. This summary provides only a relative comparison of refractory materials in rocket nozzle exhaust species.

Table IV indicates that iridium and iridium-base alloys provide the best corrosion resistance in all environments. Several materials are resistant to fluorine and hydrogen fluoride, but addition of oxygen to fluorine and hydrogen fluoride limits the applicable materials drastically. Hydrogen fluoride is least corrosive of the environments evaluated since most of the refractory metals demonstrate much lower corrosion rates than in fluorine. This is attributable to the stability of the hydrogen fluoride molecule, even at temperatures above 5000°F. Exceptions to this general behavior in hydrogen fluoride include borides, nitrides, and graphite (above 5000°F). The behavior of nitrides may be attributable to decomposition of the nitrides resulting in a surface layer rich in the reactive metals tantalum and hafnium.

The behavior of borides and graphite in hydrogen fluoride is probably due to hydrogen, since these are the only materials with stable hydrogen-containing corrosion products at high temperatures. For example, reaction of borides and graphite could proceed as follows:

TABLE IV

SUMMARY OF COMPATIBILITY OF REFRACTORY MATERIALS
WITH GASEOUS ROCKET NOZZLE EXHAUST SPECIES

| Material | Minimum Melting Temperature, | | Resistance to Given Environment[a] at 3000°-5000°F | | | | | B[b] |
	$^\circ$C	$^\circ$F	O_2	F_2	HF	F_2-O_2	HF-O_2	
Iridium	2440	4450	E	F-E	E	F-E	E	M
Ir-33Re	~2800	~5070	E	F-E	E	F-E	E	M
Rhenium	3180	5755	F[b]	F-E	E[b]	P[b]	G-E[b]	M
Re-35Ir	2860	~5180	F[b]	G-E	E[b]	F[b]	E-G[b]	M
Graphite (ATJ)	~3700	~6700 (Sub)	P[b]	G-F	E-G	P-VP	F[b]	E
W-26Re	3315	6000	F[b]	F-G	E[b]	P[b]	G[b]	G
Tungsten	3410	6170[b]	F	F-E	E	P	E-G	G
W-25Re-20Ir	2550	~4600[b]	F	G-E	E	F	E-G	F
Tantalum	3000	5430	VP[b,d]	P	G	VP[b]	P[b]	G
TaC-20 v/o C	3450	6240	F-VP[d]	G-E	E	P-VP	E-VP	G
HfC-33 v/o C	3150	5705	G-P[c]	G-F	E-G	P-VP	E-VP	G
HfB$_2$	3060	5545	G[b,c]	F	F	F-P[b]	F-P[b]	E
ZrB$_2$	3000	5430	G[b,c]	F	F	F-P[b]	F-P[b]	E
HfB$_2$-SiC	2400	~4400[b]	E[b,c]	G	G	F-P[b]	F-P[b]	E
ZrB$_2$-SiC-C	2400	~4400[b]	E[b,c]	G	G[b]	F-P[b]	F-P[b]	E
HfN	3310	5900	F[b,d]	F	F[b]	P-VP[b]	F-P[b]	G
TaN	3360	6080	F[b,c]	F	F[b]	P-VP[b]	F-VP[b]	G
(Hf-20Ta)N	~3300	~5940[b]	F[b,c]	F	F	P-VP[b]	F-VP[b]	G

[a] Rating refers to atmospheres in IITRI-B6058-40, 5.4v/oO_2, 6.5v/oF_2 10v/oHF, 6.5 v/o F -5.4 v/o O_2, 10 v/o HF-2.3 v/o O_2.

E-Excellent <1 mil/min   P-Poor 4-6 mils/min
G-Good 1-2 mils/min   VP-Very poor >6 mils/min
F-Fair 2-4 mils/min   M-Eutectic melts below 3500°F

NOTE: F-E denotes decreasing reaction with increasing temperature
     E-G denotes increasing reaction with increasing temperature

[b] Estimated-no experimental data.

[c] Solid oxide formed

[d] Melting point of oxide ~3400°F.

$$HfB_2 + HF \rightleftharpoons B_xH_y + Hf_xF_y$$

$$C + HF \rightleftharpoons C_xH_y + C_xF_y$$
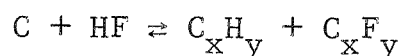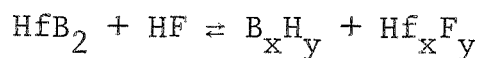
Thus, thermally stable materials which indicate high corrosion rates in hydrogen fluoride will also tend to be reactive in hydrogen. Carbide-graphite composites should be included in this group. The relatively low recession rate of carbide materials at 3500°-4500°F presumably was due to high thermodynamic stability of the carbides an or slow reaction kinetics. HfC-C composites did indicate a considerable increase in recession rate at 5000°F, as did ATJ graphite.[1]

In Table IV, estimates of the reactivity in boron-containing atmospheres are presented to indicate whether potential problems exist due to eutectic melting. The basis for an adverse rating is a eutectic melting below 3500°F. Of the materials in Table IV, a definite problem area exists only for iridium, rhenium, and their alloys. However, a number of the borides melt in the range of 4000°-5000°F (Table II). Thus, the presence of free boron could present problems at 4000°-5000°F with most of the refractory materials shown in Table IV, except perhaps the borides. In any case, the influence of boron in the exhaust stream on refractory materials is not adequately defined at the present time.

A general summary of the properties of refractory materials of interest in this program, excluding metals, is contained in Table V. All of the elements with melting points above 4000°F have been discussed in detail previously, except osmium, ruthenium, and hafnium. Because of their low melting points, ruthenium and hafnium do not appear to provide any advantage over other refractory metals. Furthermore, hafnium would be very reactive in fluorine and hydrogen fluoride based on data for HfN.

Osmium has not been considered to date, although it does have the highest melting point (5450°F) of the platinum group metals. Considering the behavior of iridium, osmium and ruthenium may be resistant to fluorine and hydrogen fluoride at high

TABLE V

SUMMARY OF ESTIMATED COMPATIBILITY

OF REFRACTORY MATERIALS WITH ROCKET ENGINE EXHAUST SPECIES

Material	High Melting Systems	Remarks
Borides	HfB_2, ZrB_2, TaB_2, CbB_2, WB	High melting points obtainable. Thermal shock problems, based on the data for ZrB_2 and HfB_2. Selected borides can provide good oxidation (1) and fair fluorine resistance (1, 27). Oxidation resistance depends on formation of solid oxides. Fair resistance to HF and fluorine, but less resistance to atmospheres containing both oxygen and fluorine (1). Generally, borides are more reactive than carbides in halogen-containing atmospheres (1, 27, 28). There is some evidence indicating that borides may be useful in boron-containing atmospheres (31) although graphite was considered the prime candidate.
Carbides	HfC, TaC, ZrC; carbide-graphite composites, complex carbides	Very high melting points obtainable. Thermal shock difficulties, but can be improved by graphite additions. Only fair oxidation resistance and then only at temperatures where solid oxides are formed. Good resistance to fluorine and HF to at least 5000°F (1, 27, 34). Poor to very poor resistance to oxygen in combination with fluorine and HF (1).
Nitrides	HfN, TaN, ZrN, TiN; complex nitrides	High melting points obtainable. Thermal shock problems. Tend to be unstable above 4000°F. Oxidation resistance depends on development of stable oxides. Poor resistance to fluorine and HF due to decomposition, resulting in highly reactive metal phases (26).
Silicides	Hf_2Si, B_3Si, Ta_9Si, Ta_5Si_3, Ta_2Si, Nb_5Si_3	Maximum melting point obtainable about 4500°F. The few specific data available on fluorine and HF compatibility indicate poor resistance (35, 36). SiC appears to improve fluorine corrosion resistance of ZrB_2. Excellent oxidation resistance to about 3000°F.

TABLE V (cont.)

Material	High Melting Systems	Remarks
Sulfides	CeS, CaS	Maximum melting point obtainable about 4500°F. No specific data available in fluorine and HF. Generally poor oxidation resistance.
Phosphides	Ba_3P, Pa_3P_2	Maximum melting point obtainable about 5500°F. No specific data available in fluorine and HF. Generally poor oxidation resistance.
Oxides	HfO_2, ThO_2, ZrO_2; Complex oxides	High melting temperatures obtainable. Thermal shock problems. Obviously best resistance is to oxygen (37, 38, 39, 40). Generally poor resistance to fluorine and HF (31, 33, 35, 37). Poor resistance of oxides to fluorine and HF is indicated by high corrosion rate of carbide-graphite composites in F_2-O_2 and HF-O_2 (Table IV.
Intermetallics	$HfRe_2$, Ir_3Hf, Ir_3Ta, Re_3W, Re_3Mo_2	Highest melting point obtainable 5720°F. Little data available in literature. Re-W and Re-Mo intermetallics should behave similar to pure metals in F_2 and HF. Fair to poor oxidation resistance likely. Ir-Hf and Ir-Ta compounds have good oxidation resistance, but oxidize internally (25). Should have good resistance to F_2 and HF above 3000°F. May be good additives for improving resistance of carbides and borides to O_2 and combined O_2-F_2 and O_2-HF atmospheres.

temperature. However, osmium has much poorer oxidation resistance than iridium.[4] Therefore, any advantage in melting point is offset by decreasing oxidation resistance.

Table V represents an attempt to summarize the general properties of carbides, borides, nitrides, silicides, phosphides, oxides, and intermetallics. Data in the literature on the compatibility of these materials with fluorine or hydrogen fluoride not presented in Table IV are included. Although fluorine corrosion is limited, the data in the literature on fluorine compatibility do not deviate appreciably from that presented in Table IV. Thus, it must be concluded that the only new materials potentially useful for fluorine-containing exhausts products are the intermetallics, and possibly BN.

The corrosion data presented in Table IV represented experimental measurements of the recession rate of refractory materials of interest in 6.5 v/o fluorine, 5.4 v/o oxygen, 10 v/o hydrogen fluoride, 6.5 v/o F_2-5.4 v/o O_2, and 10 v/o HF-2.3 v/o O_2. All of these data were obtained at a gas velocity of 400 fps, a total gas flow rate of 10 cfh, and a 45° impingement angle. These data can be employed to estimate the relative recession rate of these materials in actual rocket nozzle environments.

Estimates of the recession rate in refractory materials in HF-F_2, HF-F_2-O_2, and HF-F_2-O_2-B atmospheres are presented in Table VI. These atmospheres can be expected in the exhaust of propellant systems of current interest. For example, the HF-F_2 atmosphere represents the major corrosive species for a N_2H_4-F_2 propellant system, and the HF-F_2-O_2-B atmosphere represents the major corrosive species for a B_2H_6-OF_2 propellant system.

Obviously, the throat recession rates in Table VI will apply only if the arrival rate of corrosive species at the nozzle is reasonably close to that used for the corrosion tests. The delivery rate of corrodent species for the recession rates shown in Table VI was 6-12 x 10^{-5} lb-moles in^2/min at an impingement angle of 45°. Furthermore, the relative concentration of corrosive

TABLE VI

ESTIMATED SURFACE RECESSION RATE OF REFRACTORY MATERIALS

IN SELECTED ROCKET NOZZLE EXHAUST ATMOSPHERES AT 4000-5500°F

| Nozzle Wall Temperature, °F | Estimated Recession Rate in Given Exhaust Atmospheres | | | | | |
| | $HF-F_2$ | | $HF-F_2-O_2$ | | $HF-F_2-O_2-B$ | |
	Material	Recession Rate, mils/min	Material	Recession Rate, mils/min	Material	Recession Rate, mils/min
4000	Iridium	<0.5	Iridium	<0.5	Iridium	(a)
	Ir-33Re	<1	Ir-33Re	1.0	Ir-33Re	(a)
	W-25Re-20Ir	1	W-25Re-20Ir	2.5	W-25Re-20Ir	(a)
	Re-35Ir	1.3	Re-35Ir	~3.0	Re-35Ir	(a)
	Graphite (ATJ)	1.5	Rhenium	4.0	Rhenium	(a)
	TaC-C	1.5	ZrB_2-SiC-C	4.5	ZrB_2-SiC-C	4.5
	HfC-C	1.5	Graphite (ATJ)	4.5	Graphite (ATJ)	4.5
	Rhenium	1.5	Tungsten	5.5	Tungsten	5.5
	ZrB_2-SiC-C	2.0	HfC-C	5.5	HfC-C	5.5
	Tungsten	2.5	HfB_2	~5.5	HfB_2	~5.5
	HfB_2	2.8	TaC-C	6.0	TaC-C	6.0
	TaN-HfN	3.5	TaN-HfN	~7.0	TaN-HfN	~7.0
	Tantalum	3.5	Tantalun	~8.0	Tantalum	~8.0
4500	Ir-33Re	<0.5	Ir-33Re	0.5	Ir-33Re	(a)
	TaC-C	<1.0	W-25Re-20Ir	2.5	W-25Re-20Ir	(a)
	W-25Re-20Ir	1.0	Re-35Ir	~3.0	Re-35Ir	(a)
	HfC-C	1.0	Rhenium	4.5	Rhenium	(a)
	Re-35Ir	1.0	Tungsten	5.5	Tungsten	(a)
	Rhenium	1.0	HfC-C	6.0	HfC-C	6.0
	Graphite (ATJ)	2.0	HfB_2	~6.0	HfB_2	6.0
	Tungsten	2.5	Graphite (ATJ)	6.5	TaC-C	~7.0
	HfB_2	~3.0	TaC-C	~7.0	Tantalum	~10
	Tantalum	~3.5	Tantalum	~10	Graphite (ATJ)	(a)
	Iridium (melts 4450°F)					
	ZrB_2-SiC-C (melts ~4400°F)					

TABLE VI (cont.)

Nozzle Wall Temperature, °F	HF-F_2		HF-F_2-O_2		HF-F_2-O_2-B	
	Material	**Recession Rate, mil/min**	**Material**	**Recession Rate, mil/min**	**Material**	**Recession Rate, mil/min**
5000	Re-35Ir	<0.5	Re-35Ir	~3.5	Re-35Ir	(a)
	Rhenium	<0.5	Rhenium	4.0	Rhenium	(a)
	TaC-C	1.0	Tungsten	6.0	Tungsten	(a)
	Tungsten	2.0	Graphite (ATJ)	7.0	Graphite	(a)
	Graphite (ATJ)	2.2	HfC-C	~7	HfC-C	(a)
	HfC-C	2.2	HfB$_2$	~7	HfB$_2$	~7
	HfB$_2$	~4.0	TaC-C	>10	TaC-C	>10
	Tantalum	~4.0	Tantalum	>10	Tantalum	>10
	Ir-33Re (melts ~4900°F)					
	W-25Re-20Ir (Melts ~4500°F)					
5500	Rhenium	~1.0	Rhenium	~4.0	Rhenium	(a)
	Tungsten	1.0	Tungsten	5.6	Tungsten	(a)
	TaC-C	~2.0	Graphite (ATJ)	~8.0	Graphite	(a)
	Graphite (ATJ)	~3.0	HfC-C	>10	HfC-C	>10
	HfC-C	~4.0	TaC-C	>10	TaC-C	>10
	Tantalum (melts ~5400°F)					
	HfB$_2$ (melts ~5400°F)					

(a)Inadequate data to define.

species in a nozzle exhaust depends on the combustion conditions and mixture ratio. Changes in the fluorine-oxygen ratio could have an appreciable effect on the corrosion rate. Thus, the estimated recession rates in Table VI represent a relative ranking of nozzle materials for each environment at wall temperatures of 4000°, 4500°, 5000°, and 5500°F. Wherever corrosion data were not available, recession rates were estimated by extrapolation of available corrosion data.

Table VI indicates that the lowest recession rates can be expected for the HF-F_2 atmosphere below 5000°F. Several materials including iridium, rhenium, and their alloys have recession rates of less than 1 mil/min in this environment. At 5500°F, tungsten and rhenium also indicate recession rates of about 1 mil/min. Carbide-graphite composites, particularly TaC-C, can also be used to a wall temperature of at least 5000°F.

Introduction of oxygen into the HF-F_2 system considerably reduces the number of materials exhibiting low recession rates to only iridium and Ir-33Re. Above 4500°F, the most resistant materials are Re-35Ir and rhenium with recession rates in the range of 3.5-4.0 mils/min.

The most corrosive environment is the HF-F_2-O_2-B atmosphere since no material appears acceptable for low recession rates above 4000°F based on current information. This is due primarily to the quantitative data on the influence of free boron on iridium and rhenium containing alloys. Boron could also influence the recession of other materials due to low-melting boron compounds. For example, degradation of graphite could be increased above 4500°F because B_4C melts at about 4450°F.

The primary objective of the literature survey was to generate data for the selection of new composite systems for oxidation-corrosion tests. It was clear from the survey that no new individual materials were promising with good oxidation-corrosion. The only new materials not previously considered were a few intermetallic compounds ($HfIr_3$, $TaIr_3$, $HfRe_2$) and boron

nitride. Without considering the boron problem, iridium and iridium-rich alloys provided the best resistance to combined fluorine-oxygen and hydrogen fluoride-oxygen above 3000°F. Thus, iridium-rich alloys were the most promising second-phase addition in composite systems for the development of improved oxidation-corrosion. Also, the metallic systems W-Re-Ir and Re-Ir appeared to provide some promise at temperatures above 4000°F.

A summary of seven systems selected for further evaluation based on the literature survey is presented in Table VII. Two of these systems were the metallic alloy systems W-Re-Ir and Re-Ir, and the remainder iridium-rich alloys and intermetallics in a carbide, boride, or graphite matrix. Thus, the potential oxidation-corrosion resistant systems rely heavily on iridium since it has represented the only metal with sufficiently high resistance to significantly affect the corrosion behavior of the composite. Included in Table VII are the fabrication methods or methods that were considered appropriate for each system. The composite systems generally were expected to require hot pressing, whereas normal metalworking and/or plasma spraying are probable fabrication methods for the metals. In general, refractory systems inherently require special fabrication techniques to obtain high-density materials.

Also included in Table VII are the melting ranges expected for the materials based on existing high-temperature data. The lowest melting point for each system represents the melting point that would be obtained if the composites were thermally unstable. On the other hand, the highest melting point is that which would be obtained in a thermally stable composite. For example, the melting points of the composite systems with iridium-rich second phase are controlled by the melting points of $HfIr_3$ (4450°F), $TaIr_3$ (4420°F), or the Ir-C eutectic (4000°-4200°F). Since a phase diagram exists for both the W-Ir and Re-Ir systems,[1] melting points in these systems were available. However, no melting point data were found for W-Re-Ir alloys, or

TABLE VII

SUMMARY OF PROPOSED OXIDATION-CORROSION RESISTANT SYSTEMS

System	Expected Melting Point, $^{\circ}F$	Potential Fabrication Method
W-Re-Ir	4400-5500	Arc melting/working, plasma spray
Re-Ir	4800-5500	Arc melting/working, plasma spray
TaC-(20-30 v/o)TaIr$_3$	3500-4450	Hot press
HfC-(20-30 v/o)HfIr$_3$	3500-4470	Hot press
HfB$_2$-(20-30 v/o)HfIr$_3$	3000-4470	Hot press
Graphite-(20-30 v/o)Ir-30Re	4200-4700	Hot press
Graphite-(20-30 v/o)TaIr$_3$	4000-4450	Hot press

IITRI-B6102-13
(Final Report)

the composites. Consequently, melting temperatures were determined for these materials and are discussed in Section II-C-3.

B.   Fabrication

The W-Re-Ir and Re-Ir alloys were prepared by nonconsumable arc melting of blended and presintered powders to insure homogeneity. Powders, nominally -325 mesh, were blended, cold pressed at 48 tsi, and sintered in vacuum at 3300°F for 2 hr. Finally, nominal 10 g samples were nonconsumable arc melted, with at least 6 remelts. Metallographic examination of the W-15Re-10Ir alloy showed that a two-phase structure existed in this alloy. The solubility of iridium in tungsten is about 5 w/o at 3250°F and about 10 w/o at the peritectic temperature (4550°F);[2] rhenium is soluble to about 25 w/o in tungsten.[2] Thus, most of the W-Re-Ir alloys produced in this program consisted of the tungsten-rich W-Re-Ir solid solution with the σ and/or ε W-Ir intermetallic compounds as the second phase. The σ phase decomposes eutectoidally at about 3240°F to ε and the tungsten-rich solid solution.

No metallography was conducted on the Re-Ir alloys. The solubility of iridium in rhenium is about 40 w/o.[2] Thus, the Re-25Ir and Re-35Ir alloys prepared in this program were single-phase rhenium-rich solid solution.

The TaIr$_3$ and HfIr$_3$ intermetallic compounds were also fabricated by arc-melting. In contrast to the other metallic alloys, these materials were prepared by combining melt stock of hafnium and tantalum with presintered Ir powders prepared as described previously. Again, no metallography was conducted on these alloys. However, arc-melting of bulk materials produced single-phase alloys in previous work.[25] Vendor analyses of the tungsten, rhenium, iridium, hafnium, and tantalum are summarized in Table VIII.

None of the composites consisting of iridium-rich alloys in a carbide, graphite, or boride matrix were prepared in this program. The result of interaction studies described in

TABLE VIII

NOMINAL ANALYSES OF METALLIC RAW MATERIALS

Element	Concentration of Impurity Element, ppm				
	W[a] (99.95+)	Hf[b] (98.0)	Ta[c] (99.9+)	Re[d] (99.99+)	Ir[e] (99.9+)
C	5	<13	100	-	-
H	1	<13	20	-	-
O	4	<30	100	-	-
N	3	<10	50	-	-
Fe	3	<100	-	18	400
MN	10	<10	-	-	-
Al	-	<35	-	<1	-
Cr	10	<10	-	<1	-
Cu	-	-	-	<1	-
Mg	<10	<10	-	<1	-
Ni	5	<15	-	<1	-
Si	<5	<20	-	<1	70
Cb	<10	<35	-	-	-
Ti	<10	34	-	-	-
Pt	-	-	-	-	100
Pd	-	-	-	-	40
Ru	-	-	-	-	120
Au	-	-	-	-	10
Ag	-	-	-	-	-
Rh	-	-	-	-	200
Others	-	2.0Zr			

[a] Fansteel Metallurgical Corp., commercial purity.
[b] Nuclear Metals Inc., crystal bar.
[c] Fansteel Metallurgical Corp., commercial purity.
[d] Cleveland Refractory Metals, commercial purity.
[e] Mathey-Bishop, Inc., Alloy 2000.

Section II-C-3 and the necessity for corrosion testing in BF_3 precluded preparation of these systems. However, it is expected that these composites could be prepared by hot pressing below the melting temperatures obtained (Section II-C-3). The only exception would be the HfB_2-$HfIr_3$ compounds because of the low melting temperature (~3200°F) occurring in this system.

A limited study of the hot workability of Ir-33Re, Re-25Ir, Re-35Ir, W-15Re-15Ir, and W-20Re-20Ir alloys was conducted. This study was performed on alloys remaining after oxidation-corrosion tests. An attempt was made to hot roll these alloys at 1800° and/or 2200°F; the results are summarized in Table IX. Only the Ir-33Re alloy indicated any tendency for hot working, even at 2200°F. This alloy exhibited surface cracks after about 15% reduction whereas the other alloys cracked badly on the first 10% pass. It is possible that corrosion testing developed grain boundary effects in the cast alloys which influenced their hot workability. However, these results suggest that the hot working temperatures for the Re-Ir and W-Re-Ir alloys might be very high. Fabrication of nozzles by hot spinning, therefore, might be very difficult or impossible.

C.   Thermal Stability Studies

1.   Oxidation-Corrosion Tests

The oxidation-corrosion rates of a variety of refractory materials in fluorine, oxygen, fluorine-oxygen, and hydrogen fluoride-oxygen atmospheres have been reported previously.[1] Corrosion studies during this program were initially intended to study new materials defined by the literature search. Finally, composites fabricated on the program were to be evaluated in these atmospheres. The majority of the oxidation-corrosion tests were conducted on W-Re-Ir alloys, Re-25Ir, Re-35Ir, Ir-23Hf ($HfIr_3$), and Ir-23.9Ta ($TaIr_3$). The literature survey also indicated a potential problem with boron in combustion gases. Consequently,

TABLE IX

HOT ROLLING BEHAVIOR OF Ir-Re AND W-Re-Ir ALLOYS

Alloy Composition, w/o	Nominal Rolling Temperature, °F	Nominal Reduction, %	Comments
Ir-33Re	1800	15	Cracked after 2nd 0.010 in. pass.
	2200	19	Cracked after 2nd 0.010 in. pass.
Re-25Ir	2200	0	Cracked 1st pass.
Re-35Ir	2200	0	Cracked 1st pass.
W-15Re-15Ir	2200	0	Cracked 1st pass.
W-20Re-20Ir	2200	0	Cracked 1st pass.

corrosion studies were extended to boron-containing gases to indicate the influence of boron at high temperatures on the corrosion of selected materials.

The individual corrosive elements present in the combustion gases of potential fluorine-containing propellant systems which must be considered in oxidation-corrosion of materials are presented in Table X. Obviously, the combustion gases of engines will contain numerous other species including monatomic forms of the elemental gases and complex combustion products. The concentration of these products will depend on the mixture ratio and combustion efficiency.

Hydrogen fluoride is included, although it is not on individual species, because it will be the major constitutent of all combustion gases. Tests conducted previously suggest that the stability of the hydrogen fluoride molecule precludes reaction with many refractory materials below 5000°F. Execptions are the reactive refractory metals (Ta, Hf) and borides. Recession rates of many materials in hydrogen fluoride are in the range of two orders of magnitude less than oxygen or fluorine. Thus, hydrogen fluoride can generally be considered the carrier gas for the other corrosive species present in the gas stream.

While hydrogen also appears as a corrodent species in all combinations, it will not affect the corrosion of metallic materials. Hydrogen becomes a corrosion factor only in graphites, carbides, carbide-graphite composites, and borides--i.e., only those materials which exhibit high-temperature stable gaseous reaction products with hydrogen. These are generally limited to the C_xH_y and B_xH_y type compounds. The effect of hydrogen will be important primarily for graphites because these materials are the only potential nozzle materials in which carbon is present in an uncombined form. Carbides are much more resistant to hydrogen than carbon is because the corrosion rate is determined

TABLE X

INDIVIDUAL CORROSIVE SPECIES PRESENT
IN COMBUSTION GASES OF POTENTIAL LIQUID PROPELLANTS

Propellant System	Individual Corrosive Species
H_2-F_2	HF, F_2, H_2
H_2-OF_x	HF, F_2, O_2, H_2
$N_2H_4-F_2$	HF, F_2, H_2, N_2
$N_2H_4-OF_x$	HF, F_2, O_2, H_2, N_2
CH_4-F_2	HF, F_2, H_2, C
CH_4-OF_x	HF, F_2, O_2, H_2, C
$B_2H_6-F_2$	HF, F_2, H_2, B
$B_2H_6-OF_x$	HF, F_2, O_2, H_2, B

by the temperature-dependent relative thermodynamic stability of the carbides and C_xH_y reaction product. This thermodynamic balance obviously prevails for graphites, and consequently the recession rate in hydrogen is determined by the kinetics of the $C-H_2$ reaction. It was shown in previous phases that $C-H_2$ reaction probably does influence the reaction rate of carbide-graphite composites with HF above 4500°F.[1] However, it will also be shown subsequently that the $C-H_2$ reaction is a secondary problem for graphitic rocket nozzle materials.

The previous oxidation-corrosion work had considered only HF, F_2, O_2, H_2, and their combinations--i.e., propellant systems in which elemental hydrogen was the fuel. However, the use of space-storable hydrogen fuels interjects other potential corrosive species including carbon, and boron.

Nitrogen generated in hydrazine reaction products is generally not a problem for any of the systems of interest in this program. Nitrides are unstable and/or form high-melting compounds at high temperatures.

On the other hand, boron and carbon can influence the corrosion rates of refractory materials in rocket nozzle exhausts. Unlike fluorine and oxygen which volatilize, boron and carbon will form low-melting compounds with some of the systems of interest. Surface recession due to carbon and boron, therefore, will consist of surface melting rather than volatilization of corrosion products. High-temperature interaction data (Section II-A) suggest that more problems will be encountered with boron than carbon because the melting temperatures are generally lower for boron interactions.

The equipment for oxidation-corrosion testing has been reported in detail previously.[1] Test samples supported on tungsten rods were induction-heated in a stainless steel chamber containing a sight port for optical temperature measurements. All tests were run under identical conditions, unless

IIT RESEARCH INSTITUTE

IITRI-B6102-13
(Final Report)

otherwise noted: (1) total gas flow rate--10 cfh (400 fps);
(2) exposure time--5 min, (3) impingement angle--45°, (4) nozzle
distance--1 in. The nominal sample size was 0.5 x 0.5 x 0.125 in.,
and surface recession calculations were made using the impinge-
ment surface and edges as the effective reaction surface area.
Temperature measurements were made with an L & N optical pyrom-
eter, and temperature corrections made using the published values
for emittance of the various materials.

A limited number of corrosion tests were conducted in
fluorine for Re-Ir and W-Ir alloys previously,[1] but no work
had been done on W-Re-Ir alloys or the MIr_3 intermetallics.
Accordingly, corrosion tests of these materials in fluorine,
hydrogen fluoride, fluorine-oxygen, and hydrogen fluoride-oxygen
were conducted to determine the high-temperature resistance of
these materials. Data for the Re-Ir alloys in fluorine were
taken from previous work.

The lack of information on the influence of boron-
containing gaseous species demonstrated that experimental work
in these atmospheres was required. Accordingly, the work scope
was modified to permit oxidation-corrosion tests in BF_3, BF_3-O_2,
and BF_3-H_2 atmospheres. The BF_3-H_2 atmosphere was selected to
assure generation of free boron by the reaction.

$$2BF_3 + 3H_2 \rightleftharpoons 6HF + 2B$$
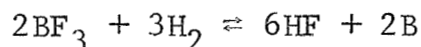
It was found that tests could be conducted in these
atmospheres as readily as the tests in combined fluorine and
hydrogen fluoride, and that free boron was generated according
to the above equation.

The results of oxidation-corrosion tests are plotted
in Figures 1 to 8. Experimental data are contained in
Appendix A.

Surface recession data for W-Re-Ir and Re-Ir alloys,
$HfIr_3$, and $TaIr_3$ in flowing argon with 6.5 v/o fluorine at
3000°-5000°F are plotted in Figure 1. Data for rhenium,
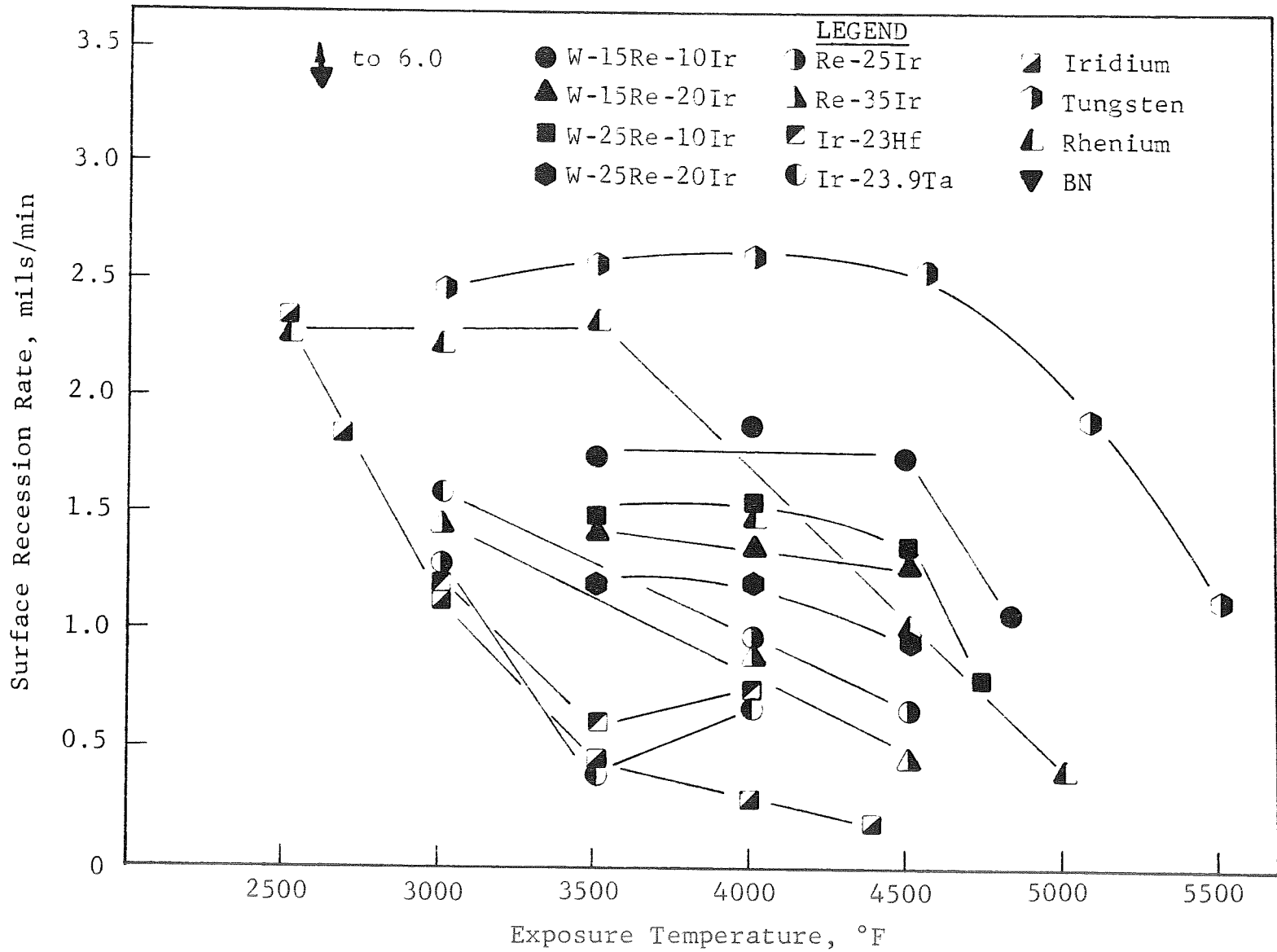
Fig. 1 – Surface Recession Rate of Refractory Materials in Flowing Argon-6.5 v/o Fluorine.

tungsten, and iridium obtained previously are included. The tungsten-base alloys exhibited the highest recession rates of the new materials. Generally, the recession rate of W-Re-Ir alloys decreased with Ir/Re concentration; the lowest recession was obtained for the W-25Re-20Ir alloy. Over the range of 3500°-4500°F, the W-Re-Ir alloy had a recession rate of about 1 mil/min; about one-half that of unalloyed tungsten.

The lowest recession rates at 3000°-3500°F were measured on the $TaIr_3$ and $HfIr_3$ intermetallic compounds. These materials were similar to unalloyed iridium in this range, but increased in recession rate at 4500°F. This was apparently due to more aggressive attack of hafnium and tantalum in the alloys; both exhibit very high recession rates in fluorine. At 4500°F, the lowest recession rates were obtained on the Re-Ir alloys-- as expected, based on the data shown for iridium and rhenium.

Since no data existed on boron nitride (BN) in fluorine, several samples of this material were also exposed to fluorine and hydrogen fluoride. Boron nitride cannot be heated inductively because of its high dielectric strength; consequently, 0.060 in. thick samples were heated with a tungsten samples as a susceptor. The maximum temperature attainable by this method was about 3000°F uncorrected optical temperature. The results obtained from these tests indicate that the calculated surface recession rate of BN at 2750°F (uncorrected optical temperature) in an argon-6.5 v/o fluorine atmosphere was very high--in the order of 6.0 mils/min. At 2900°F (uncorrected) the reaction rate of BN in argon-10 v/o HF was determined to be 0.32 mil/min. These rates are high compared to most of the other materials tested. This is the highest rate determined in this program for fluorine corrosion. These tests demonstrate that BN would not be an attractive material for operation in fluorine-containing environments.

Surface recession data in flowing argon-10 v/o hydrogen fluoride are plotted in Figure 2. In this atmosphere,

IIT RESEARCH INSTITUTE

IITRI-B6102-13
(Final Report)
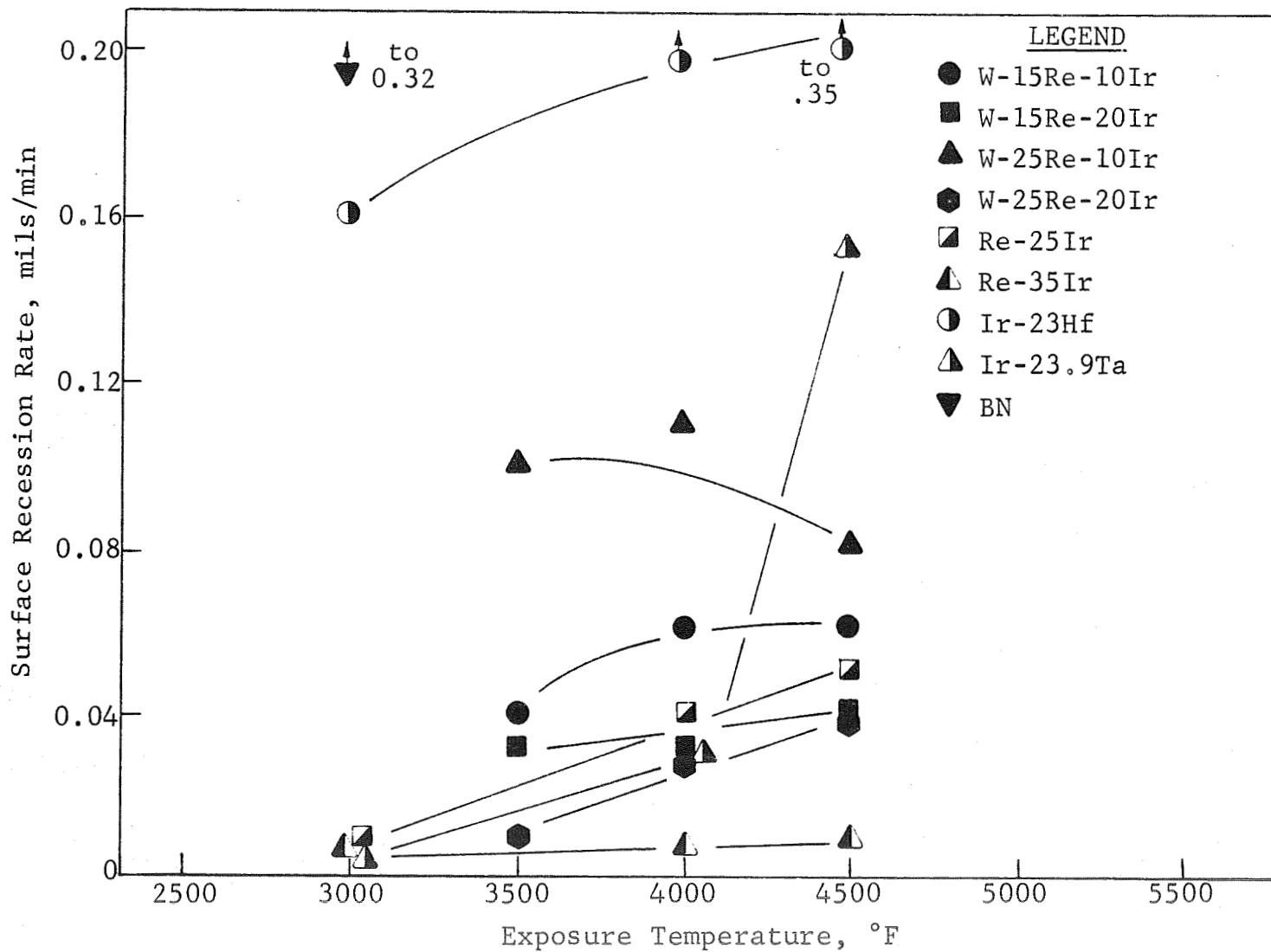
Fig. 2 - Surface Recession Rate of Refractory Materials in Flow-
ing Argon-10 v/o Hydrogen Fluoride.

except for BN, the highest rates were measured for $HfIr_3$, although both $HfIr_3$ and $TaIr_3$ had relatively high rates of 0.15 to 0.35 mil/min at 4500°F. The lowest recession rates were obtained on the W-Re-Ir and Re-Ir alloys; recession of these alloys was in the range of 1.5 to 2 orders of magnitude less than in 6.5 v/o F_2.

Surface recession rates in flowing argon-6.5 v/o F_2-5.4 v/o O_2 are plotted in Figure 3. This atmosphere is the most aggressive employed in this program. Again, data obtained previously for tungsten, iridium, and ATJ graphite are included. The lowest calculated recession rates obtained in this atmosphere were for $Hf-Ir_3$ and $TaIr_3$, both of which exhibited temperature dependence similar to unalloyed iridium. Re-35Ir had a uniform recession rate of about 2 mils/min over the range of 3500°-4500°F. Finally, the W-Re-Ir alloys exhibited surface recession rates of at least a factor of two less than tungsten and ATJ graphite above 3500°F.

Surface recession data for W-Re-Ir and Re-Ir alloys, $HfIr_3$, and $TaIr_3$ in argon-10 v/o hydrogen fluoride-2.3 v/o oxygen are plotted in Figure 4. In this atmosphere, most of the weight loss results from interaction with oxygen. It is not surprising, therefore, that the lowest recession rates were obtained for the $HfIr_3$ and $TaIr_3$ intermetallic compounds. These materials, in fact, had weight gains because of the development of oxide films. The $TaIr_3$ intermetallic exhibited a weight gain at 3000°F and $HfIr_3$ at 4000°F. Re-35Ir had a linearly temperature-dependent recession rate varying from about 0.3 mil/min at 5000°F to 0.6 mil/min at 4500°F. The W-Re-Ir alloys and Re-25Ir had recession rates in the range of 0.8 to 1.5 mils/min.

As previously discussed, the influence of boron-containing gaseous species in the corrosion of refractory materials was undefined in existing data. Accordingly, selected materials were exposed in BF_3, BF_3-O_2, and BF_3-H_2 atmospheres.
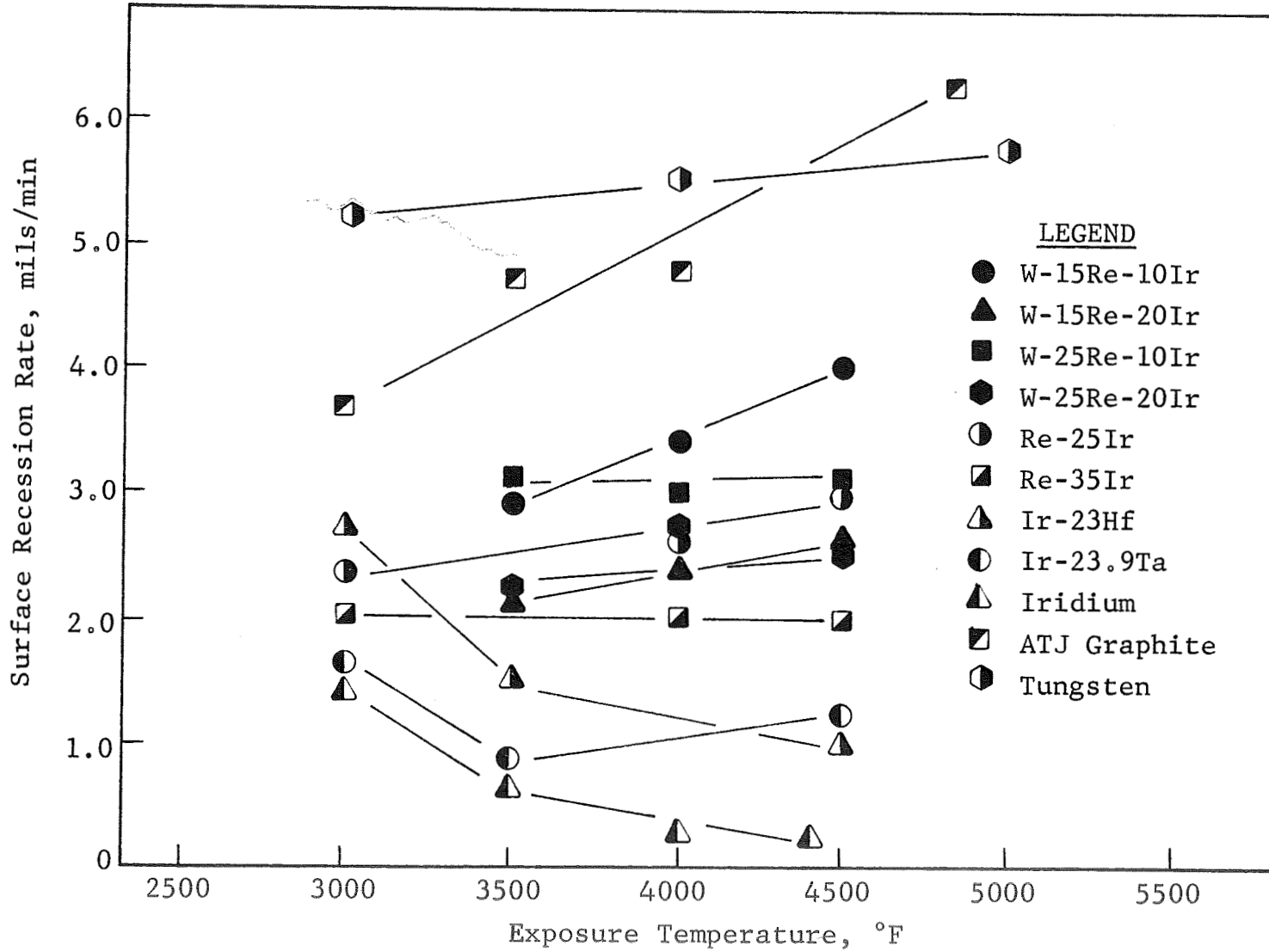
Fig. 3 - Surface Recession Rate of Refractory Materials in Flow-
ing Argon-6.5 v/o F_2-5.4 v/o O_2.
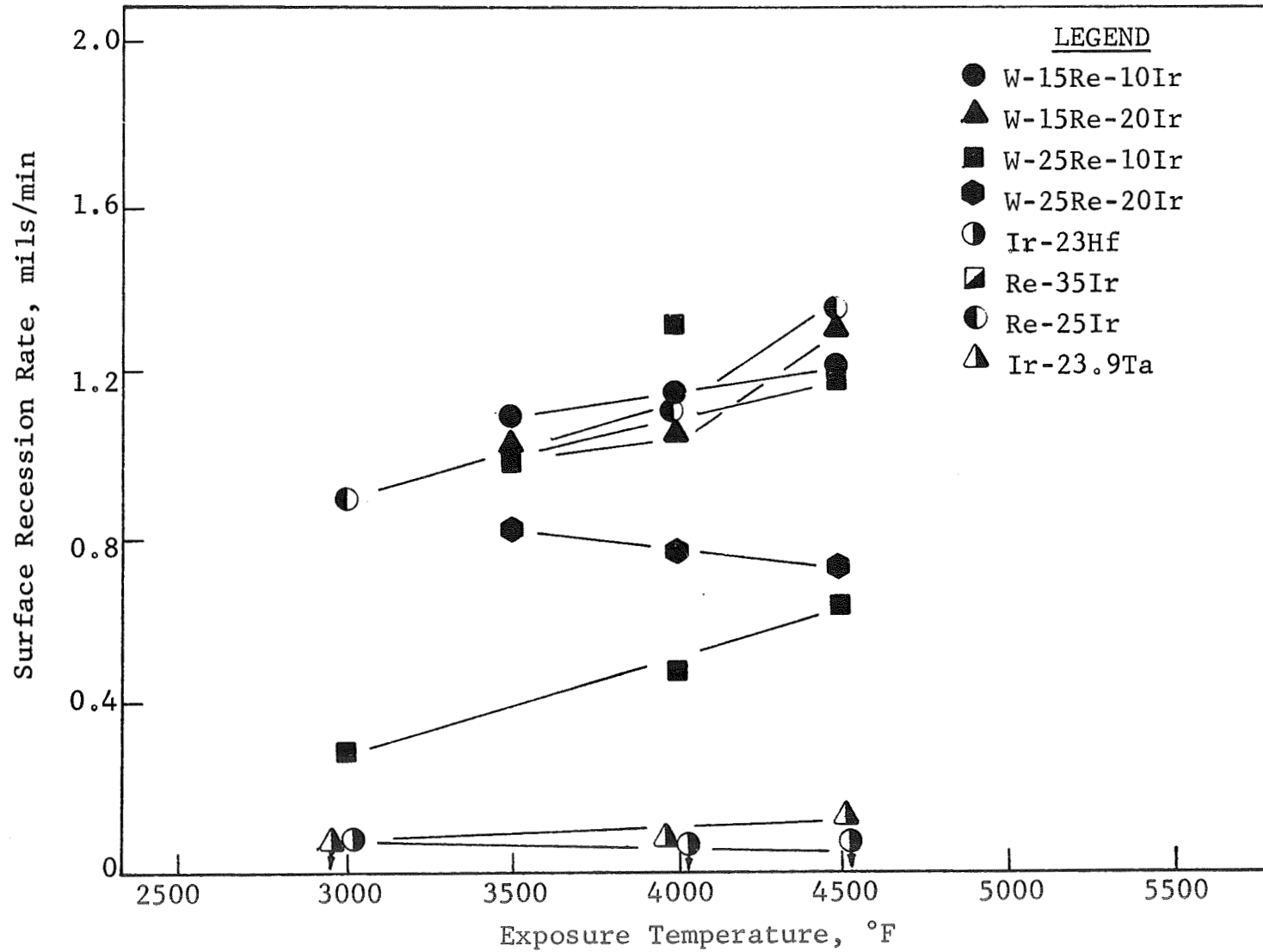
Fig. 4 - Surface Recession Rate of Refractory Materials in
Flowing Argon-10 v/o HF-2.3 v/o O$_2$.

The latter atmosphere was intended to provide free boron via reaction to form the stable HF molecule. The results of oxidation-corrosion tests in boron-containing atmospheres are plotted in Figures 5 through 7.

Figure 5 shows the surface recession rate of tungsten, iridium, and ATJ graphite in argon-10 v/o BF_3 from 3000°-5500°F. Data for Re-25Ir and Re-35Ir at 4000°F only are included. Except for ATJ graphite, the recession rate in 10 v/o BF_3 is about equivalent to that in 10 v/o HF, in the range of 0.01 to 0.07 mil/min. ATJ graphite increased rapidly in recession rate from about 0.08 mil/min at 3500°F to 0.2 at 4800°F. Examination of the sample surfaces after exposure in a low-power microscope did not indicate any surface melting reactions with the boron in BF_3. Thus, reaction with BF_3, like HF, appears to be a secondary problem in rocket nozzle environments for the materials evaluated.

Surface recession rates of tungsten and ATJ graphite in argon-4.3 v/o BF_3-4.0 v/o O_2 are plotted in Figure 6. Also included are data previously obtained in argon-6.5 v/o F_2-4.0 v/o O_2, which provides the same fluorine and oxygen mass flow rates as the BF_3-O_2 atmosphere. The surface recession rates of ATJ graphite are slightly higher in BF_3-O_2, and tungsten slightly lower, than in argon-4 v/o oxygen.[1] Thus, these tests again indicate only a minor effect of BF_3 on the surface recession rate. It appears that the recession rate of ATJ graphite is about equivalent to the sum of the recession rates in the individual BF_3 and O_2 environments. For tungsten, lower oxidation-corrosion in BF_3-O_2 may be due to interactions producing $B_xO_yF_z$ species which reduce the effective oxygen concentration.

Figure 7 is a plot of the recession rates of tungsten, iridium, ATJ graphite, Re-25Ir, and Re-35Ir in argon-10 v/o BF_3-10 v/o H_2. This atmosphere was intended to produce free boron by interaction of the gases to produce hydrogen fluoride and

IITRI-B6102-13
(Final Report)
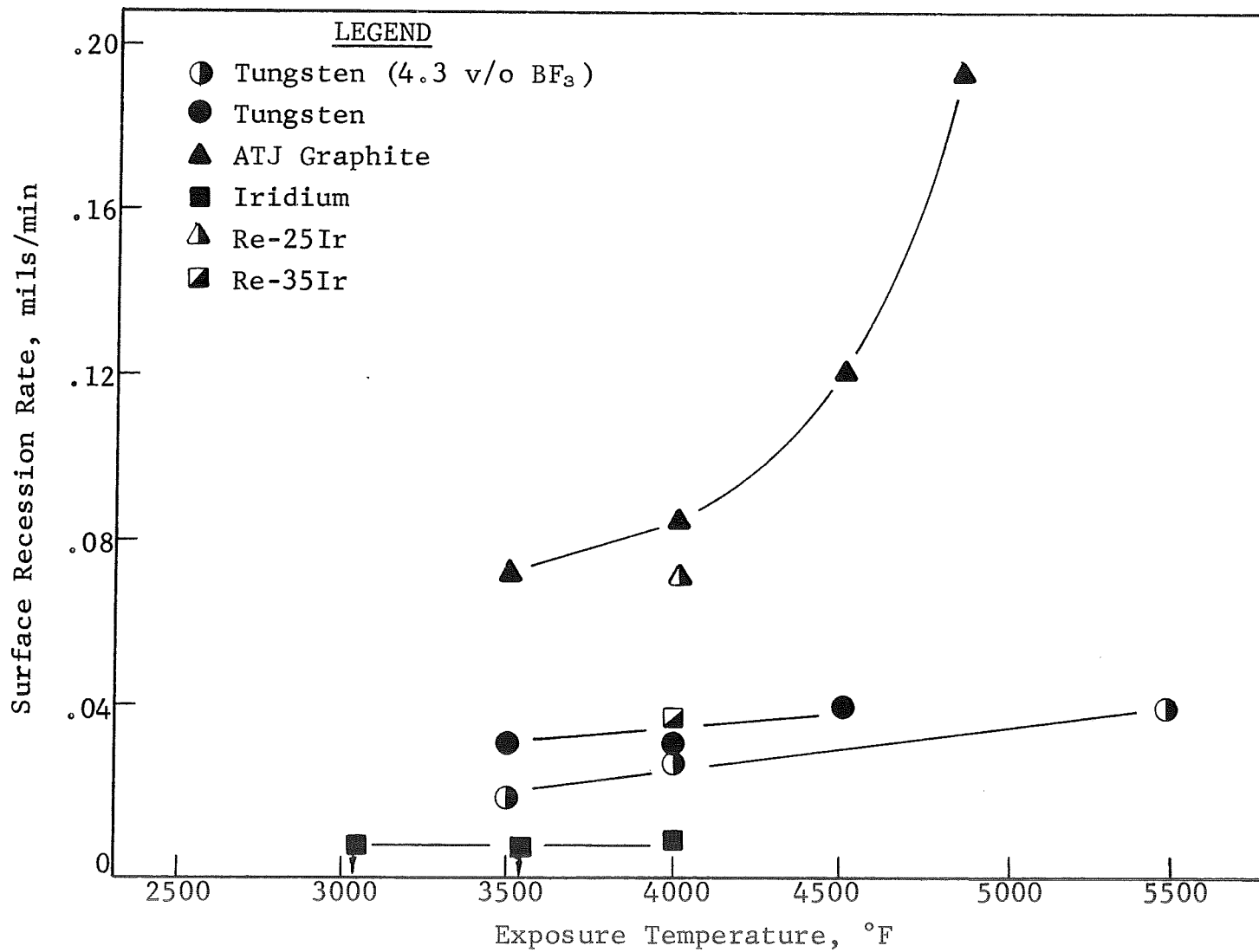
Fig. 5 — Surface Recession Rate of Refractory Materials
in Flowing Argon-10 v/o BF_3.
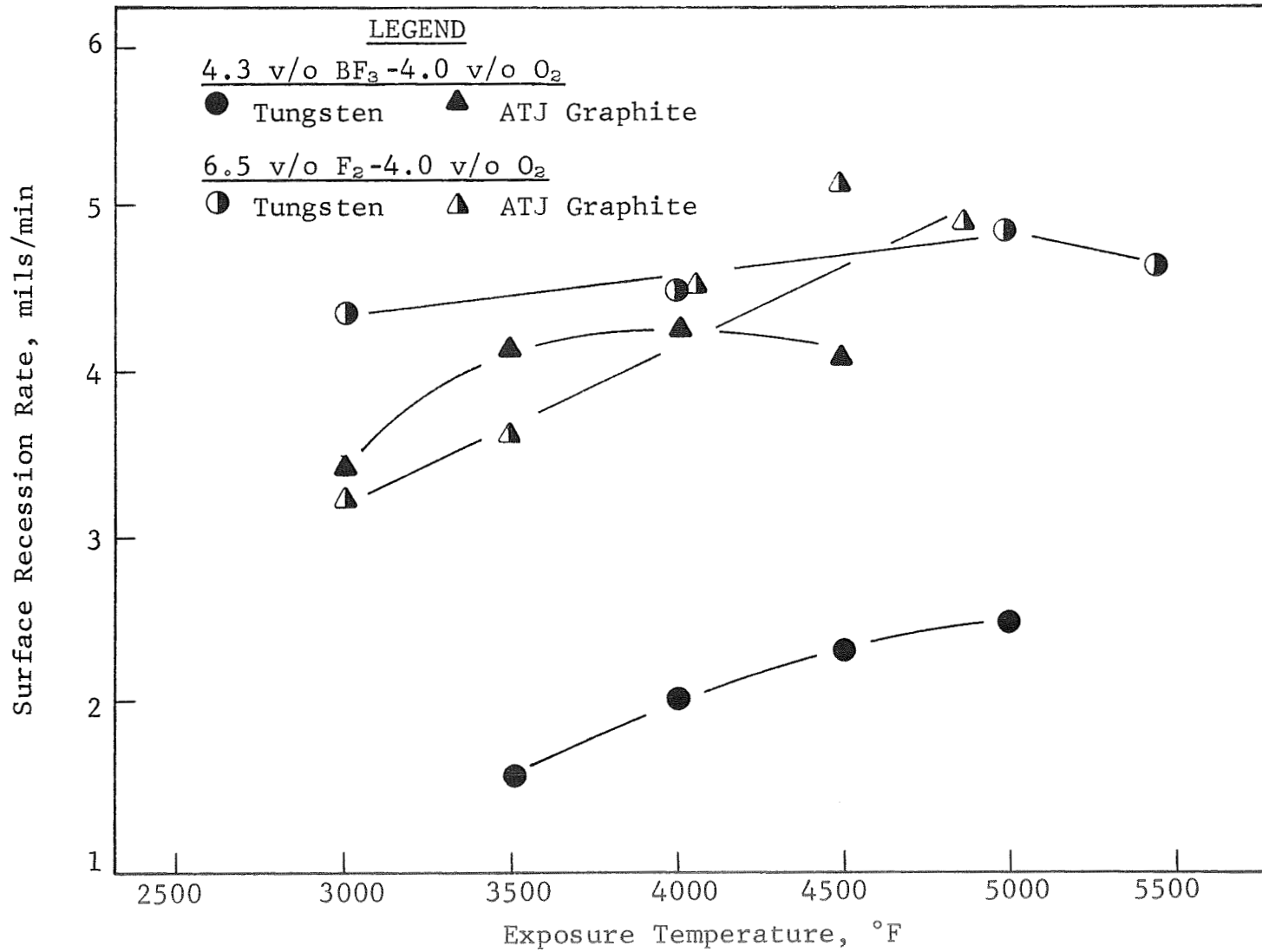
Fig. 6 – Surface Recession Rate of Tungsten and ATJ Graphite in Flowing Argon-4.3 v/o BF_3-4.0 v/o O_2 and Argon 6.5 v/o F_2-4.0 v/o O_2.
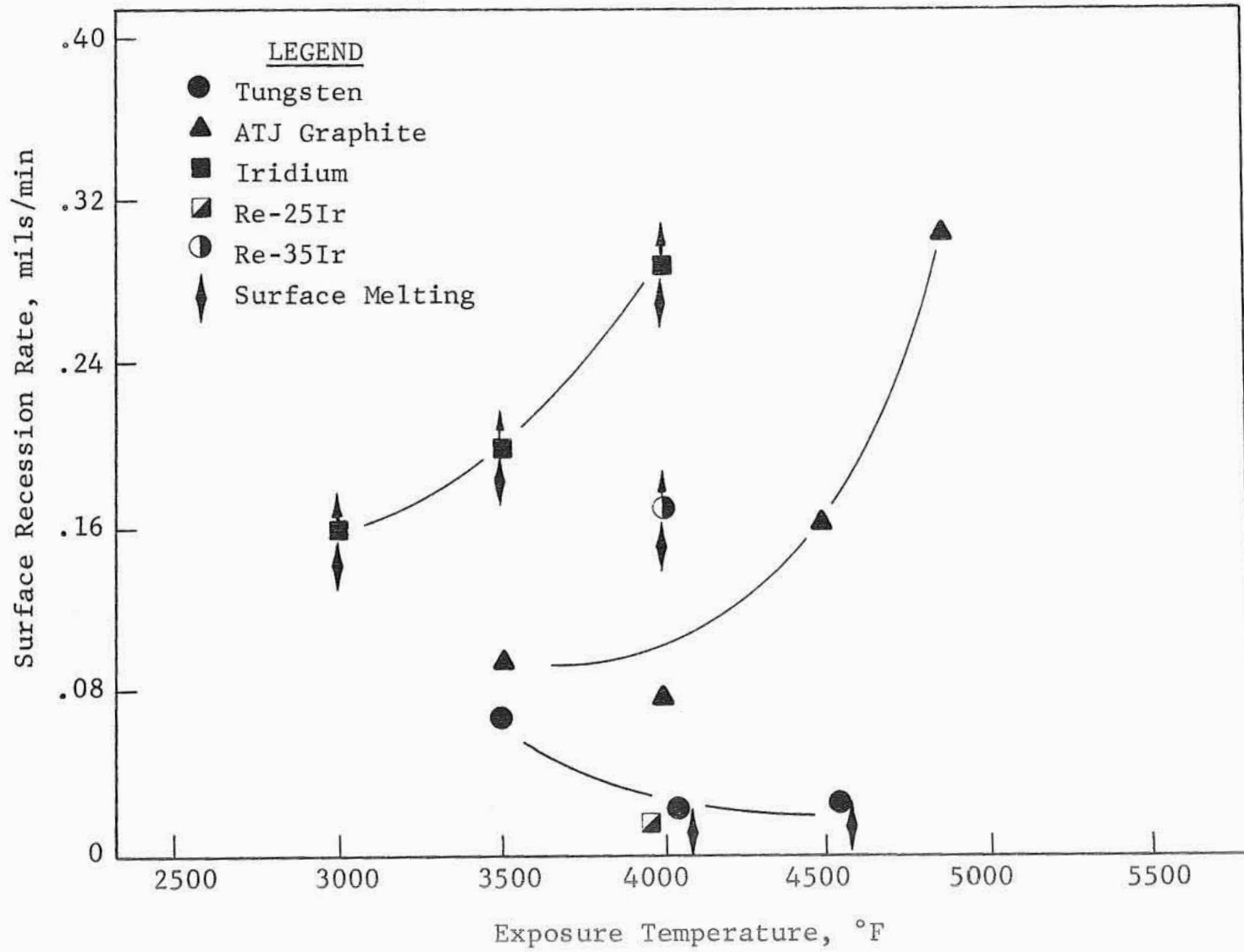
Fig. 7 - Surface Recession Rate of Refractory Materials in Flowing Argon-10 v/o BF_3-10 v/o H_2.

boron. Assuming reaction with all available hydrogen, the atmosphere at the sample surface contained BF_3, HF, and boron. Examination of the sample surfaces after exposure in a low-power microscope demonstrated that free boron was produced in these tests. Furthermore, surface melting was readily visible on both iridium and tungsten samples, but not on ATJ specimens.

Surface recession data are plotted in Figure 7 for iridium and Re-35Ir, although recession rates could not be calculated because the samples were brazed to the tungsten rod after exposure. The data are plotted only to indicate the temperatures at which melting occurred. It was estimated that 5, 10, and 30% of the iridium samples had melted after 5 min at 3000°, 3500°, and 4000°F, respectively. Similarly, about 5% of the Re-35Ir sample melted after 5 min at 4000°F. Surface melting was also visible on the tungsten samples exposed at 4000° and 4500°F; the decrease in calculated recession rate for tungsten at 4000° and 4500°F is probably due in part to boron uptake by the tungsten samples resulting in lower weight loss.

ATJ graphite did not indicate any surface reaction with boron. The measured recession rate was similar to the combined rate of 10 v/o BF_3 and 10 v/o H_2, both in the measured rate and its temperature dependence.

The tests in BF_3-H_2 demonstrate that free boron can cause surface melting of iridium, tungsten, and Re-Ir alloys. Unfortunately, the boron eutectic is lowest for iridium, which has the best resistance to combined fluorine-oxygen at 3000°-4400°F. Thus, boron must be considered as a corrodent equivalent to fluorine and oxygen for some materials. These tests also suggest that it is likely that free carbon would also cause melting of iridium above the Ir-C eutectic (~4000°F).

The surface recession rate of graphite in argon-hydrogen mixtures is plotted in Figure 8. Also shown is the weight loss in the absence of hydrogen resulting from mechanical
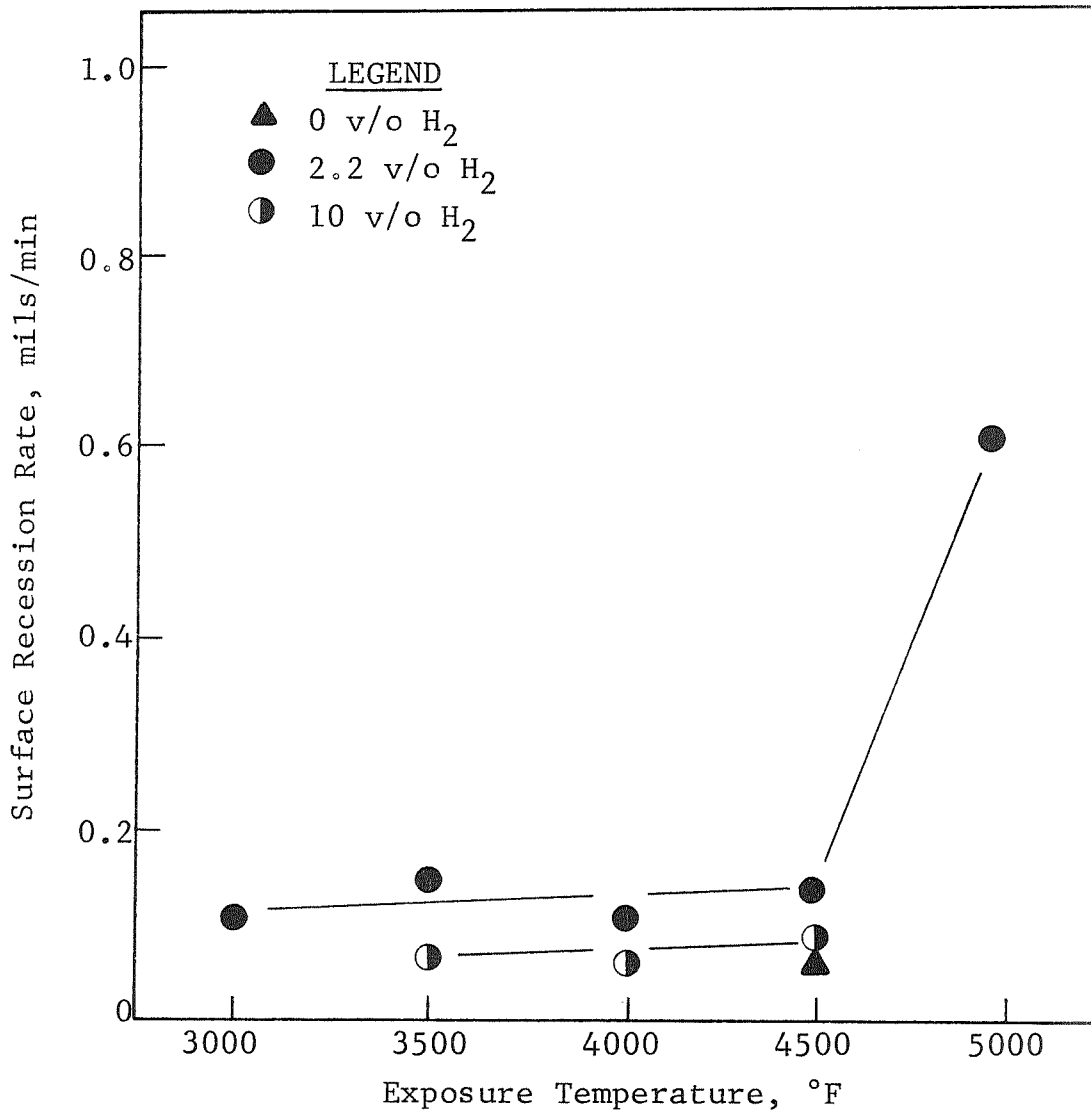
Fig. 8 - Surface Recession Rate of ATJ Graphite in
Flowing Argon and Argon-Hydrogen.

erosion of the graphite surface. It was found that the ATJ graphite samples lost 4 to 6 mg during heating in vacuum at 4000°F. Consequently, all graphite samples were vacuum outgassed prior to corrosion tests. Data in Figure 8 indicate that the recession rate of graphite in 10 v/o hydrogen was less than 0.2 mil/min below 4500°F, but increased abruptly to about 0.6 mil/min at 4900°F. Thus, the CH_2 reaction is a secondary problem below 4500°F compared to fluorine and oxygen interactions.

2.   Mechanical Property Determinations

The composites fabricated in this program were to be evaluated by thermal shock and room-temperature transverse rupture tests in addition to oxidation-corrosion tests. Transverse rupture tests were precluded because of the following:

    1.   Additional corrosion tests in boron-
          containing atmospheres were required
          which prohibited fabrication of com-
          posites.

    2.   W-Re-Ir and Re-Ir alloys could not be
          fabricated by hot rolling, as described
          in Section II-B.

    3.   The results of boron studies indicated
          that iridium-rich secondary additions
          would melt in boron-containing
          atmospheres.

The oxidation-corrosion tests in boron-containing atmospheres were substituted for mechanical property tests by contract modification.

In effect, thermal shock tests were conducted on all materials during oxidation-corrosion tests. Nominally, test samples were induction heated to the test temperature of 3500°-5500°F in 15-25 sec. Thus, the heating rates were at least 200°F/sec. At the completion of each test, the argon was left flowing after the corrodent gas or gases were stopped. This method produced gas quenched cooling to below red heat in

IIT RESEARCH INSTITUTE

about 15 sec. Each corrosion test, therefore, consisted of a complete thermal shock cycle. In no case was thermal shock cracking observed on W-Re-Ir, Re-Ir, ATJ graphite, $HfIr_3$, or $TaIr_3$ samples. Consequently, no severe thermal shock problems are anticipated with any of these materials in rocket nozzle configurations.

An attempt was made to evaluate the thermal shock characteristics of the materials evaluated in this program using the figure of merit thermal shock formation. This parameter is expressed as: [42]

$$M = \frac{K\sigma}{\alpha E}$$

where
M = index of merit
K = thermal conductivity $(Btu-in/(hr)(ft^2)(°F)$
σ = tensile strength at temperature T
α = coefficient of thermal expansion (in/in°F)
E = effective modulus at temperature T

High values of M indicated low thermal shock sensitivity.

This parameter is, of course, oversimplified and appropriate only for comparing materials in a specific test, because the test specimen configuration and the cooling rate are primary variables. The index of merit calculation is most appropriate for evaluating brittle materials, since in an actual test a fracture stress (σ) other than the tensile strength may be appropriate. For ductile materials, plastic deformation must be taken into account in evaluating a thermal shock parameter.

Obviously, thermal shock sensitivity calculated as above will be obtained in a low tensile strength, high modulus material with low conductivity and a high expansion coefficient. Since K, σ, α, and E are all temperature dependent, it is also clear that any material may exhibit a particular temperature range of maximum shock sensitivity. This means that the properties as a function of temperature must be known to establish the minimum index of merit. These data are not known for the W-Re-Ir,

Re-Ir, Ir_3Hf, and Ir_3Ta alloys investigated in this program. However, from the rolling studies described in Section III-B, thermal shock sensitivity might be expected for the Re-Ir and W-Re-Ir alloys.

Indexes of merit at room temperature calculated from data in the literature for tungsten, rhenium, and iridium are in the range of 1×10^3 to 1×10^4. Unalloyed iron and austenitic stainless steels have merit indexes in the range of 1×10^2 to 1×10^3. The refractory metals generally have higher thermal conductivity and strength and lower expansion coefficients, which offsets the higher modulus ($60-80 \times 10^6$). Thus, thermal shock problems under normal cycling conditions with tungsten, rhenium, and iridium can only be anticipated near room temperature where ductility may be limited. The Ir_3M, Re-Ir, and W-Re-Ir alloys may exhibit thermal shock failure at higher temperatures. Although the properties are not available for these alloys, it is expected that high modulus would be retained. Thermal conductivity should be lower in the alloys than in the pure metals. Both these factors and high-temperature brittleness (Section II-B) tend to increase thermal shock sensitivity. Thus, it is possible that thermal shock cracking of Ir_3M, Re-Ir, or W-Re-Ir alloys may be encountered for specific sample geometries and/or under more extreme thermal shock conditions than were applied in this program.

3. Supplemental Investigations:
   High-Temperature Melting Studies

High-temperature melting interaction of several candidate composite materials was investigated by heating material combinations of interest until melting was observed. The material combinations and the observed incipient melting temperatures are given in Table XI. Also listed are eutectic temperatures from the literature that apply to each combination.

In this work, small pieces of Ir, Re, $HfIr_3$, and $TaIr_3$ were placed on the larger (nominally 0.5 x 0.5 x 0.125 in.)

TABLE XI

MELTING TEMPERATURES

OF SEVERAL REFRACTORY MATERIAL COMBINATIONS

Material Combination	Incipient Melting Temp.,* °F	Applicable Eutectic, Temp.	
		System	°F
Iridium-Boron	2360	Ir-B	2265
Iridium/HfB$_2$	3190	Ir-B	2265
		Ir-Hf	2606
HfIr$_3$/HfB$_2$	3860	Ir-B	2265
		Ir-Hf	2606
Iridium/HfC-33 v/oC	4080	Ir-C	4177
		Ir-Hf	2606
HfIr$_3$/ATJ graphite	4200	Ir-C	4177
		Ir-Hf	2606
HfIr$_3$/HfC-33 v/o C	4150	Ir-C	4177
		Ir-Hf	2606
TaIr$_3$/ATJ graphite	4520	Ir-C	4177
		Ir-Ta	3542
TaIr$_3$/TaC-20 v/o C	4475	Ir-C	4177
		Ir-Ta	3542
Rhenium/HfC-33 v/o C	4850	Re-C	4532
		Re-Hf	3344

*Corrected temperature using emittance of 0.85 for HfC-33 v/o C, TaC-20 v/o C, ATJ graphite, and HfB$_2$.

samples of HfC-C, TaC-C, ATJ graphite, and HfB_2. The larger
samples were induction heated in the fluorine corrosion appara-
tus under an inert atmosphere of argon. Samples were held at
50°F intervals from about 3000°F to the observed melting point.
Holding times at each temperature were 5 min. The interaction
temperatures reported were observed on the larger carbide, bo-
ride, or graphite samples. In all cases, the temperature on the
top of the Ir, Re, $HfIr_3$, or $TaIr_3$ appeared to be slightly lower
than that of the larger sample. However, the interface tempera-
ture of the material pair is the important one and should have
been best represented by the temperature of the large sample.
The observed melting temperature may be slightly higher than the
equilibrium melting temperature, since the holding time at any
particular temperature was approximately 5 min. This holding
time may not be sufficient to obtain equilibrium in these high-
melting materials.

Examination of these results indicates that in the
case of Ir/HfB_2 and Re/HfC-33 v/o C the observed melting temper-
atures are somewhat higher than may be expected from literature
values of applicable eutectic temperatures. As indicated above,
this may be due to not having achieved equilibrium conditions.

In the case of Ir/HfC-33 v/o C it appears that the
Ir-C eutectic is the limiting temperature because of the free
carbon. Examination of the results in Table XI indicates rea-
sonable correlation with published values in most cases. The
melting point of 2360°F observed for the Ir-B eutectic was only
about 100°F higher than the reported value. The data for Ir-HfB_2
indicates that this combination is unstable, as expected, al-
though the observed melting point of 3190°F is considerably
above both the Ir-B and Ir-Hf eutectics. The $HfIr_3$-HfB_2 combi-
nation melted at 3860°F, which was just below the melting point
of the carbides.

Melting points obtained for $HfIr_3$ in combination with
ATJ graphite and HfC-33 v/o C were in the range of the Ir-C

IIT RESEARCH INSTITUTE

eutectic (~4100°F). On the other hand, TaIr$_3$ exhibited melting points of about 4500°F for both graphite and the carbide composite. The observed melting temperature for Re/HfC-33 v/o C was 4850°F, about 300°F higher than the reported temperature for the Re-C eutectic.

The results of interaction studies suggested that the highest melting composites would be obtained for TaIr$_3$ in combination with either ATJ graphite or TaC-graphite composites. Addition of HfIr$_3$ in a graphite or carbide matrix does not appear to provide any significant advantage in melting point over unalloyed iridium. Other systems with promise could be rhenium-rich Re-Ir alloys in the carbide materials. These systems should provide melting points above 4400°F, in the absence of boron in the combustion gas. Boron will likely cause melting of any iridium-rich second phase of a composite below 4000°F.

The melting points of W-Re-Ir alloys were determined in a similar manner to the interaction temperatures discussed in the previous section. A comparison of the observed solidus temperature of these alloys with estimated values for the W-Ir phase diagram[2] is presented in Table XII. The melting temperatures in the W-Re-Ir system are controlled by the W-Ir system, since the eutectic temperature is about 4180°F (80 w/o Ir) in the W-Ir system. The minimum melting point in the W-Re system is about 5250°F.[3]

Table XII indicates that all of the W-Re-Ir alloys prepared in this program melt above 4500°F. The variation in estimated melting temperature results from differences in reported W-Ir phase diagrams.[2] The results in Table XII tend to verify the results of Giessen, rather than those of Tylkina et al.,[2] i.e., the lower temperatures for the eutectic at ~70 w/o W (4470°F), and the peritectic reaction at 75 w/o W (4650°F). The results also indicate that the large decrease in melting points occurs in the range of 0-15 w/o Ir. Further increase in iridium concentration to 20 w/o does not cause a significant decrease in melting point.

IIT RESEARCH INSTITUTE

TABLE XII

APPROXIMATE MELTING TEMPERATURES
OF W-Re-Ir ALLOYS

Alloy Composition, w/o	Optical Pyrometer Temp., °F		Estimated Melting Temp., °F [b]
	Uncorrected	Corrected [a]	
W-15Re-10Ir	4200	4925	4725-5070
W-15Re-15Ir	4150	4875	4600-5070
W-15Re-20Ir	3820+	4500+	4470-4890
W-25Re-10Ir	4150	4875	4600-5070
W-25Re-15Ir	4000	4675	4600-4890
W-25Re-20Ir	3870+	4500+	4470-4890

[a] Temperature corrections made using an emittance of
0.35 for these alloys.

[b] From Reference 2.

A limited study of the potential of coating and/or impregnating ATJ graphite with iridium-rich alloys was conducted. ATJ graphite samples were slurry-coated with -325 mesh iridium, or iridium-rich powders, and heated in argon above 4200°F in the corrosion apparatus. The ATJ samples were outgassed in vacuum at 4200°F for 5 min prior to application of the slurry. The results of these tests are summarized in Table XIII.

All of the coatings tended to dewet after melting, producing a thin, discontinuous surface coating along with large globules of metal. In all cases, the metal was converted to a gray, shiny material. Addition of 3 and 5 w/o Hf minimized the formation of metal globules, but did not produce a coating of uniform thickness. Rhenium additions produced higher melting temperatures, as expected, but did not influence wetting significantly. The most uniform coating was obtained with unalloyed iridium heated at 4200°F, just above the Ir-C eutectic (~4100°F).

In general, no significant impregnation of the graphite was obtained. This was evident upon fracturing the coated samples and examining the fracture surface with a low-power microscope. Surface reaction was generally superficial, except beneath the metal globules where more extensive reaction with the graphite occurred. Bonding of the metallic surface material was normally excellent for all compositions. However, this technique did not appear to be a promising method of coating and/or impregnating graphite with iridium. Consequently, work on iridium-coated graphite was discontinued. Some success in plasma-arc deposition and gas pressure bonding iridium on grahpite is reported in reference 44.

4. Metallography

Selected W-Re-Ir alloys were examined metallographically in the arc-melted condition and after exposure in fluorine at 4500°F. It was expected that exposure in fluorine above 3500°F would result in the development of iridium-rich surface layers

TABLE XIII

BEHAVIOR OF IRIDIUM-RICH ALLOYS
MELTED ON ATJ GRAPHITE

Alloy Composition, w/o	Applied Alloy Thickness		Heating Condition		Comments
	mg/cm^2	mils[a]	Temp., °F	Time, min	
Iridium	240	4.3	4600	6	Extensive dewetting
Iridium	110	2.0	4600	3	Dewetting, uniform superficial metal coating.
Iridium	124	2.2	4200	3	Slight dewetting, uniform metal coating.
Ir-20Re	220	3.9	4750	3	Dewetting, superficial metal coating.
Ir-20Re	112	2.0	4600	3	Dewetting, superficial metal coating.
Ir-3Hf	182	3.5	4200	3	Some dewetting, uniform, rough metal coating.
Ir-5Hf	80	1.4	4200	3	Some dewetting, uniform, rough metal coating.

[a]Average calculated thickness of fully dense iridium.

on W-Re-Ir alloys because of selective attack of tungsten and rhenium. Metallography of exposed samples verified this hypothesis.

The microstructures of W-15Re-10Ir and W-15Re-15Ir are shown in Figure 9. Both alloys are two-phase, consisting of the pro-peritectic W-rich solid solution in a matrix of either the ϵ or σ (W-Ir) intermetallic compound. Rhenium may also be dissolved in the matrix phase; the solubility of rhenium in the W-Ir intermetallic compounds is unknown. The higher iridium alloy is somewhat more brittle as indicated by internal cracking induced by metallographic preparation (Figure 9b).

Iridium-rich surface layers developed on W-25Re-10Ir and W-15Re-15Ir by exposure in fluorine are shown in Figure 10. The layers are probably primarily Ir-Re alloys since tungsten should be selectively removed at 4500°F. No evidence of melting exists although the samples were exposed above the melting point of iridium (4450°F). This indicated that the surface layers are probably Ir-Re, rather than iridium. These surface layers result in decreasing corrosion rate with time for W-Re-Ir alloys. The layer is more dense and adherent on the W-25Re-15Ir alloy (Fig. 10b) than on the lower iridium alloy. Corrosion mechanisms of this type provide the basis for improving the oxidation-corrosion resistance of composites by additions of a corrosion-resistant second phase in a suitable matrix.

5. Discussion

a. Oxidation-Corrosion of Tungsten-Base Alloys

In addition to the oxidation-corrosion tests described in Section II-C-1, corrosion tests were also conducted in fluorine to investigate specific corrosion mechanisms. These tests included: (1) determination of the time dependence of surface recession rate of W-Re-Ir alloys, (2) measurement of the influence of impingement angle on the calculated surface recession of tungsten and ATJ graphite in argon-6.5 v/o fluorine, and (3) comparison of the surface recession rate of W-15Re-20Ir and ATJ
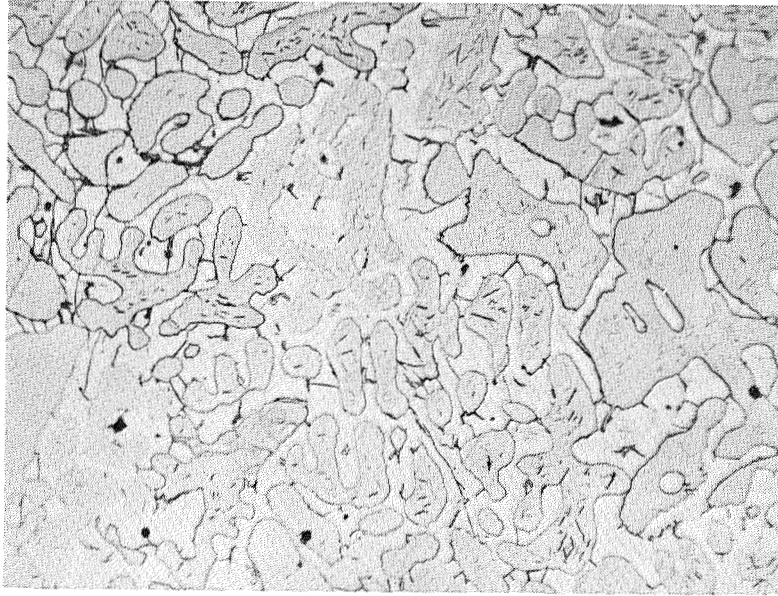
Neg. No. 37940   X200

(a) W-15Re-10Ir
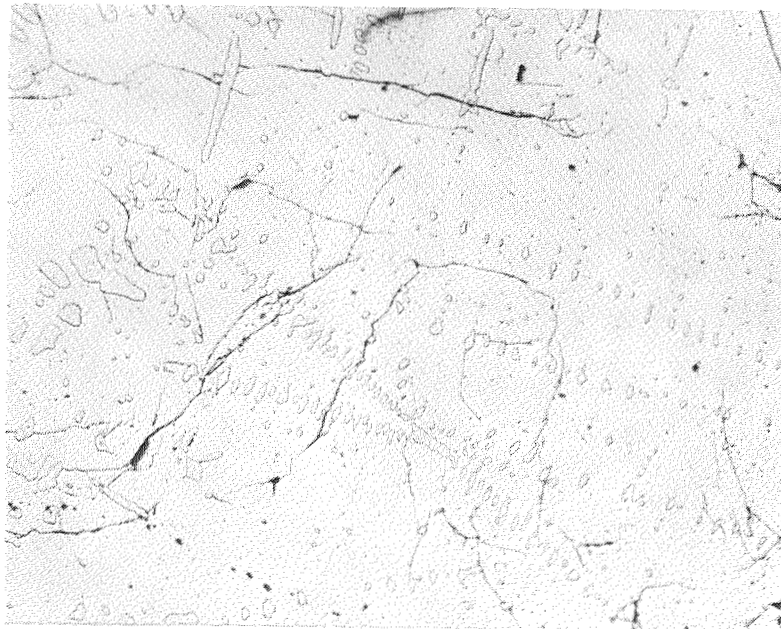
Neg. No. 37939   X200

(b) W-25Re-15Ir

Fig. 9 - Microstructure of W-Re-Ir Alloys
        As Arc-Melted.

60
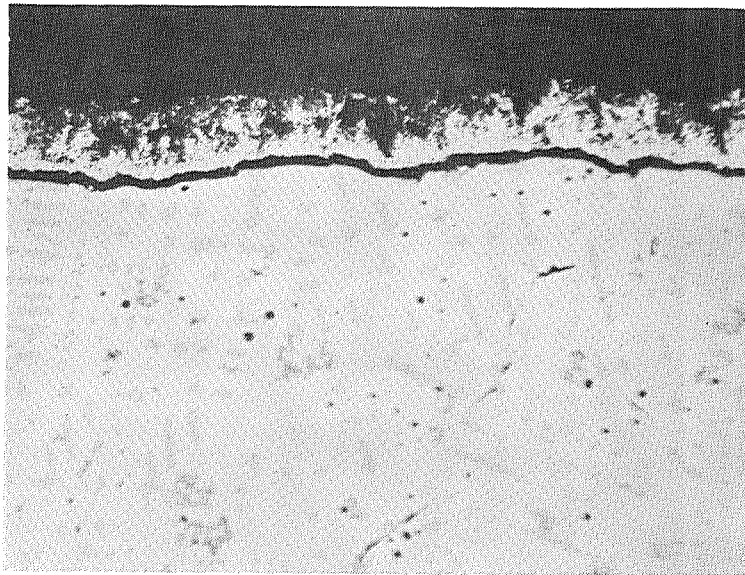
Neg. No. 37936   X200
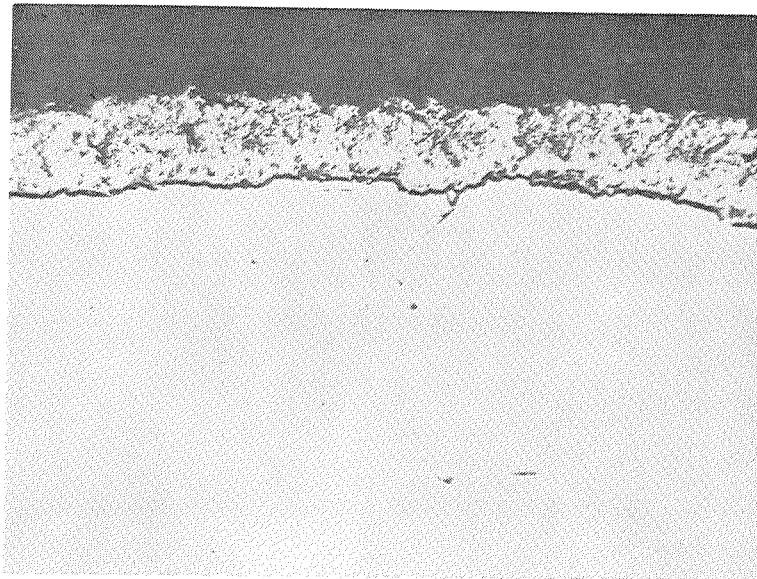
(a) W-25Re-10Ir

Neg. No. 37937   X200

(b) W-25Re-15Ir

Fig. 10 - Iridium-Rich Surface Layers Developed
on W-Re-Ir Alloys Exposed in Argon-
6.5 v/o Fluorine at 4500°F for 9 min.

IITRI-B6102-13
(Final Report)

graphite in flowing fluorine. Experimental data for these tests
are summarized in Appendix A, Tables A-IX through A-XII.

The results of metallographic examination of W-Re-Ir
alloys, described in the previous section, verified that
iridium-rich surface layers were developed on these alloys at
4000°F. Iridium-rich surface residues were expected based on
the relative corrosion rates of unalloyed tungsten, rhenium, and
iridium in fluorine. Development of these layers is kinetically
similar to the mechanism by which refractory carbon chars are
developed on ablative materials, and they can be similarly ef-
fective in decreasing the surface recession rate. However, it
was not known whether the surface material developed from alloys
containing 10-20 w/o iridium would be adherent in a high-
velocity gas stream. If iridium-rich surface layers developed
were adherent, nonlinear recession rates were expected.

Samples of W-Re-Ir alloys were exposed in argon-6.5
v/o fluorine for incremental exposure of 0.5, 0.5, 1, and 2 min.
Recession rates were calculated from the cumulative weight loss
for each period at 0.5, 1, 2, and 4 min. It was recognized that
data scatter would be high for the 0.5 min exposures. Calculat-
ed recession rates as a function of exposure time for W-Re-Ir
alloys at 4000° and 4500°F are plotted in Figures 11 and 12, re-
spectively.

All of the W-Re-Ir alloys exhibit decreasing corrosion
rate with increasing exposure time. However, the W-15Re-10Ir
and W-25Re-10Ir alloys had equivalent or higher recession rates
at 4500° than 4000°F. This was unexpected since the recession
rates of rhenium in fluorine decrease rapidly above 4000°F.
Thus, it was expected that rhenium would also contribute to any
protective layer formed at 4500°F. The corrosion data in Fig-
ures 11 and 12 suggest that this did not occur.

Surface recession rates for the W-15Re-15Ir and W-
25Re-15Ir alloys were generally comparable within the data scat-
ter at 4000° and 4500°F. On the other hand, the two alloys with

IIT RESEARCH INSTITUTE
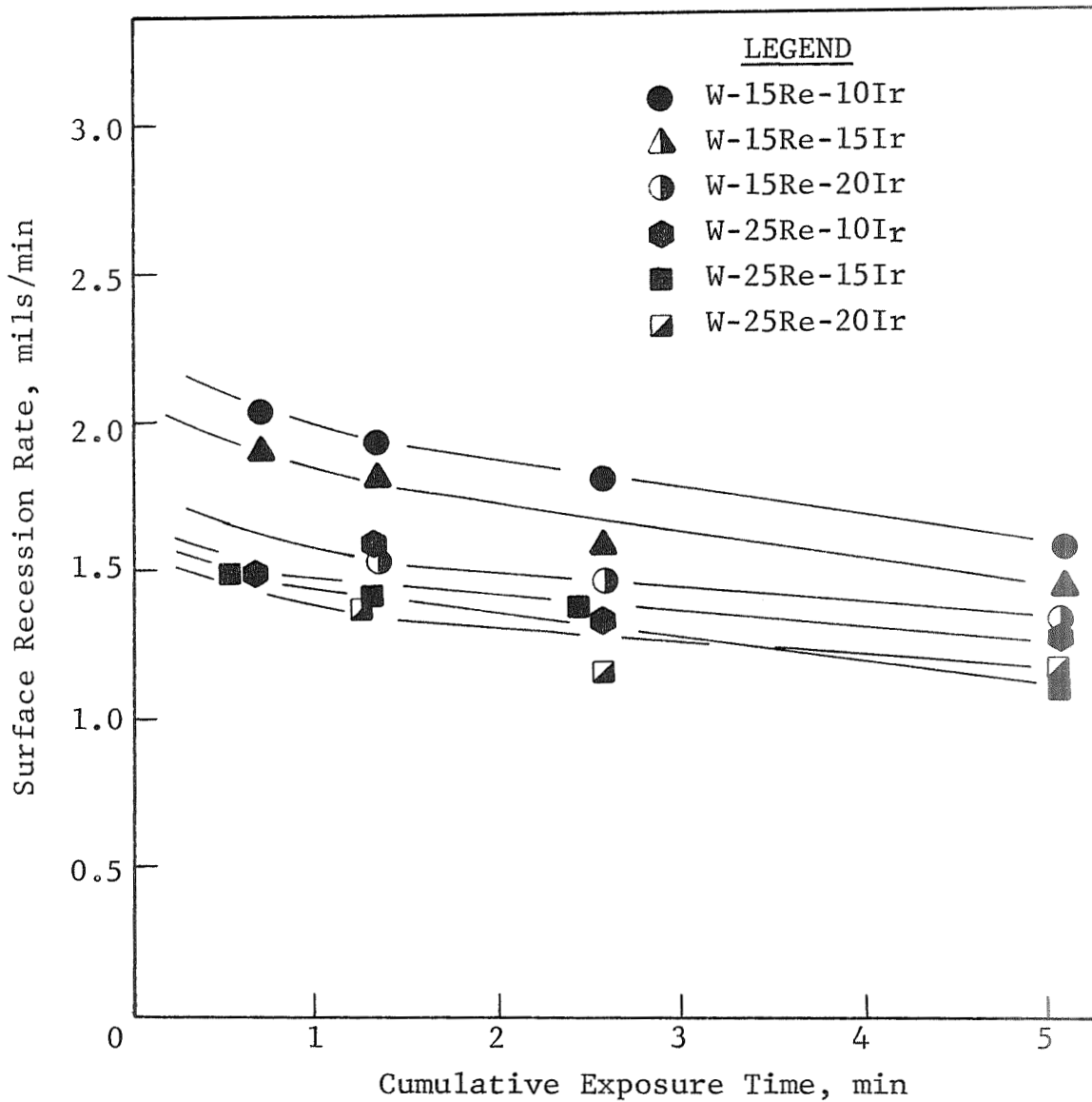
Fig. 11 - Effect of Exposure Time on the Surface Recession Rate of W-Re-Ir Alloys in Argon-6.5 v/o Fluorine at 4000°F.

IITRI-B6102-13
(Final Report)
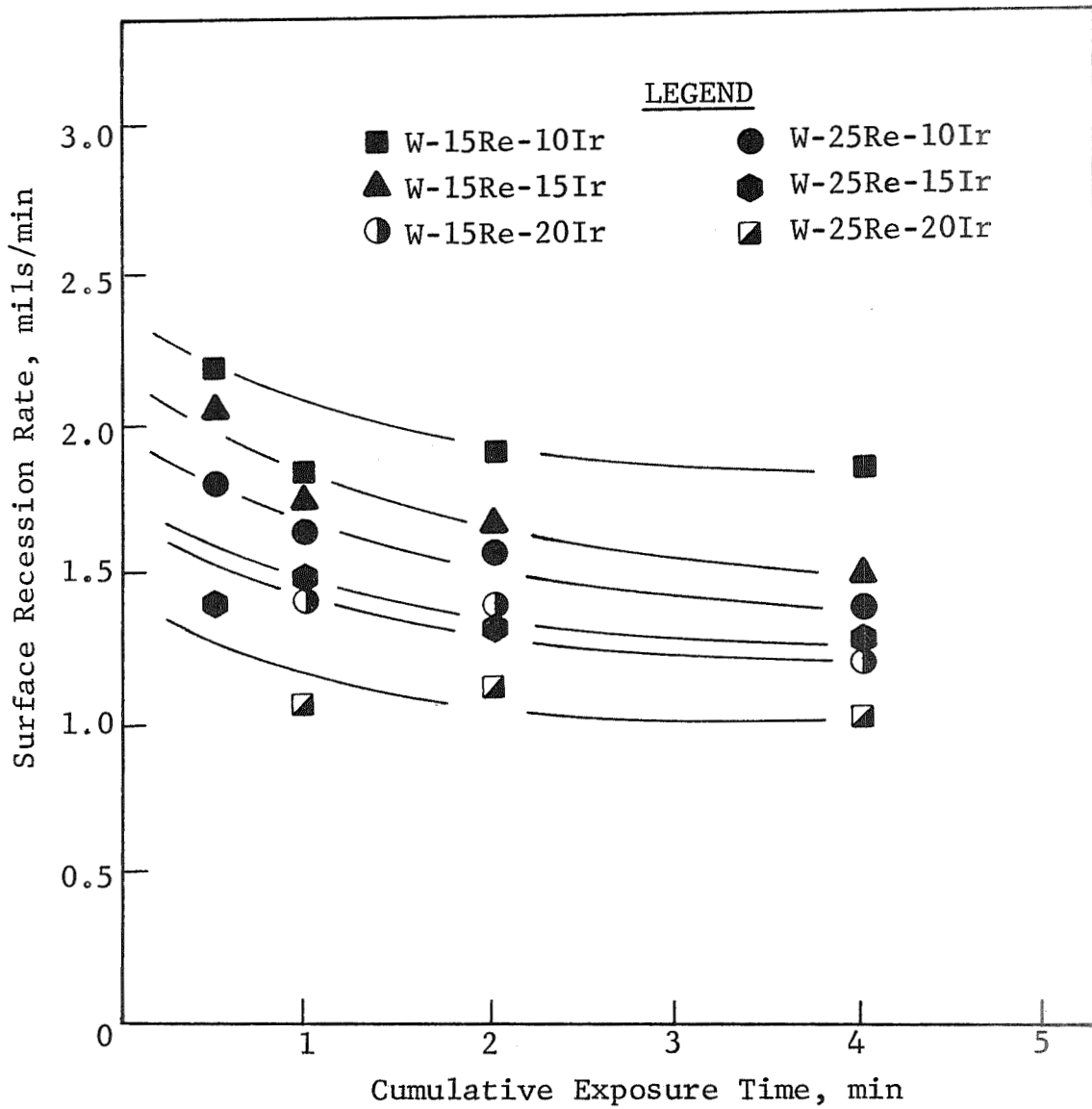
Fig. 12 - Effect of Exposure Time on the Surface Recession Rate of W-Re-Ir Alloys in Flowing Argon-6.5 v/o Fluorine at 4500°F.

20 w/o iridium exhibited lower recession rates at 4500°F than at 4000°F, particularly for the W-25Re-20Ir alloys. These results suggest that the measured difference in time-dependent corrosion rates for the various alloys was due to the development of iridium-rich surface layers. At 10 w/o iridium, the surface layer formed was not sufficiently dense and/or uniform to be protective. Melting of the iridium-rich layer did not occur at 4500°F, 50° above the melting point of iridium (4450°F). The results illustrate that adherent layers with reasonably high density were obtained only at 15 and 20 w/o iridium. This is consistent with the microstructures shown in Figure 10. The absence of melting at 4500°F was probably due to the presence of rhenium, which increased the melting point of the iridium-rich layer. Thus, protective iridium-rich surface films can be developed in situ on W-Re-Ir alloys in fluorine, and probably in fluorine-oxygen.

The apparent tendency toward nonadherence and low density of surface layers developed on W-Re-Ir alloys at low iridium concentration does not mean that some reduction in recession is not obtained in these alloys. The initial oxidation-corrosion rates ($t \cong 0$) can be estimated by assuming that the total recession is the sum of the individual recession rates for the constituents of the alloys:

$$R_t = R_a \text{ (v/o a)} + R_b \text{ (v/o b)} + R_c \text{ (v/o c)} \ldots R_i \text{ (v/o i)}$$

where R_t = total recession

R_i = recession of the individual constituents

v/o i = volume fraction of the individual constituents.

In W-Re-Ir alloys, the volume fraction is about equivalent to the concentration in weight percent.

The initial surface recession rates calculated as above for the W-15Re-10Ir alloy at 4000° and 4500°F are about 2.1 and 4.9 mils/min in 6.5 v/o F_2 and 6.5 v/o F_2-5.4 v/o O_2, respectively. The corresponding zero time recession rates for

the W-25Re-20Ir alloy are 1.8 and 4.2 mils/min. Comparison with the data in Tables A-I and A-II (Appendix A) shows that the 5 min average recession rate is about 15% less than the initial rate for the W-15Re-10Ir in fluorine and about 25% less in fluorine-oxygen. In the W-25Re-20Ir alloy, the reduction in the metal recession rates is the range of 35% for both atmospheres.

Although the highest reduction is obtained for the higher iridium alloy, an appreciable change is also obtained for the W-15Re-10Ir alloy, particularly in the most aggressive atmosphere (F_2-O_2). It is also interesting to notice that the calculated initial rate is approximated by the 30 sec rate for the W-15Re-10Ir alloy (Figure 11 and 12). On the other hand, the higher iridium alloy is nearly at the average rate after only 1 min of exposure in fluorine. These results indicate that changes in surface composition do decrease the recession rates, even for the low iridium alloys.

The influence of iridium and rhenium additions in tungsten alloys is best illustrated by the plot of recession rate in 6.5 v/o fluorine vs. Ir + Re concentration in Figure 13. This plot is based on continuous 5 min exposures from the data in Table A-I (Appendix A). From the previous discussion, the plotted surface recession rates are clearly the average recession rate in 6.5 v/o fluorine as a linear function of the Ir + Re concentration at 3500°-4500°F.

A similar plot of the surface recession rate vs. concentration of W-Re-Ir alloys in argon-6.5 v/o fluorine-5.4 v/o oxygen is shown in Figure 14. Here, the recession rate is generally independent of the rhenium concentration, depending only on the iridium concentration. The only exceptions were the W-15Re-20Ir alloys at 4500°F, which had higher recession at 3500°F than the W-25Re base alloys. Rhenium has no influence in fluorine-oxygen because the recession rates of rhenium and tungsten in oxygen are approximately equal.[1] In both 6.5 v/o
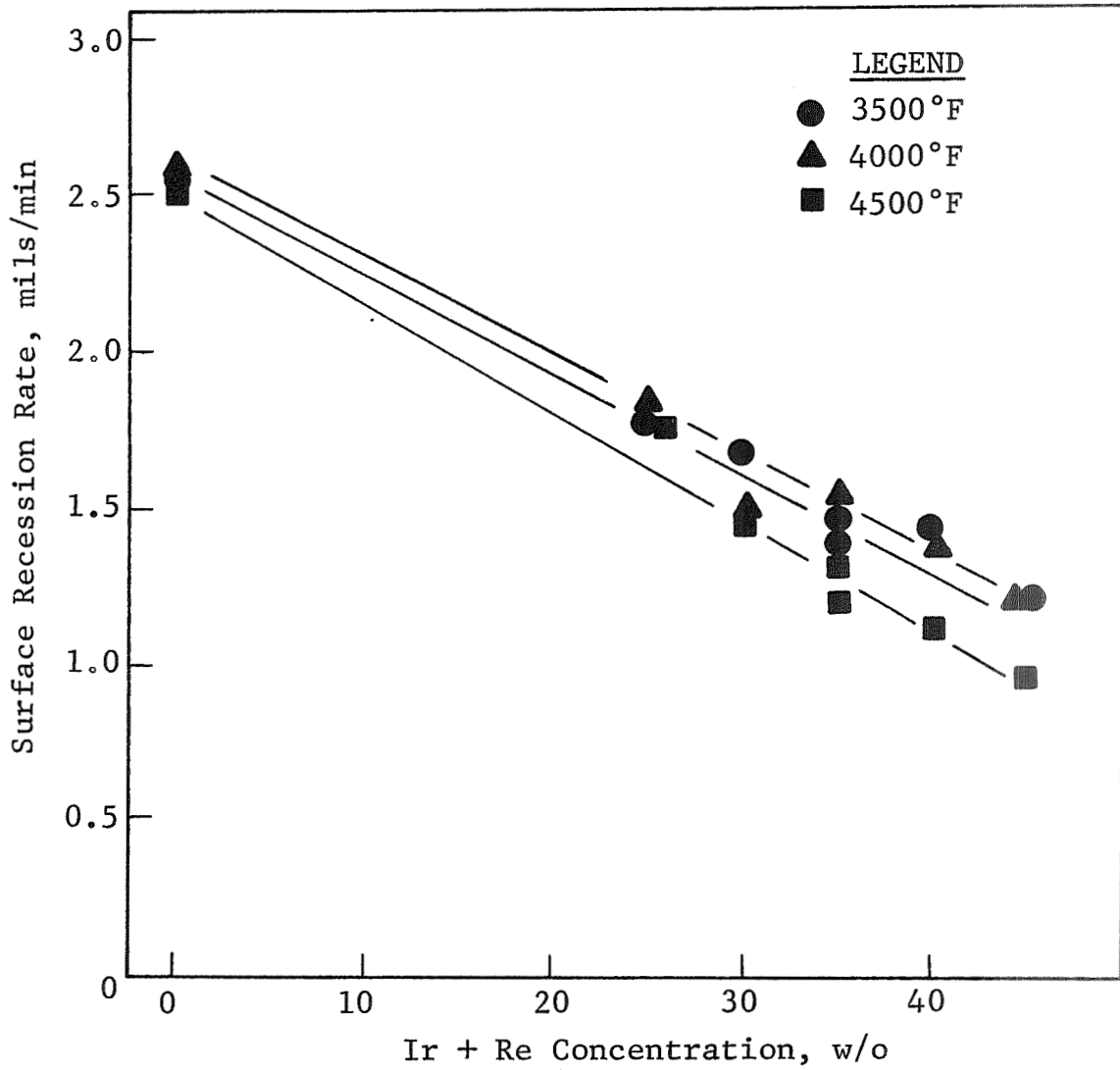
Fig. 13 - Effect of Ir + Re Concentration on the
Surface Recession Rate of W-Re-Ir Alloys
in Flowing Argon-6.5 v/o Fluorine.
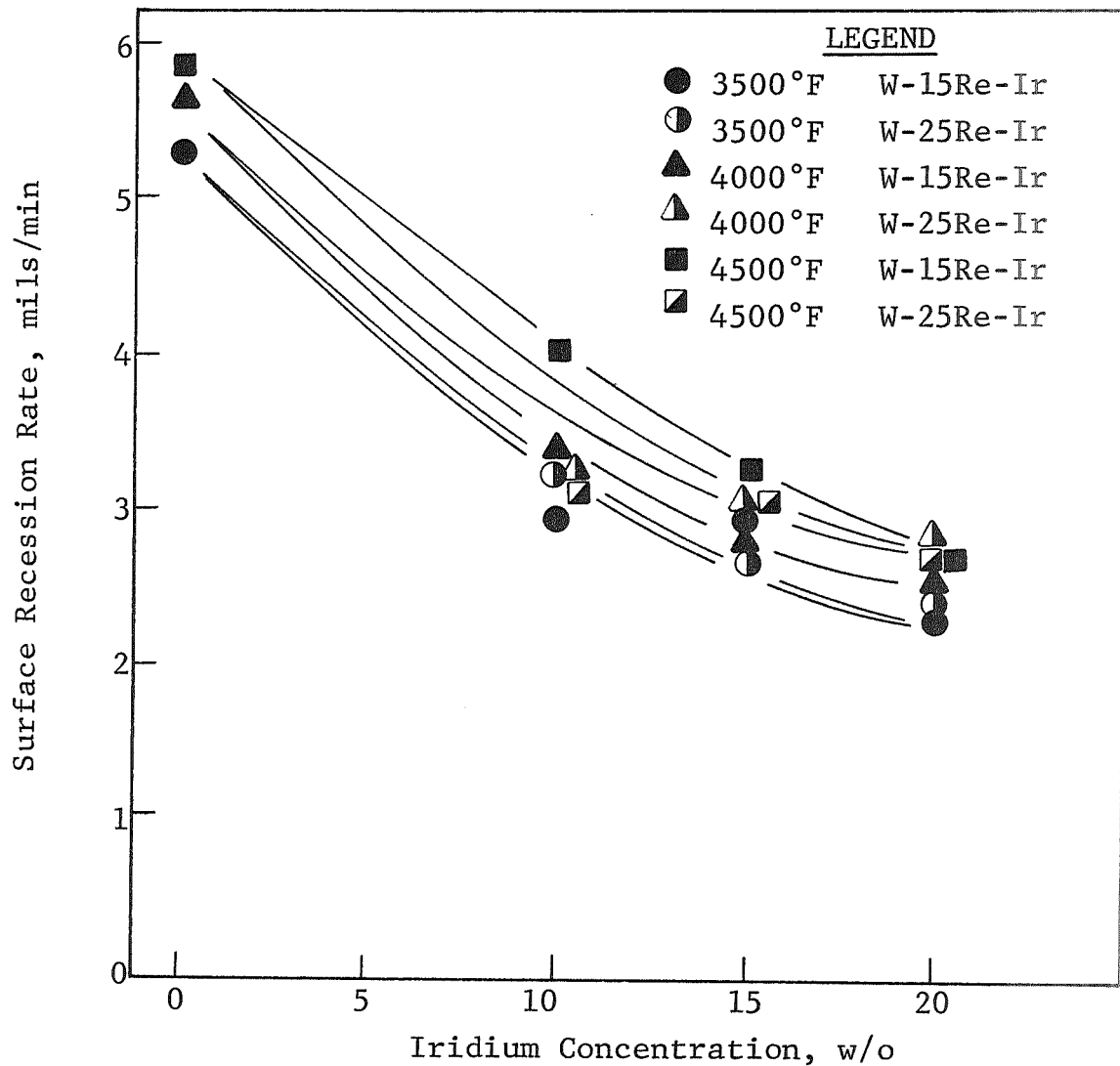
Fig. 14 - Effect of Iridium Concentration on the
Surface Recession Rate of W-Re-Ir Alloys
in Flowing Argon-6.5 v/o Fluorine-5.4 v/o
Oxygen.

IITRI-B6102-13
                                        (Final Report)

fluorine and 6.5 v/o fluorine-5.4 v/o oxygen, W-15Re-20Ir and W-25Re-20Ir had recession rates at least a factor of two less than unalloyed tungsten for 5 min exposures. The time dependence of the recession rates demonstrated for W-Re-Ir alloys indicated that the total surface recession for the ternary alloys would be even less for longer exposures than would be predicted by the 5 min data.

The previous discussion indicates that addition of iridium-rich phases in a suitable refractory matrix as a means of developing oxidation-corrosion resistance in composites for fluorine-oxygen-boron is questionable. Although protective surface layers can be developed, the concentration of iridium-rich phase necessary to provide protection in a variety of materials has not been defined. In the W-Re-Ir alloys, the iridium-rich phase was the matrix and not the dispersed phase. In composites, the iridium-rich addition will obviously be the dispersed phase. This difference could modify the concentration of iridium-rich addition required to obtain adherence of the surface layer. It is likely that a higher concentration of iridium will be required in the composites than was shown to be required in W-Re-Ir alloys. For this reason, the dispersed second phase should be as fine as possible within the constraints of the fabrication technique. Although a large concentration of boron in the exhaust atmosphere will be deleterious, a small boron concentration could, in fact, be beneficial. Boron could aid uniform distribution of iridium-rich material over the surface by superficial melting.

b.   Gas-Solid Reactions

All oxidation-corrosion tests described in Section II-C-1 were conducted with a gas impingement angle of 45°. The impingement angle in a rocket nozzle will generally be considerably less than 45°, except at the throat inlet where angles approaching 45° can prevail. Accordingly, a limited number of tests were conducted on ATJ graphite and tungsten in argon-6.5 v/o fluorine

IIT RESEARCH INSTITUTE

IITRI-B6102-13
(Final Report)

at impingement angles of 30° and 90° from the horizontal. The results of these tests are plotted in Figure 15 and summarized in Tables A-X and A-XI (Appendix A). Data obtained previously for a 45° impingement angle are included in Tables A-X and A-XI.

Figure 15 indicates that the recession rates of ATJ graphite at all temperatures and of tungsten at 5500°F increase linearly with the impingement angle. The slope of the curve is similar for all of these tests. At 3500° and 4500°F, tungsten exhibits a departure from linearity at low angles. For tungsten at 4000°F and 4500°F the 30° impingement angle produced about 20% decrease in recession rate compared to the 45° impingement angle. In all other tests, the decrease in recession was about 10% less at 30°. These results do indicate that the measured recession rates are a function of impingement angle, but the effect is relatively small at the low impingement angles that prevail in rocket nozzles.

The recession rates of ATJ graphite and W-15Re-20Ir in 100% fluorine were measured at 3000° and 4000°F. It was not possible, because of the limitation of the fluorine flowmeter, to conduct these tests at a total flow rate of 10 cfh. Accordingly, these tests were conducted at a total flow rate of 0.65 cfh--the mass flow rate of fluorine used for argon-6.5 v/o fluorine tests. The results are summarized in Table A-XII (Appendix A). Data for argon-6.5 v/o fluorine are included for comparison.

Calculated recession rates in 100% fluorine were approximately double those in argon-6.5% fluorine. This was the result of two factors: (1) an increase in the dwell time of fluorine molecules on the surface and (2) very localized attack causing extensive "cratering" of the test samples. Cratering results in an increase in the effective sample surface area of the specimen, whereas the slower flow rate increases the probability of reaction.

Also shown in Table A-XI is a calculated parameter defined as the utilization factor. This is an empirical parameter

IIT RESEARCH INSTITUTE
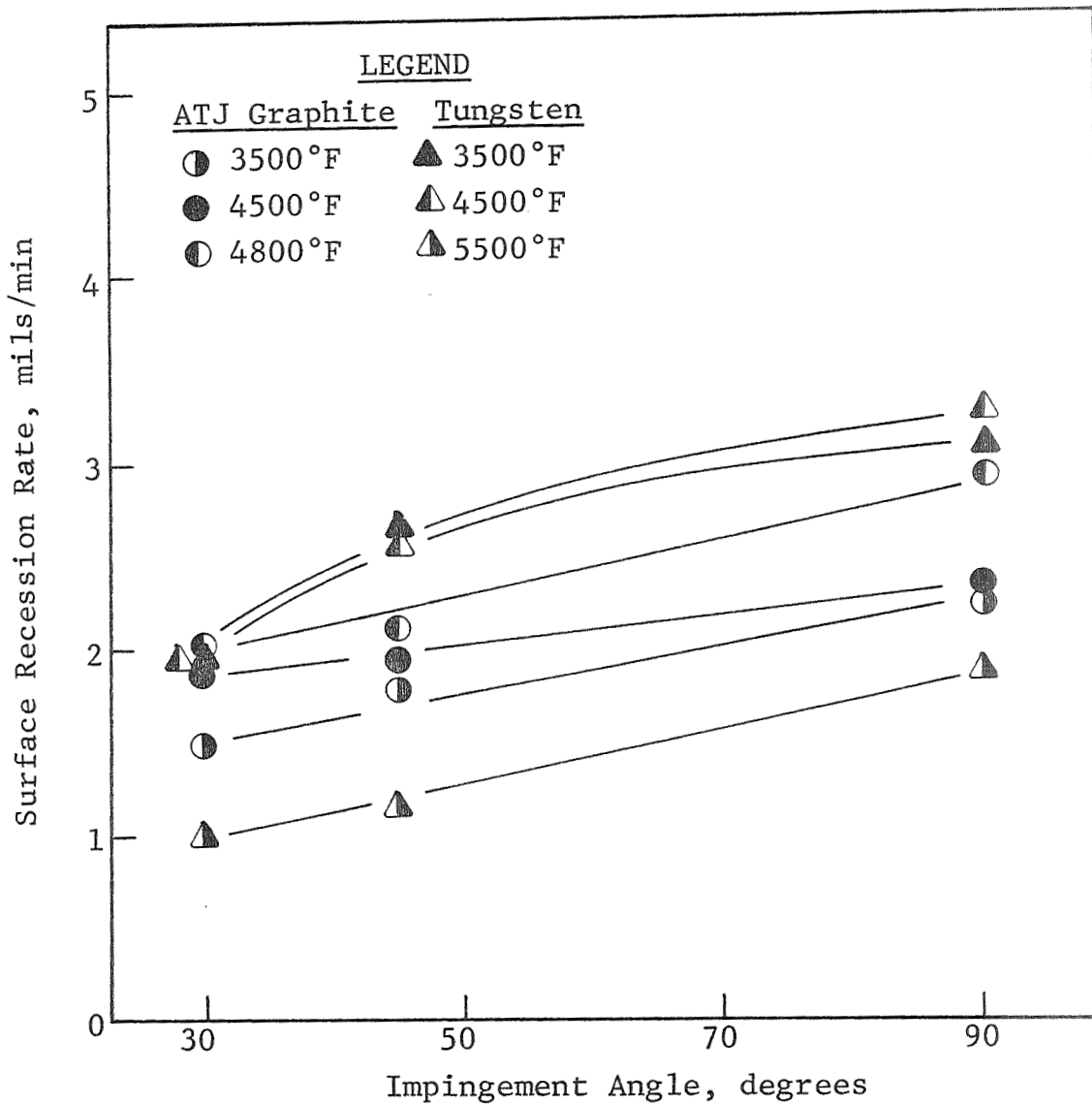
Fig. 15 - Effect of Impingement Angle on the Surface
Recession Rate of ATJ Graphite and Tung-
sten in Flowing Argon-6.5 v/o Fluorine.

IITRI-B6102-13
          (Final Report)

indicating the fraction of the fluorine flow that is consumed by reaction with tungsten. The utilization factor can be readily derived from the total flow as follows:

$$F_t = F_B + F_i \tag{1}$$

where F_t = total mass flow rate of corrodent

F_B = mass flow bypassing the specimen

F_i = mass flow impinging on the specimen.

Since there is no reason to assume that all of the fluorine that impinges on the test specimen reacts, Equation 1 should be written more generally as:

$$F_t = F_B + KF_i + (1 - K)F_i \tag{2}$$

where K has values from 0 to 1. The third term on the right side of Equation 2 is that portion of the total flow that impinges on the specimen without reaction.

Since the mass flow that bypasses the specimen is indistinguishable from that which impinges without reaction, Equation 2 can be rewritten as:

$$F_t = F'_B + KF_i \tag{3}$$

where $F'_B = F_B + (1 - K)F_i$.

Dividing Equation 3 by F_t and rearranging,

$$\frac{KF_i}{F_t} = \frac{F_t - F'_B}{F_t} = UF \tag{4}$$

or

$$F_t UF = KF_i \tag{5}$$

where UF is defined as the <u>utilization factor</u>. Clearly UF, like K, can only have values of 0 to 1. If UF = 0, no reaction occurs; and if UF = 1, all of the corrodent gas reacts with the test sample.

Obviously, Equation 5 could be rewritten directly as $F_t UF = F_r$, where F_r is the flow rate of gas that does react.

IIT RESEARCH INSTITUTE

However, it is written as shown to demonstrate that UF is determined by a factor controlled by the reaction kinetics (K), and a factor related to the geometry of the test (since $F_i = F_t - F_B$). Generally, the geometric relationship is controlled by F_B. Furthermore, F_B should be a minimum for gas impingement angles normal to the test specimen surface and should increase with increasing angle from the normal.

The term KF_i probably has both geometric and kinetic terms in the coefficient. It is, in fact, similar to the "sticking coefficient" often used in low flow rate kinetic calculations to account for reactant molecules which come in contact but do not react. A geometric factor is also usually incorporated in the "sticking coefficient" to account for the angle of impingement of the reactants (probability of reaction). Here, an additional term involved in K, related to the dwell time of gas molecules in contact with the surface, may also be important because of the high flow rates.

The usefulness of Equation 5 is that only F_t is known during experimentation. If UF is known, the weight of solid removed per unit time can be written as:

$$M_R = (F_t UF)(M_F)(M_S),\qquad (6)$$

where M_R = weight of solid removed per unit time

M_F = molar ratio of solid to gas in the reaction

M_S = molecular weight of the solid.

In terms of linear recession, Equation 6 is:

$$R = \frac{(F_t UF)(M_F)(M_S)}{AC}\qquad (7)$$

where R = linear recession rate

A = area of specimen

C = conversion factor to obtain linear rates.

Since F_t, A, and M_S are known for any test, UF can be calculated from experimental recession rate data if the

IIT RESEARCH INSTITUTE

stoichiometry of the reaction (M_F) is known. The term M_F is, of course, subject to change with temperature, depending upon the stability range and number of reaction products. Furthermore, it does not necessarily predict the stoichiometry of the reaction product which is desorbed from the surface. Rather, it defines the stoichiometry (or average stoichiometry) of the reaction products formed without distinguishing whether the final product is obtained at the surface or in the gas stream after desorption. For example, the product leaving the surface may be MF_2, but reaction in the adjacent gas stream results in a MF_6 product. In this case, the utilization factor is obviously determined only by the final reaction product, since it is a measure of the total reactant gas consumed in the reaction.

In order to make the UF calculation, the stoichiometry of the reaction products must be known or assumed. It was shown by Hill,[1] that the reaction product of tungsten in fluorine at 3000°-5800°F is likely WF_6. The decrease in recession rate of tungsten above 5000°F was shown to be the result of thermal decomposition of the WF_6 molecule. Utilization factors shown in Table A-IX, therefore, were calculated assuming that the WF_2 reaction product is WF_6.

As previously stated, UF is an empirical parameter determined by both the mechanism and kinetics of the gas-metal reaction, and a geometric factor associated with the test method. Clearly, the variation in recession rate with impingement angle is controlled by the geometric factor. There is no reason to assume any variation in reaction product stoichiometry with impingement angle. The data in Table A-XI indicate that about 30% of the fluorine reacts with the tungsten sample at a 30° impingement angle. Utilization factors for tungsten in 6.5 v/o fluorine at 45° and 90° are about 0.4 and 0.5, respectively. This should be expected, since the fraction of the gas stream bypassing the specimen (F_B) should increase with decreasing impingement angle.

The significance of the utilization factor is shown in a comparison of experimental measurements and recession rates calculated from Equation 7 for tungsten in flowing 2.5, 6.5, and 10 v/o fluorine in Figure 16. Calculated rates were obtained based on a UF of 0.4 and WF_6 reaction product (W + $3F_2 \rightarrow WF_6$; M_F = 1/3). The utilization factor was obtained from the experimental rate of tungsten in 6.5 v/o fluorine; the fluorine flow rate for tests in 6.5 v/o fluorine was 1.37×10^{-2} gram-moles/min.

Figure 16 indicates that excellent agreement is obtained for all three atmospheres to about 4500°F. Departure from the calculated rates occurs above 4500°F because of thermal decomposition of the WF_6 molecule above 5000°F.[1] The excellent agreement shown in Figure 16 is not surprising since it merely suggests that WF_6 is the most stable reaction product and the value of K in Equation 5 remains constant in atmospheres containing 2.5-10% fluorine. This means that the recession rate is directly proportional to the fluorine mass flow rate. Hill showed that this was true for the WF_2 reaction at 4000°F for atmospheres containing 2.5 to 26 v/o fluorine and flow rates from 2.5 to 12.5 cfh (100-500 fps).[27]

While the results shown for the WF_2 reactions are not unexpected, correlation of experimental rates with calculated rates for other materials using the utilization factor of 0.4 developed for tungsten cannot be expected. These comparisons for ATJ graphite, iridium, and rhenium are shown in Figure 17. Again, excellent correlation is obtained for rhenium at 2500°-3500°F and for iridium at 2500°F in argon-6.5 v/o fluorine for a MF_6 reaction product. As for tungsten, the correlation breaks down when the reaction product molecule becomes thermally unstable. Thus, it appears that the stable reaction product for both iridium and rhenium is the hexafluoride. Furthermore, the value of K (Equation 5) is independent of the solid, at least for the three metals, which suggests that UF cannot exceed 0.4. It is possible that the reaction product, for example, might be MF_3;
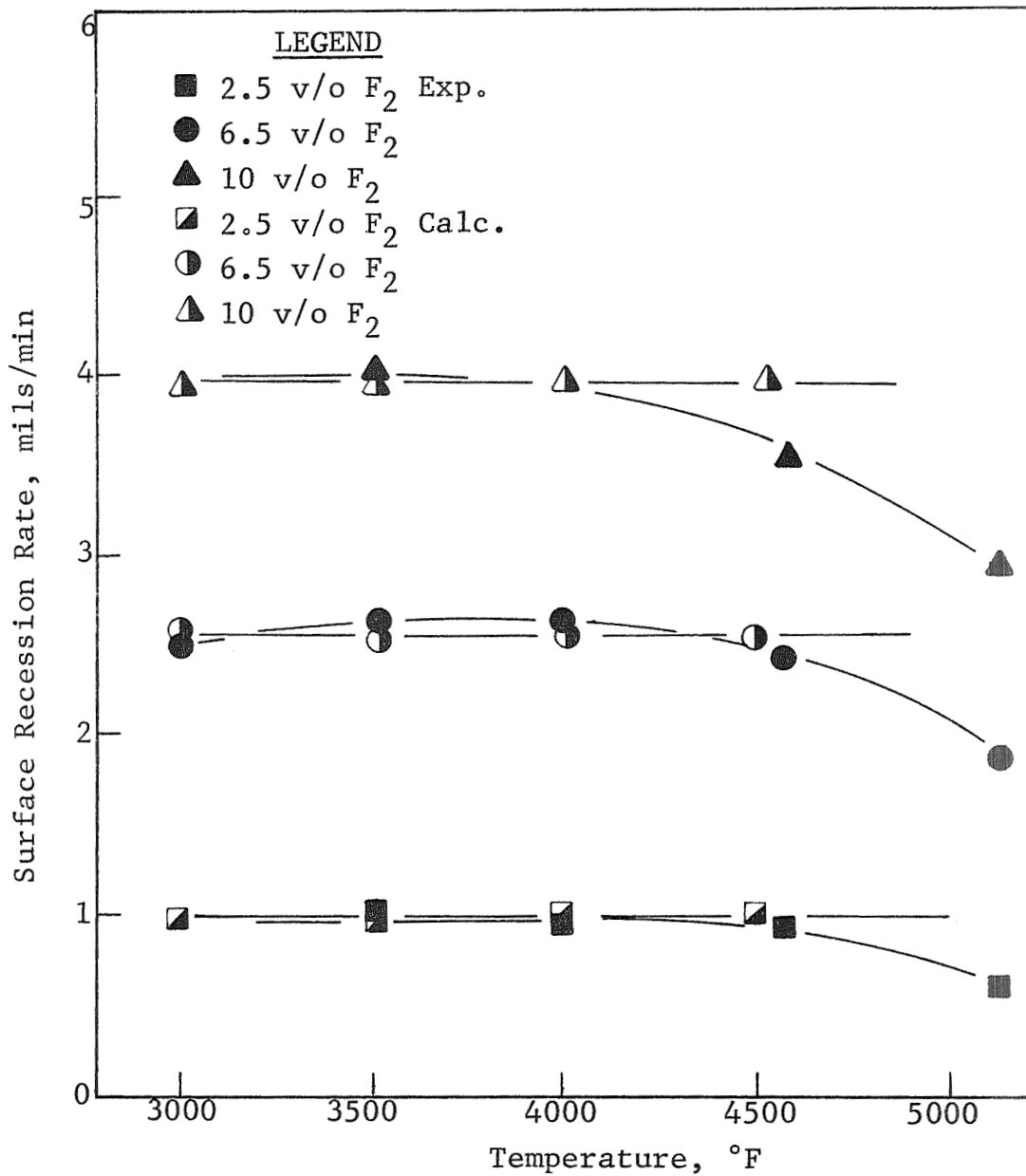
Fig. 16 - Comparison of Experimental and Calculated
Recession Rates of Tungsten in Flowing
Fluorine for UF = 0.4.

IITRI-B6102-13
(Final Report)
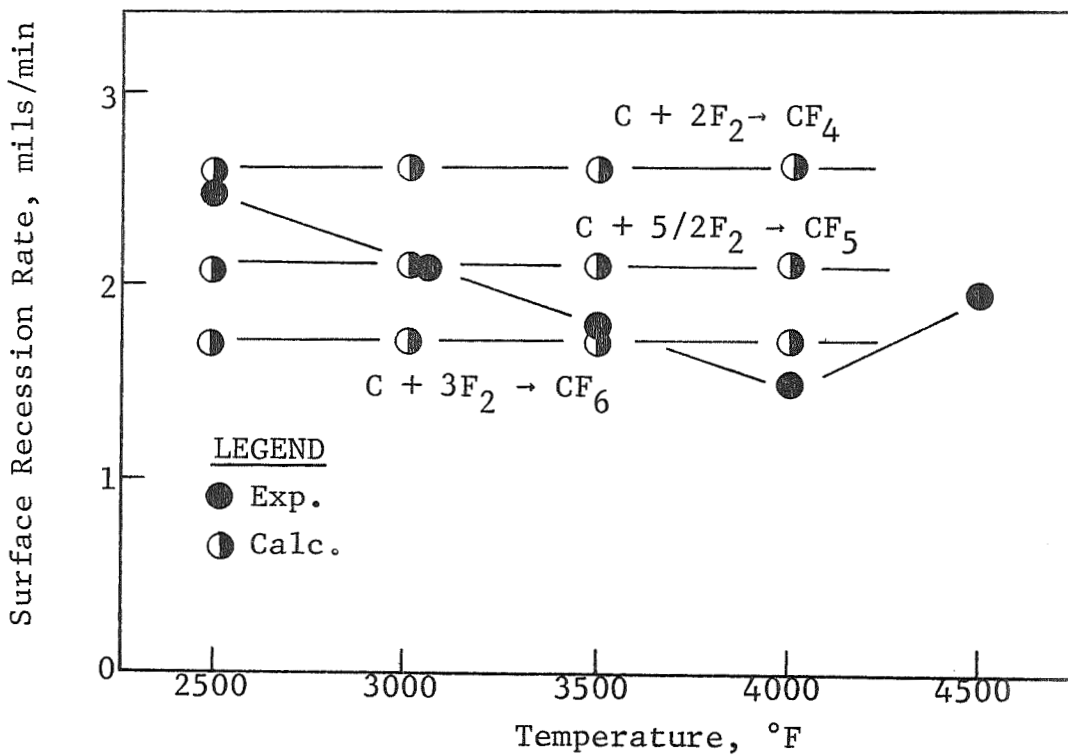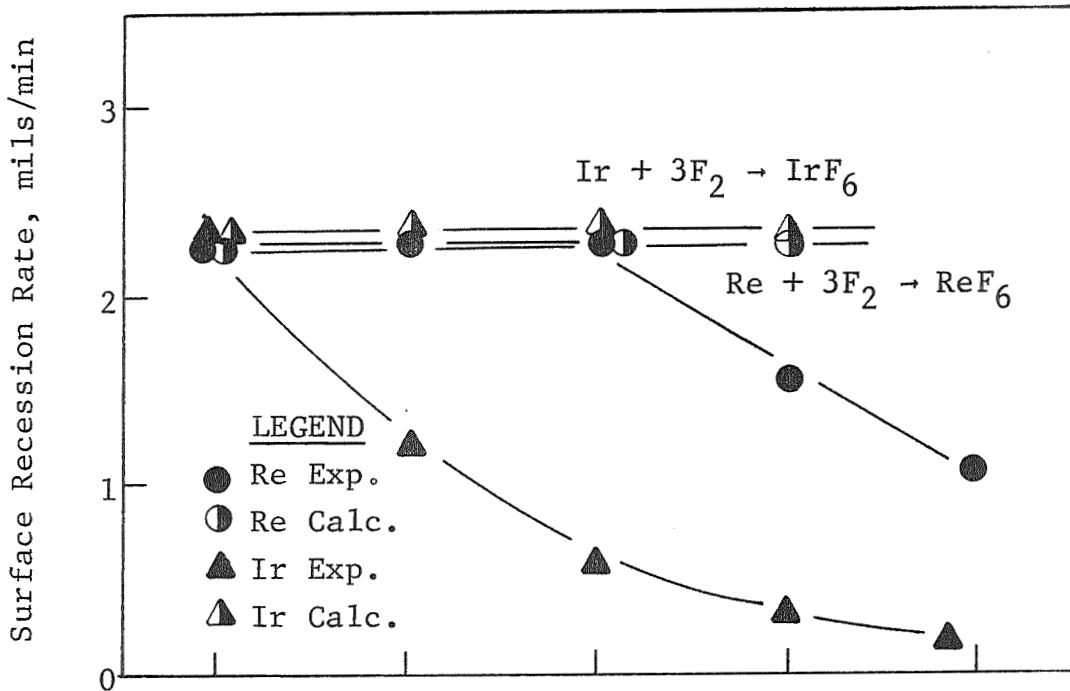
Fig. 17 - Comparison of Experimental and Calculated Recession Rates of Iridium, Rhenium, and ATJ Graphite in Flowing Fluorine for UF = 0.4.

the utilization factor would then be 0.2. It is unlikely that variation in both M_F and UF would result in the excellent correlation obtained for rhenium and iridium.

The lower plot in Figure 17 shows the experimental recession rate of ATJ graphite vs. calculated rates based on several possible reactions assuming UF = 0.4. Experimentally, ATJ graphite decreases in recession rate at 2500°-4000°F, followed by a rate which increases with increasing temperature.[1] For the assumed utilization factor, the average reaction product at 2500°F is approximately that of the tetrafluoride. The decrease in rate at 2500°-4000°F is apparently due to thermal instability of CF_4, or higher carbon fluorides. Increasing recession rate with temperature above 4000°F appears to be associated with a different stable product, possibly CF_5 or CF_6.

The plot for ATJ graphite does point out some interesting conclusions regarding variation in recession rate with temperature. At a constant corrodent flow rate (constant F_i) recession rates will decrease with increasing temperature only if: (1) the major reaction product becomes unstable, or (2) a product having a higher fluorine concentration becomes stable. On the other hand, an increase in the shape of the recession rate curve, without an inversion as shown for ATJ graphite, indicates the emergence of a stable reaction product with a lower fluorine concentration. These conclusions are based on the assumption that K (Equation 5) should not decrease with temperature for a stable product. In fact, the converse should be true, since K is dependent on the rate of reaction and reaction rates generally increase with increasing temperature. Finally, the stoichiometry of the reaction, such as that shown in Figure 17 for ATJ graphite, cannot be determined from the utilization factor calculations.

The utilization factor concept appears to work reasonably well for fluorine corrosion of some pure materials. Furthermore, the maximum value of UF in Equation 5 appears to be independent of substrate material. It could, therefore, also be

independent of the corrodent gas. The use of UF to compare calculated and experimental oxidation rates of tungsten, ATJ graphite, and rhenium is shown in Figures 18 through 20.

Figure 18 shows the experimental oxidation rate of tungsten in argon containing 3.25, 4.0, and 5.4 v/o O_2 at a 400 fps flow rate.[1] The recession rates in all three atmospheres increase with temperature at 3000°-4000°F, but approach a constant rate at 4000°-5000°F. Thus, tungsten in oxygen at 4000°-5000°F behaves similar to tungsten in fluorine at 3000°-4500°F. It is generally recognized that the reaction product of W-O_2 reaction is very nearly WO_3.[42] The calculated rate in 5.4 v/o O_2 at UF = 0.4 is slightly higher than the experimental rate at 4000°-5000°F. Correlation is obtained with the experimental rates in 5.4 v/o O_2 at 5000°F for UF = 0.36. Again, excellent correlation is obtained for 3.25 and 4.0 v/o O_2 at UF = 0.36 in the temperature range of 4000°-4500°F, i.e., UF is constant for atmospheres containing at least 3.25 to 5.4 v/o O_2. The results in Figure 18 indicate that UF approaches a constant value at lower temperatures as the oxygen concentration decreases; UF is essentially constant over the range of 3500°-5000°F in 3.2 v/o O_2, whereas it approaches a constant value only above 4500°F for the 5.4 v/o O_2 atmosphere. Thus, correlation of calculated rates and experimental rates should also be obtained at oxygen concentration less than 3.25 v/o, within the range that WO_3 is the reaction product.

The plot of oxidation rates for ATJ graphite in Figure 19 illustrates a condition in which more than one well-defined reaction product is possible. Both CO and CO_2 are possible reaction products, although CO is the more stable product at very high temperatures. Obviously, formation of CO will be fostered by low oxygen flow rates and high exposure temperatures. Figure 19 shows that the experimental rates lie between the calculated rates for CO and CO_2 reaction products for UF = 0.4, as expected. Experimental data scatter is high in 4.0 v/o O_2.[1] However, in
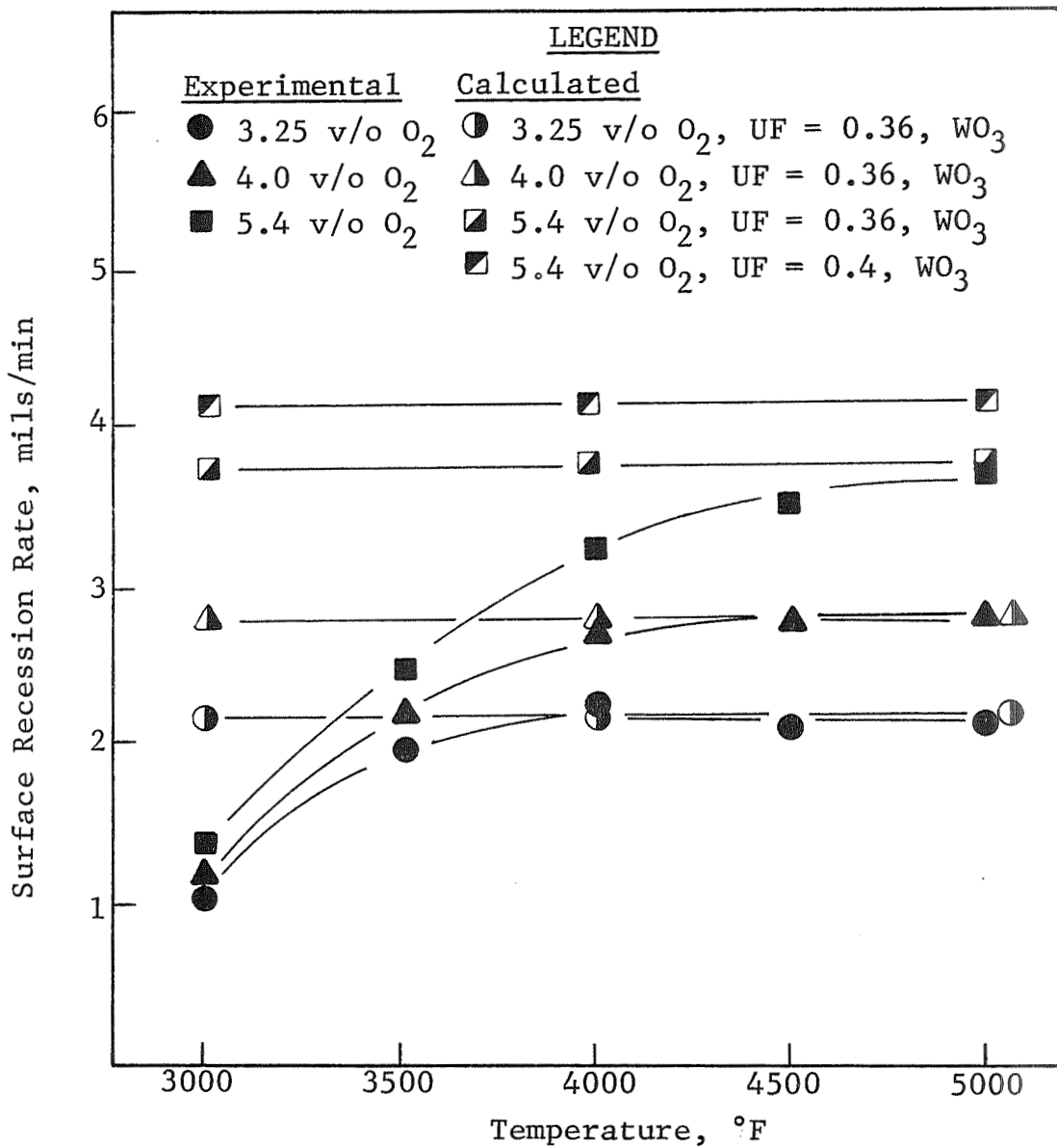
Fig. 18 - Comparison of Experimental and Calculated
Recession Rates of Tungsten in Flowing
Oxygen.

IITRI-B6102-13
(Final Report)
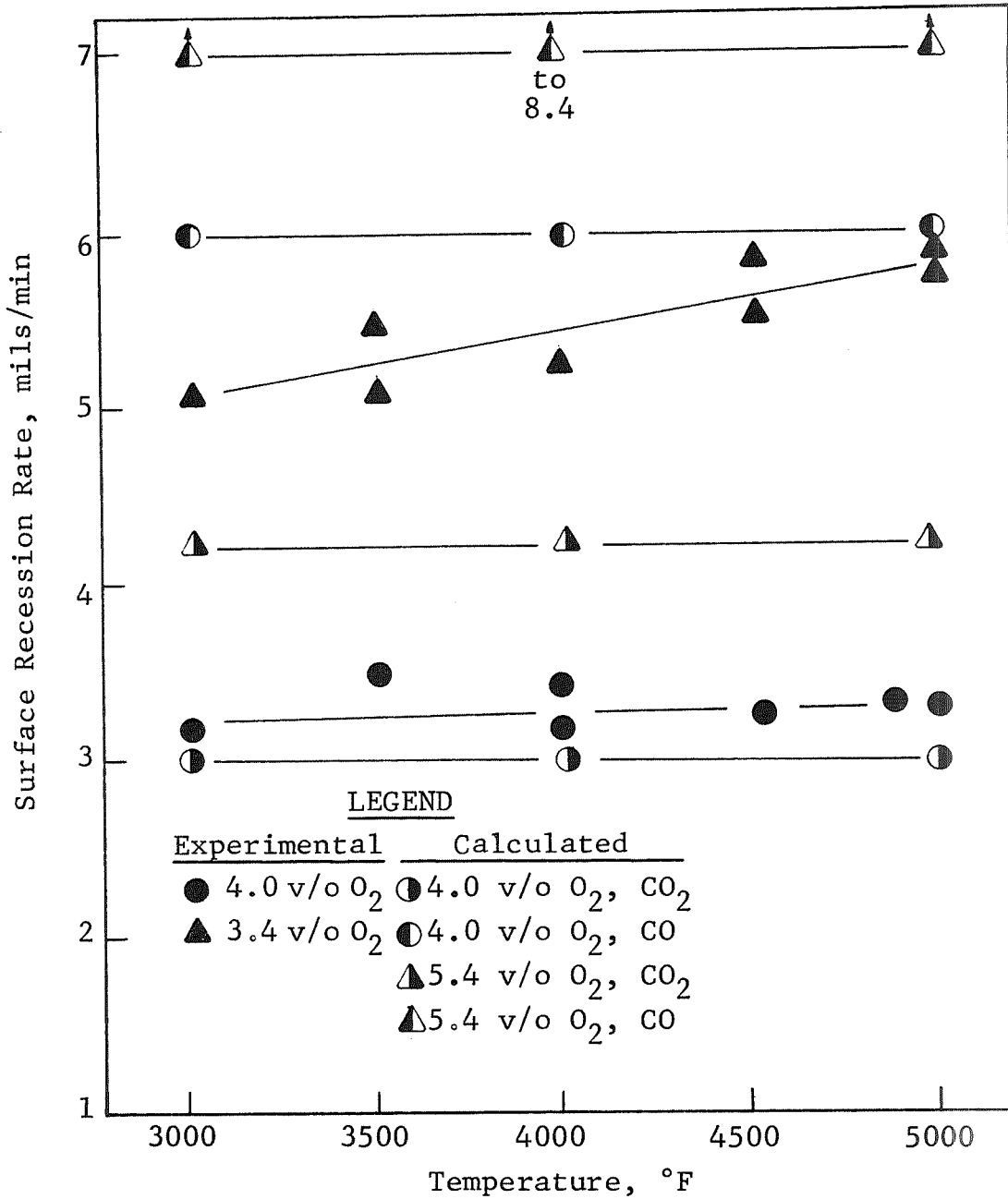
Fig. 19 - Comparison of Experimental and Calculated
Surface Recession Rates of ATJ Graphite
in Flowing Oxygen for UF = 0.4.

IITRI-B6102-13
(Final Report)

5.4 v/o O_2 the recession rate clearly increases with temperature. This means that if UF is constant for the test condition used, the concentration of CO in the reaction products increases with increasing temperature.

Figure 20 is a plot of the calculated and experimental rates for rhenium in 2.3 and 5.4 v/o O_2.[1] Although the experimental data are limited, the recession rates appear to increase slightly with increasing temperature. The experimental rates lie between the calculated rates for ReO_5 and Re_2O_7 reaction products for UF = 0.4. Both atmospheres indicate approach to an Re_2O_7 reaction product at high temperature although UF may not be constant over the range of 3500°-5000°F. It is interesting that reasonable correlation is also obtained for HF-O_2 mixtures for UF = 0.4. The experimental rates in 10 v/o HF-0.56 v/o O_2 and 10 v/o HF-2.5 v/o O_2 are about 0.15 and 1.0 mils/min at 5200°F, respectively.[1] Calculated rates, assuming all recession is due to oxygen, are about 0.29 and 1.2 mils/min.

Thus, the utilization factor concept can be useful in analysis of experimental data for systems of a single corrodent gas and a pure solid material, particularly in the range where UF is constant with temperature. However, the concept can also be extended to regions where UF is not constant. For convenience, it can be assumed that K = 1 for experimental conditions where K is constant. This means that all of the corrodent gas impinging on the surface or in the surface layers reacts with the solid. It would appear that this is the case, since the recession rates are directly proportional to the corrodent mass flow rate for constant UF and a well-defined reaction product stoichiometry. However, K contains terms which define: (1) the rate of reaction and (2) the "dynamic equilibrium" between the reactants and products. Thus, some of the impinging gas materials can remain unreacted for constant UF and a single reaction product. Increasing UF with temperature means that the rate of arrival of corrodent gas molecules exceeds the rate at which they
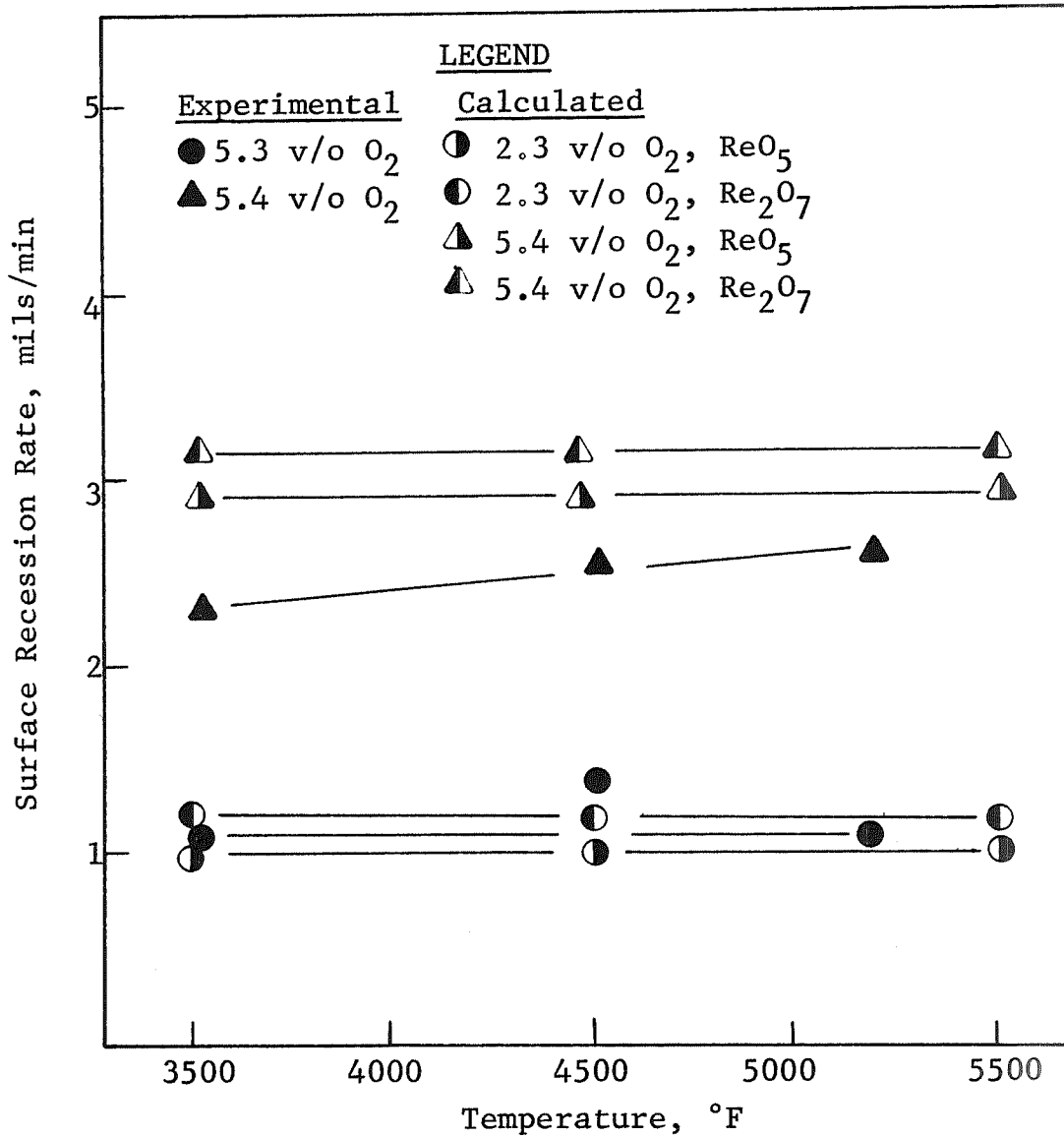
Fig. 20 - Comparison of Experimental and Calculated
Surface Recession Rates of Rhenium in
Flowing Argon-Oxygen for UF = 0.4.

IITRI-B6102-13
(Final Report)

are consumed in the reaction $[(1 - K)F_i \neq 0]$. Decreasing UF with temperature indicates that the "dynamic equilibrium" is shifted toward the reactants; i.e., the reaction product becomes unstable. The former case is represented by the W-O_2 reaction below 4000°F (Figure 18), and the latter case by the Ir-O_2 reaction above 2500°F (Figure 17). In either case, UF can be calculated for the reaction at any temperature from experimental data. The effect, in either case, is simply a reduction in the apparent molar ratio, M_F, in Equation 7.

The previous discussion has demonstrated that the utilization factor concept is useful in examining the recession rate data for some pure materials and a single reaction product, particularly for conditions where UF is constant. Further insight into the data can be obtained by examination of the schematic plot of recession rate (and UF) versus temperature for the general case in Figure 21. This plot represents the recession rates for a single reaction product. Obviously, a plot of this type can be generated for each possible reaction product of the gas-solid reaction. The flat portion ($KF_i = C$) of the curve occurs at high recession rates for high values of M_F. Furthermore, it is clear that the plot shown represents a plane section through a three-dimensional plot in which the Z axis can be either flow rate, corrodent concentration in the atmosphere, or for that matter, pressure. The curve shown, therefore, represents the contour of a three-dimensional surface. Thus, the curve shape will change depending on whether this Z axis represents variable flow rate at constant corrodent concentration, or variable corrodent concentration at constant flow rate. In either case, the boundary of the solid evaporation region will remain essentially invariant at constant pressure.

A recession rate curve such as that shown in Figure 21 can prevail whether the atmosphere is static or flowing. As will be discussed later, the effect of flow rate is to shift the temperature of the boundaries. In any case, a condition $KF_i = C$
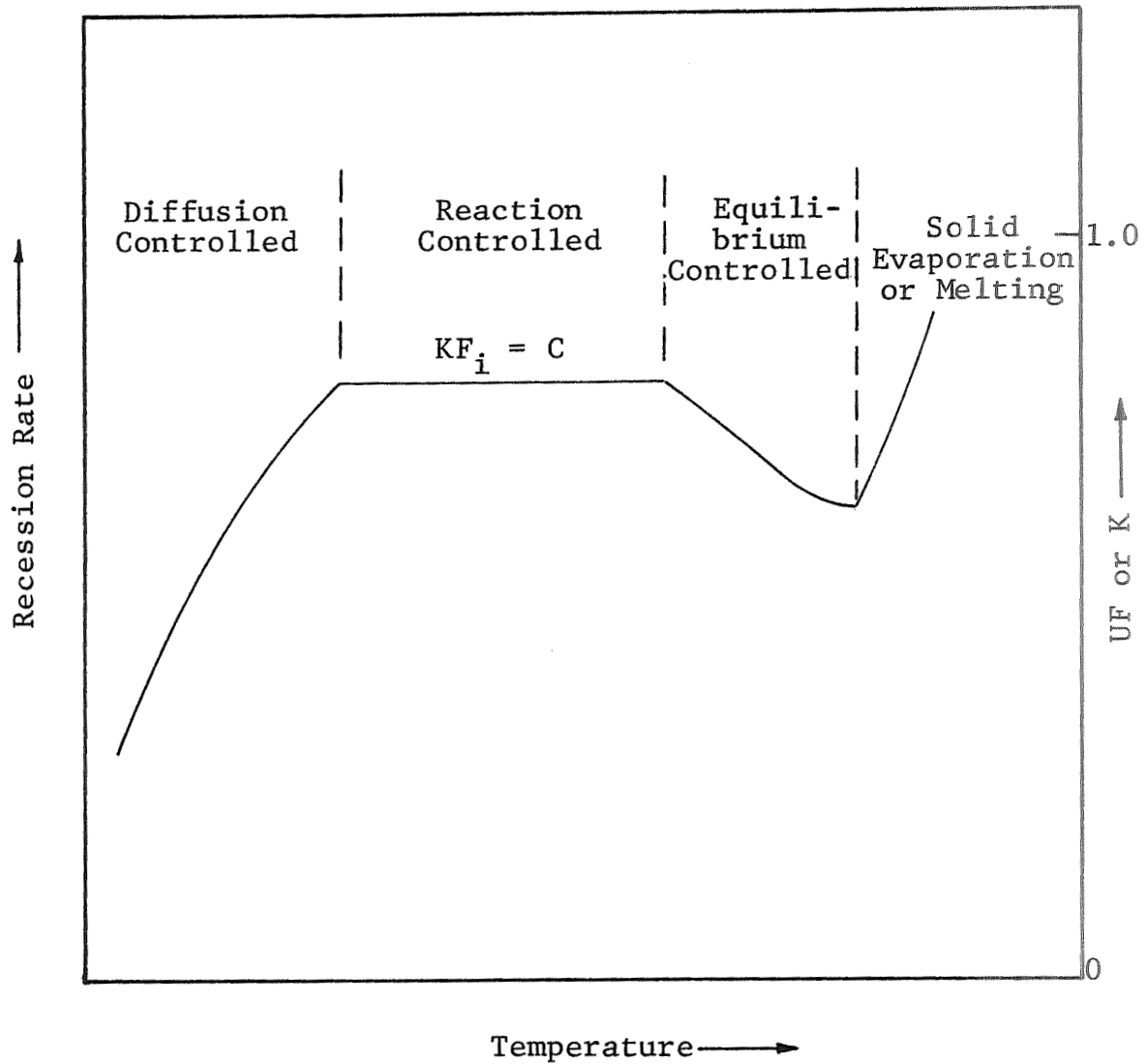
Fig. 21 - Schematic Diagram of the Variation in Recession Rate With Temperature for a Single Volatile Reaction Product.

constant must always prevail for the gas-solid reaction; the limiting condition is always $KF_i = F_i$. A region of dynamic equilibrium control can only exist if the reaction product becomes unstable at high temperature, such as that shown previously for the metal fluorides. Melting will occur at a specific temperature for essentially all experimental conditions, but the location of the boundary for solid evaporation will be pressure dependent.

A complete curve such as that shown in Figure 21 is rarely realized in low-pressure static tests of gas-metal reactions because the diffusion region can extend to very high temperatures. The two lower boundaries may be coincident. In the absence of an equilibrium-controlled region, evaporation or melting of the solid material may occur before the diffusion-controlled boundary is reached. Furthermore, thermal instability of the reaction product is not always observed.

In the diffusion-controlled region, the recession rate is controlled by the rate of arrival of gas molecules at the surface. More specifically, the recession rate is controlled by the arrival rate of gas molecules with sufficient kinetic energy to surmount the energy barrier to the reaction. (The energy of dissociation of diatomic gas molecules contributes to this barrier.) This suggests a reason that a curve as shown in Figure 21 can exist for both dynamic and static atmospheres. The additional kinetic energy imparted by the pressure drop in a dynamic system is insufficient to permit all the impinging gas molecules to surmount the energy barrier. The effect of high flow rates of the corrodent gas is, therefore, to simulate a temperature-accelerated arrival rate, without imparting a comparable increase in kinetic energy. For example, the gas product is employed in this program were about 400 fps. In contrast, the average velocity of oxygen atoms at 0°C calculated from kinetic theory is about 1300 fps,[43] and increases with temperature. Thus, the kinetic energy due to flow is a minor, although not negligible, part of the total kinetic energy, particularly at high temperatures. The major effect

IIT RESEARCH INSTITUTE

86   IITRI-B6102-13
                                      (Final Report)

of a flowing system is therefore to shift the boundary of the diffusion-controlled region to a lower temperature. The diffusion controlled region provides the familiar Arrhenius plot used for calculation of the apparent activation energy for the reaction.

The region $KF_i = C$ is less clearly defined than any other regions in the plot. This condition is normally called the reaction-controlled region, since the recession rate is considered to be dependent on the solid-gas surface reaction. Surface reaction control means that the recession rate is dependent on the slowest of the five fundamental steps in the overall reaction process. These steps include: (1) adsorption of the corrodent gas on the solid surface, (2) dissociation of the corrodent gas molecules, (3) formation of reaction products, (4) desorption of the reaction product, and (5) diffusion of the reaction product away from the solid surface. These basic steps are conventionally defined as important in the reaction process, and each can produce the condition constant KF_i. For example, if step 4 is the slowest, the reaction product will accumulate on the surface and limit the accessibility of surface for adsorption of gas molecules. Clearly, each of the other steps can similarly restrain the overall reaction. There is some question whether all of these steps are limiting, as will be discussed subsequently.

It would appear that the condition KF_i = constant can also prevail in any given test independent of any of the five basic steps as defined. In flowing systems, the condition can be obtained without surface reaction control. Examination of Figure 16 indicates that the condition is obtained if K = 1 ($KF_i = F_i$). This situation can be obtained independent of whether the Z axis is either flow rate or corrodent concentration at constant flow rate. It simply means that all corrodent gas molecules impinging on the surface react. In this context, the difference between the diffusion-controlled and reaction-controlled region is in the kinetic energy of the impinging gas molecules.

IIT RESEARCH INSTITUTE

87   IITRI-B6102-13
                            (Final Report)

Recession in the diffusion-controlled region is dependent on the fraction of impinging gas molecules with sufficient kinetic energy to surmount any energy barrier to reaction. In the region $KF_i = F_i$, all gas molecules have sufficient energy to surmount the barrier; all molecules which impinge eventually react. Obviously, this could be construed as equivalent to step 1 in the overall reaction process.

It was stated previously that Figure 16 represents a plane section through a three-dimensional plot, where the Z axis is variable flow rate at constant corrodent concentration, or constant flow rate with variable corrodent concentration. The other possible variable is, of course, total pressure. Increasing total pressure will increase the recession rate for both of the above conditions, probably by increasing F_i. Thus, the increase in recession rate will not likely be a linear function of total pressure.

Variation in both flow rate and corrodent concentration will modify somewhat the curve shown in Figure 16. An increase in corrodent concentration at constant flow rate will result in an increase in the recession rate; in the region where KF_i is constant, the recession rate will be directly proportional to the corrodent concentration. This is shown in Figure 16 for tungsten in fluorine. In this region, increasing total flow rate will similarly result in a directly proportional increase in recession rate; both variations increase F_i. There will, however, be a shift in the diffusion-reaction boundary depending on the method of increasing F_i.

The magnitude of the shift in the reaction-diffusion boundary in Figure 21 will be dependent on the test method, i.e., whether a hot or cold gas is employed. All of the tests in this program were hot substrate-cold gas tests. In a rocket nozzle, an inverse relationship exists --a hot gas-cold wall condition prevails. In order to compare the two conditions, it is necessary to define the temperature in Figure 21 as either that of

IITRI-B6102-13
                                    (Final Report)

the gas or the solid. If it is assumed that the temperature indicated in Figure 21 is that of the solid, the influence of hot or cold gas at constant flow rate can be assessed. The general shape of the curve will not be changed, only the boundaries between the various regions will be shifted.

For a hot gas test, the diffusion-surface reaction boundary will tend to be shifted downward in temperature from a cold gas test because the hot gas molecules have higher kinetic energy. The reaction-equilibrium boundary must be unaffected or also shift downward for the same reason. The recession rate for a hot gas test in the diffusion-controlled region is therefore always higher than for a cold gas test. Increasing the flow rate (Z axis) at constant corrodent concentration in a hot gas test will result in an increase in the solid surface temperature. An increase in the corrodent gas concentration, will probably have a similar effect, since rate of generation of exothermic energy per unit area will increase. Thus, variation of both corrodent concentration and flow rate will result in an apparent shift of the whole curve downward in temperature for the same initial solid temperature.

For a cold gas test, an inverse effect will likely be obtained. Here, some of the impinging gas molecules may require excitation at the surface to surmount the energy barrier. The effect will be to reduce the solid surface temperature, particularly if unreactive gas molecules, such as the argon used in this program also impinge on the surface. Increasing either the corrodent concentration or flow rate will tend to shift the curve upward in temperature, particularly the diffusion-reaction boundary. This effect can be seen in the plot for the $W-O_2$ reaction in Figure 18. Corrosion tests in this program minimized the cooling effect by stabilizing the specimen temperature with the argon flowing prior to introduction of the corrodent gases.

The above discussion suggests that the major effect of test method on the schematic plot in Figure 21 is in the

diffusion-controlled region and at the diffusion-reaction boundary. Shift of the diffusion-reaction boundary upward in temperature is maximum for a static test. For a flowing cold gas test, increasing either flow rate or corrodent concentration will tend to reduce the temperature range of constant KF_i by increasing the temperature of the diffusion-reaction boundary.

Finally, the exothermic energy released at the solid surface by the reaction can also influence the oxidation-corrosion behavior. This energy is probably dissipated in several mechanisms. One method is thermal conductance into the solid material. At low temperatures, the solid surface can increase in temperature with exposure time, as was observed for the $W-F_2$ corrosion tests at 2000°-2500°F.[1] Dissipation by radiation to the surroundings will also occur. Exothermic energy can also be absorbed by excitation of the impinging gas molecules under cold gas-hot wall conditions. Finally, a portion of the energy can be employed in imparting translational motion to the gaseous reaction products evolving from the surface. Reaction products leaving the surface must have a kinetic energy at least equal to that they would have at the surface temperature of the solid. Since the thermal velocity is considered greater than the pressure-induced velocity, a concept of "sweeping" away reaction products appears questionable. In a static system, ejection of reaction products will likely be random, although the mean ejection direction is normal to the surface. In a flowing system, collision with incoming unreacted molecules must occur; gas flow would apparently only bias ejection in the direction of the free stream flow.

Examination of the experimental corrosion rates in Figures 16 through 20 illustrates several conditions indicated by Figure 21. Only for the $W-F_2$ reaction (Figure 16) is a reasonably complete curve obtained. Although not shown in Figure 16, the measured recession rate in 6.5 v/o F_2 decreases slightly below 3000°F. Thus, the $W-F_2$ reaction approximates the reaction-

controlled region including both boundaries in the range of
2500°-5500°F. Figure 17 indicates that the Ir-F_2 and Re-F_2 plots
are in the region of the reaction-equilibrium boundary. In con-
trast, the W-O_2 plots are near the diffusion surface reaction
boundary (Figure 18). The C-F_2 (Figure 16) plots appear to be in
the equilibrium-controlled region and the C-O_2 (Figure 19) reac-
tion in the diffusion-controlled region. Location of the plotted
data for ATJ graphite is not clear since the possibility of sev-
eral reaction product stoichiometries suggests that the experi-
mental recession rates may be due to overlapping recession curves
of the various stable species. A similar situation may prevail
for rhenium in oxygen (Figure 20).

Thus far, discussion has been concerned only with reac-
tions of one corrodent gas with an unalloyed solid material. It
is also possible to extend the analysis to more than one reactant
gas or an alloyed solid material. For a condition of combined
corrodent gases, Equation 7 can be written as:

$$R_t = \frac{F_{ta}UF_a M_{Fa}M_{sa} + F_{tb}UF_b M_{Fb}M_{sb} + \cdots F_{ti}UF_i M_{Fi}M_{si}}{AC} \qquad (8)$$

where F_{ta} = flow rate of corrodent a

F_{tb} = flow rate of corrodent b

M_{Fa} = molar ratio for reaction with corrodent a

M_{Fb} = molar ratio for reaction with corrodent b

Equation 8 can be employed provided that the reaction
products produced by the various corrodent gases are distinguish-
able, i.e., no complex products are formed. In the region where
KF_i is constant, UF is constant. Thus, for two reactant gases,
an unalloyed solid material and constant UF, Equation 8 is:

$$R_t = \frac{M_s UF}{AC} \; (F_{ta}M_{Fa} + F_{tb}M_{Fb}) \qquad (9)$$

Equation 9 means that the recession rates due to the
individual corrodent gases can be summed to obtain the total

recession rates. This can be accomplished within the restraints imposed by increasing the total corrodent concentration as discussed previously. Obviously, formation of a complex product will result in a deviation in total recession from that given by Equation 9 because the values of M_{Fa} and M_{Fb} will change.

Recession rates calculated from Equation 9 and experimental data[1] for tungsten at 4000°F and for rhenium at 3500°-5200°F in fluorine-oxygen are plotted in Figures 22 and 23, respectively. The data are summarized in Tables A-XIII and A-XIV (Appendix A). Also shown in Table A-XIII is the average utilization factor for the overall reaction of tungsten in oxygen and fluorine-oxygen at 4000°F. The values for UF in oxygen and in fluorine-oxygen, with the exception of 0.108 cfh oxygen, are in the range of 0.32 to 0.37. This is not surprising since the value of UF for oxygen at 4000°F was about 0.36 (Figure 17).

The plot of calculated versus experimental rates for tungsten in oxygen and fluorine-oxygen in Figure 22 indicates that the calculated rates are generally higher than the experimental. This is expected because of the reduction in UF. In oxygen, reasonable comparison is obtained up to flow rates of about 0.325 cfh (7 x 10^{-3} mils/cm^2/min). Deviation at higher flow rates is due to the influence of corrodent concentration on the diffusion-reaction boundary as discussed previously.

In fluorine-oxygen, a similar effect is observed. However, increasing oxygen concentration in the range of 0-0.163 cfh (0-1.63 v/o O_2) has little influence on the experimental recession rate. Above a flow rate of 0.325 cfh the curves for calculated and experimental rates are about the same shape. These results suggest that a F_2-O_2 reaction producing O_xF_y compounds may occur, contributing to the reduction in UF.

Figure 23 compares the calculated and experimental rates for rhenium in fluorine-oxygen at 3500°-5200°F. The value of UF (Table A-XIV) for the Re-F_2 reaction above 3500°F was calculated from the recession rate of rhenium in fluorine.[1] Good

IIT RESEARCH INSTITUTE

IITRI-B6102-13
                                   (Final Report)
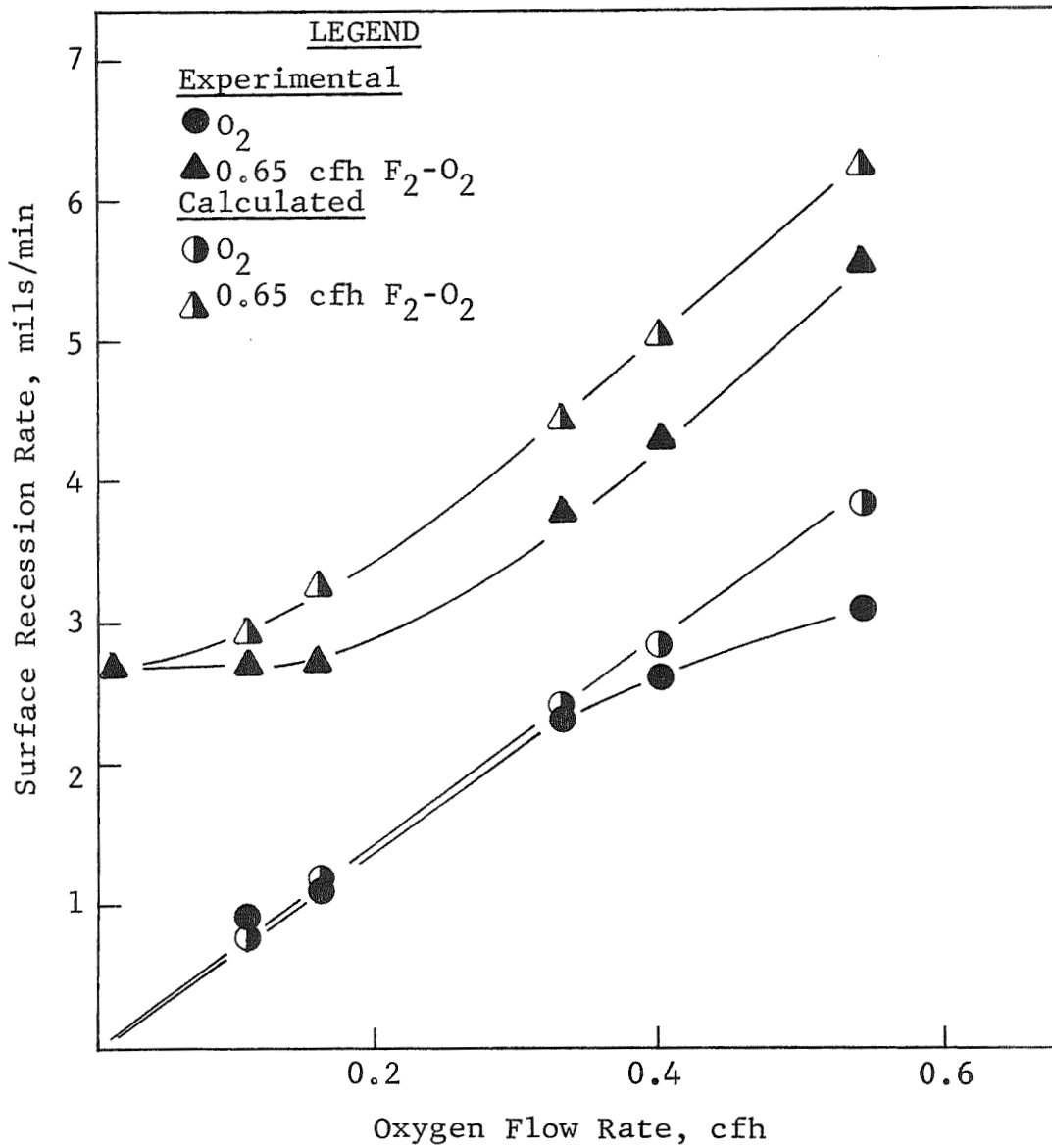
Fig. 22 - Comparison of Calculated and Experimental
Recession Rates of Tungsten in Flowing
Oxygen and Fluorine-Oxygen at 4000°F.
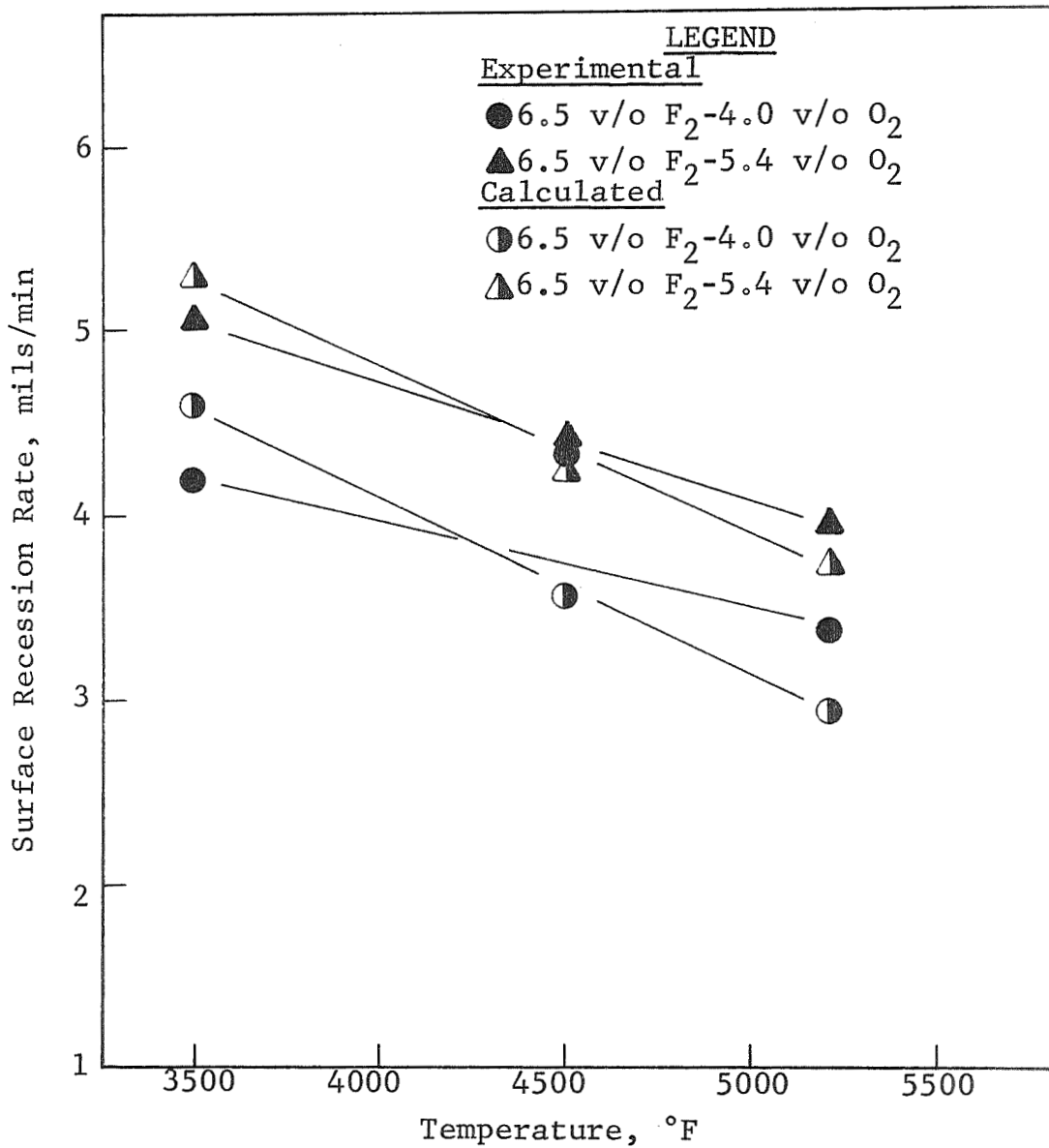
IITRI-B6102-13
       (Final Report)

Fig. 23 - Comparison of Calculated and Experimental
Recession Rates of Rhenium in Flowing
Fluorine-Oxygen.

IITRI-B6102-13
       (Final Report)

correlation is obtained for 0.65 cfh F_2-0.54 cfh O_2 (6.5 v/o F_2-5.4 v/o O_2), but deviations are evident for 0.65 cfh F_2-0.4 cfh O_2. It is probable that most of the deviation for the lower oxygen flow rate is due to experimental error.

Equation 9 can also probably be employed to calculate the recession rate resulting from one or more corrodent gases reacting with an alloyed (or composite) solid. In this case, the value of UF can be time dependent if the recession rates of the components of the solid material are significantly different. This condition was discussed previously concerning the time dependence of the recession rates of W-Re-Ir alloys. Equation 9 must be modified to account for the atomic percent (a/o) of the various constituents in the solid material. Thus, for two components in the solid and a single corrodent gas Equation 9 becomes:

$$R_t = \frac{F_t UF_1 M_{F1} M_{s1}}{B_1 C_1} + \frac{F_t UF_2 M_{F2} M_{s2}}{B_2 C_2} \qquad (10)$$

where B_1 = A x atomic concentration of component 1

B_2 = A x atomic concentration of component 2

If the recession rates of components 1 and 2 are equal, then $UF_1 = UF_2 = UF$. This also means that MF must be equal for the two components. On the other hand, if a wide difference in recession rates exists, only the initial recession rate (time = 0) is given by Equation 10. As the exposure time increases, the recession rate approaches that dictated by the term in Equation 10 giving the slowest recession rate. Measurement of the value of UF with increased time therefore becomes difficult, since several terms in the equation (UF_1, UF_2, B_1, B_2) will vary with time.

Some insight into the mechanism of oxidation-corrosion can also be obtained in systems in which other than gaseous reaction products are possible. This condition prevails in fluorine-oxygen for solid materials which develop high melting

IIT RESEARCH INSTITUTE

IITRI-B6102-13
(Final Report)

oxides, such as graphite-carbide composites. Here, both solid (or liquid) oxides and gaseous fluoride are possible reaction products.

The oxidation-corrosion behavior of HfC-33 v/o C and TaC-20 v/o C in fluorine-oxygen and hydrogen fluoride-oxygen was examined. After oxidation-corrosion tests, a thin film of oxide was usually found on the carbide composites. Furthermore, flow of liquid oxide was apparent on both composite materials above the melting point of the respective oxide. This suggested that formation of the oxide preceded generation of gaseous fluorides. Accordingly, both HfC-C and TaC-C samples were exposed for 15 sec at 3000°-5000°F. After exposure, the oxide was carefully removed and the oxidation (recession) rate calculated from the weight loss. It was hoped that the short exposure time would give a reasonable approximation of the initial oxidation rate.

The short-time oxidation rates in 2.3 and 5.4 v/o O_2 at 3000°-5000°F for HfC-33 v/o C and TaC-20 v/o C are plotted along with oxidation-corrosion rates in fluorine-oxygen[1] and hydrogen fluoride-oxygen[1] in Figures 23 and 24. Figure 23 indicates a reasonable comparison of the oxidation and oxidation-corrosion rates for HfC-C, at least above 4000°F. Better matching of the recession rates in fluorine-oxygen below 4000°F could be achieved, but the 15 sec oxidation exposure was probably too long to obtain the initial oxidation rate at 3000° and 3500°F. In hydrogen fluoride-oxygen, the higher oxidation rate below 3500°F suggests that a different mechanism might prevail at the lower temperature.

Figure 25 indicates that the oxidation rates for TaC-C are lower than the oxidation-corrosion rates. Again, this is probably due to the inability to obtain the initial rate by a 15 sec exposure. Since Ta_2O_5 melts about 3400°F, glasses were developed in oxygen at 3500°F and above, which probably also reduced initial oxidation. In any case, it appears that the oxidation-corrosion rate in fluorine-oxygen and hydrogen fluoride-

IIT RESEARCH INSTITUTE

IITRI-B6102-13
                                (Final Report)
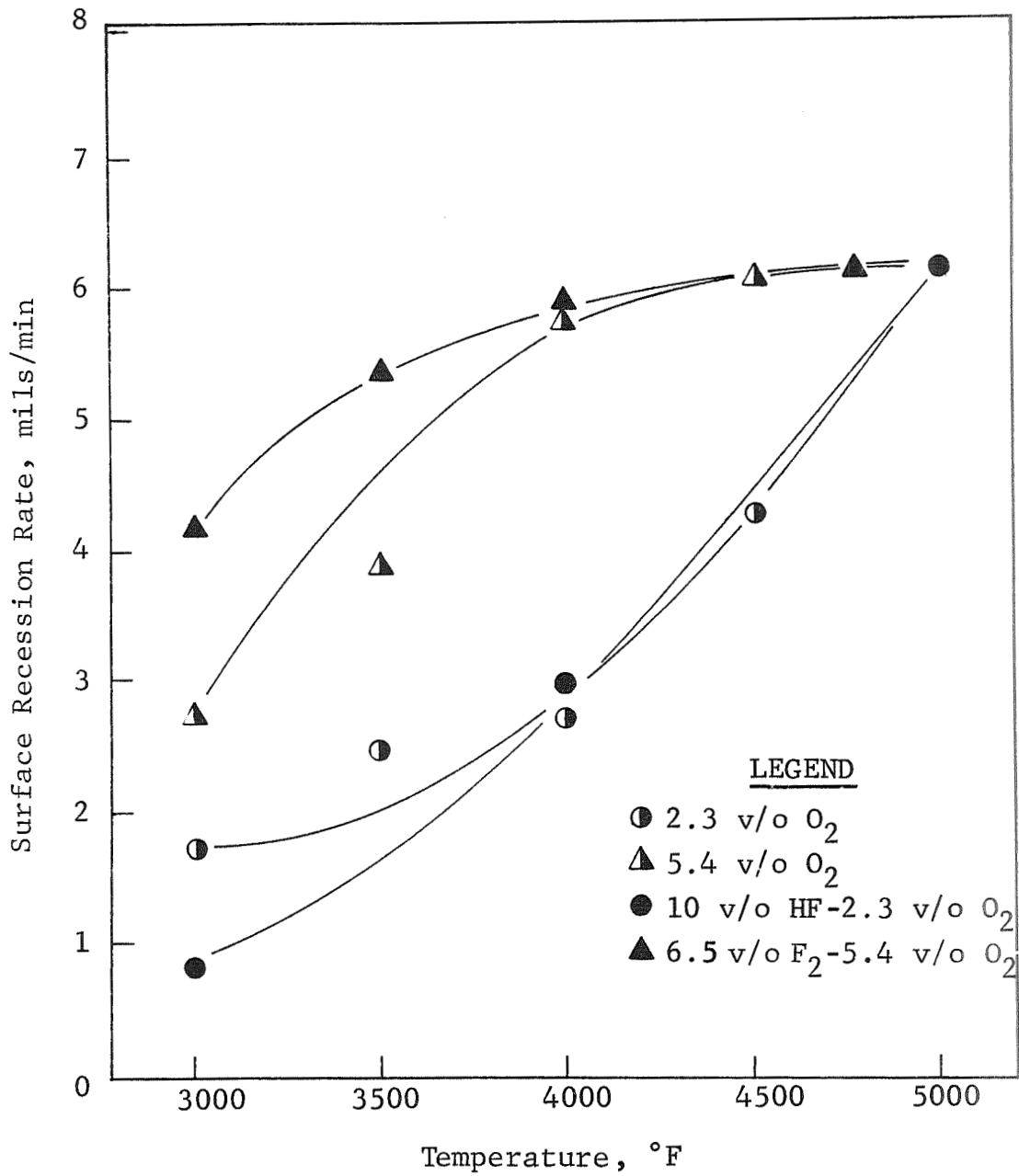
Fig. 24 - Comparison of Short Time Oxidation
and Oxidation-Corrosion Rates for
HfC-33 v/o C.
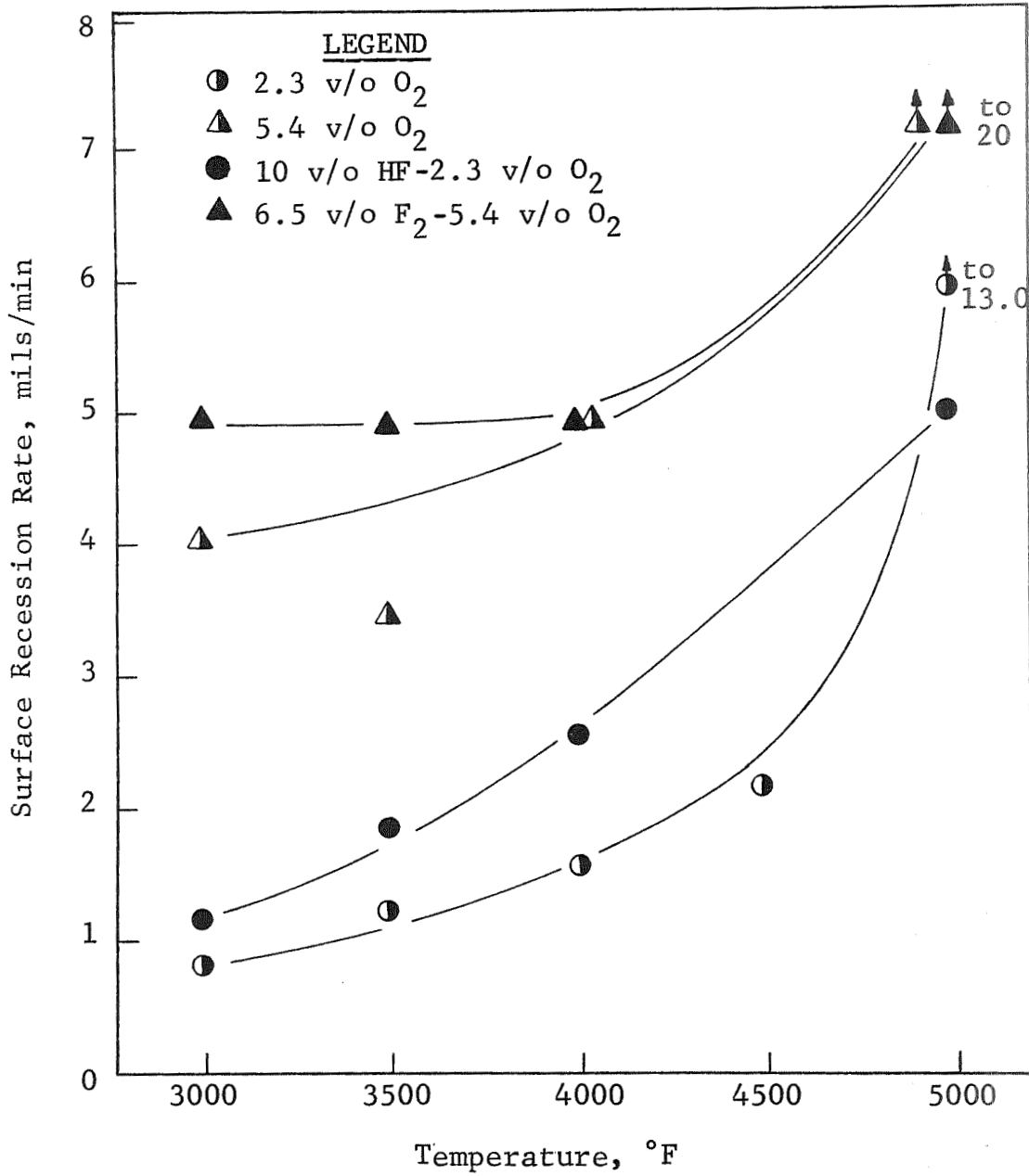
Fig. 25 - Comparison of Short Time Oxidation
and Oxidation-Corrosion Rates for
TaC-20 v/o C.

oxygen is determined by the oxide forming reaction. Carbide composites have relatively low recession rates of 1-2 mils/min in 6.5 v/o fluorine and 0.1-0.2 in 10 v/o hydrogen fluoride.[1] It therefore appears that in oxygen-containing atmospheres the oxide is developed initially, which subsequently reacts with the fluorine. In the temperature range where solid oxides are formed, the rate of reaction with fluorine is about equivalent to the rate at which the oxide is developed.

The utilization factor concept does permit calculating recession rates of refractory materials in a variety of fluorine and oxygen environments. Oxidation-corrosion tests conducted in this program represent a reasonable simulation of the conditions that should prevail in a rocket nozzle. For example, only a small fraction of corrodent gas flow through a rocket nozzle results in throat recession. Although the tests conducted herein were cold gas-hot wall tests, most of the tests were conducted in or near the reaction-controlled region. Since the recession rate is independent of the gas temperature, oxidation-corrosion data generated in this program should be applicable to the cold wall-hot gas environment of a nozzle. The major variable is total pressure since all the laboratory tests were conducted at about atmospheric pressure.

In spite of these differences, it is possible that the utilization factor concept can be employed in estimating throat recession rates in rocket nozzles. The utilization factor in nozzles should be much smaller than was obtained in the laboratory tests. In a nozzle, the lower utilization factor will be partially offset by higher mass flow rates and higher total pressure. However, it may be possible to estimate a utilization factor for nozzle configurations in a subscale laboratory test. This should permit estimation of the throat recession for nozzle materials at various nozzle temperatures, flow rates, and exhaust gas compositions. These data should be much more beneficial than relative laboratory recession rate data in establishing

engine operating conditions, nozzle design, and material selection for the thrust chambers and nozzles for fluorine engines.

III. SUMMARY AND CONCLUSIONS

A literature search was conducted to define matrix-additive combinations suitable for fabrication into oxidation-corrosion resistant composites for use in liquid rocket engine exhausts containing both fluorine and oxygen. The survey included all refractory materials melting above 4000°F, excluding oxides. Selection criteria for the composites system included: melting point above 4000°F, oxidation-corrosion resistance in fluorine-oxygen, high-temperature thermal stability, and fabricability. The results of the literature survey demonstrated that W-Re-Ir and Re-Ir alloys, $HfIr_3$, $TaIr_3$, and possibly BN warrant further evaluation. It was also shown that free boron in exhaust products could limit the potential nozzle materials. Iridium and iridium-rich alloys remained the most oxidation-corrosion resistant materials for fluorine-oxygen. These materials, however, would probably be most susceptible to attack by boron.

Attempts to fabricate W-Re-Ir and Re-Ir alloys by hot rolling at 2200°F were unsuccessful. Ir-33Re demonstrated some hot workability at both 1800° and 2200°F.

Oxidation-corrosion tests were conducted in fluorine, hydrogen fluoride, fluorine-oxygen, and hydrogen fluoride-oxygen atmospheres at 3000°-5000°F on W-Re-Ir alloys, Re-25Ir, Re-35Ir, $HfIr_3$, and $TaIr_3$. Again, the $HfIr_3$ and $TaIr_3$ compounds had the best overall oxidation-corrosion resistance in these atmospheres at 3000°-4500°F. The Re-Ir alloys also had reasonably good oxidation-corrosion resistance. W-Re-Ir alloys containing up to 20 w/o iridium exhibited oxidation-corrosion rates about one-half that of unalloyed tungsten. Surface recession rates for BN were very high in both fluorine and hydrogen fluoride.

Corrosion tests were also conducted on ATJ graphite, tungsten, iridium, and Re-Ir alloys in BF_3, BF_3-O_2, and BF_3-H_2 atmospheres at 3000°-4500°F. The results indicated that BF_3 is not a major corrosive species for these materials. The boron generated in BF_3-H_2 atmospheres caused surface melting of iridium at 3000°-4000°F, and tungsten above 4000°F. Re-35Ir also exhibited surface melting at 4000°F, but ATJ graphite was unaffected to 4800°F. Boron, therefore, is a major problem for materials that form low-melting eutectics with boron, and can cause surface recession equivalent to, or higher than, that of fluorine and oxygen for these materials.

Corrosion tests of ATJ graphite in argon-10 v/o hydrogen indicated that the recession due to hydrogen is a secondary problem below 4800°F. Surface recession rates in this atmosphere were at least an order of magnitude less than in fluorine or oxygen below 4000°F.

Melting interaction temperatures were determined for iridium, $TaIr_3$, and $HfIr_3$ in contact with carbides, borides, and ATJ graphite. The highest melting temperatures (~4500°F) were obtained with $TaIr_3$ in combination with TaC-C and graphite. $HfIr_3$ in combination with HfC-C and graphite melted near the Ir-C eutectic temperature (4170°F). The melting temperature of about 2500°F for the Ir-B eutectic was verified. Rhenium in contact with HfC-C melted at about 4850°F. These results suggest that $TaIr_3$-graphite or $TaIr_3$-TaC composites warrant further evaluation. Other systems with high-temperature potential are Re-Ir alloys in combination with graphite or carbides.

The approximate melting points of W-Re-Ir alloys were determined and shown to depend on the iridium concentrations. All of the alloys evaluated in this program had melting points above 4500°F. The lowest melting points (~4600°F) were measured on the W-15Re-20Ir and W-25Re-20Ir alloys.

The following conclusions can be drawn from the work conducted in this program:

IIT RESEARCH INSTITUTE

1. Surface melting resulting from interaction with boron is a potential problem for some high-temperature rocket nozzle materials as severe as that of fluorine or oxygen. Unfortunately, iridium-rich materials, which have the best fluorine-oxygen resistance, are susceptible to attack by free boron.

2. Hydrogen, hydrogen fluoride, and boron trifluoride generally exhibit recession rates at least an order of magnitude less than fluorine or oxygen at comparable flow rates for most refractory materials.

3. Composites combining iridium-rich ($TaIr_3$) or Re-Ir additions to carbides or ATJ graphite have some promise for fluorine-oxygen atmospheres. The other systems which offer some promise are W-Re-Ir and Re-Ir alloys.

4. Fabrication of W-Re-Ir and Re-Ir alloys by conventional hot working will be difficult. Ir-33Re probably can be hot worked at 1800°-2500°F.

5. The recession rates of nozzle materials in rocket engines could be estimated from laboratory data by correlation of the corrodent gas flow rate per unit area of nozzle surface.

IV. RECOMMENDATIONS

It is recommended that the following work be conducted as a logical continuation of the work described herein:

1. Further evaluation of refractory materials in boron-containing atmospheres should be conducted to define the magnitude of the boron problem.

2. Composites based on Re-Ir and $TaIr_3$ incorporated in a graphite and/or TaC-graphite matrix should be prepared and evaluated in fluorine-oxygen and boron-containing atmospheres.

3. Surface recession data from laboratory tests should be correlated with engine firing tests by comparison of the corrodent mass flow per unit area of laboratory test specimens and rocket nozzles.

REFERENCES

1. V. L. Hill, "Protective Coatings for Refractory Metals in Rocket Engines," Contract NAS7-431 (Final Report), August 1969.

2. F. A. Shunk, Constitution of Binary Alloys, Second Supplement, McGraw-Hill Book Co., New York, 1969.

3. R. P. Elliott, Constitution of Binary Alloys, First Supplement, McGraw-Hill Book Co., New York, 1965.

4. D. P. Harmon, "Iridium-base Alloys and Their Behavior in the Presence of Carbon," AFML-TR-66-290, Aerojet-General Corp., February 1967.

5. M. Hansen and K. Anderko, Constitution of Binary Alloys, McGraw-Hill Book Co., New York, 1958.

6. I. E. Campbell and E. M. Sherwood, High Temperature Materials and Technology, John Wiley & Sons, New York, 1967.

7. J. F. Lynch, et al., "Engineering Properties of Ceramics," AFML-TR-66-52, June 1966.

8. L. C. Long, Jr and J. R. Joiner, "Refractories in a Reactive Atmosphere," FDTR-TM-67-1, April 1967.

9. H. J. Goldschmidt, Interstitial Alloys, Plenum Press, New York, 1967.

10. E. Rudy, "Ternary Phase Equilibria in Transition Metal-Boron-Carbon-Silicon Systems," AFML-TR-65-2, Part V (Compendium of Phase Diagrams), May 1969.

11. E. V. Clougherty, D. Kalish, and E. T. Peters, "Research and Development of Refractory Oxidation Resistant Diborides," AFML-TR-68-190, October 1968.

12. I. I. Kornilov, "The Chemistry of Metallides," Consultants Bureau, New York, 1965.

13. E. K. Storms, The Refractory Carbides, Academic Press, New York, 1967.

14. J. R. Armstrong, et al., "Tungsten to Graphite Bonding," Contract DA-04-495-ORD-3028 (Final Summary Report), December 1961.

REFERENCES (cont.)

15. C. E. Brukl and E. Rudy, "Ternary Phase Equilibria in Transition Metal-Boron-Carbon-Silicon Systems," AFML-TR-65-2, Part II, Vol. XIV, July 1967.

16. V. L. Hill and R. H. Singleton, "Diffusion Barriers for Tungsten-Graphite Interface," Seventh Refractory Composite Working Group Meeting, DMIC Report 184.

17. C. E. May and P. D. Hoekstra, "Stability of Refractory Compounds in Hydrogen Between 4500°F and 5000°F, and Their Compatability With Tungsten," NASA-TN-D-844, May 1961.

18. C. R. Manning, Jr. and R. F. Stoops, "High Temperature Cermets I, Compatibility," J. Amer. Cer. Soc., 51, (8), 411-415, August 1968.

19. R. Resnick and R. Steinitz, "High Temperature Reactions Between Tungsten and Several Refractory Compounds," Fifth Meeting of Refractory Composites Working Group, Dallas, Texas, August 1961.

20. J. J. Krochmal, "Fiber Reinforced Ceramics: A Review and Assessment of Their Potential," AFML-TR-67-207, October 1967.

21. E. Rudy, "Ternary Phase Equilibria in Transition Metal-Boron-Carbon-Silicon Systems," AFML-TR-65-2, Part II, Vol. VIII, September 1966.

22. V. L. Hill, "Fifth Refractory Composites Working Group Meeting," Dallas, Texas, August 1961.

23. F. J. Lally and R. H. Hiltz, "Tungsten--Its High-Temperature Reactivity," J. Metals, 14, 424-428, June 1962.

24. D. A. Beckley, "Development of Cermet Rocket Nozzles," Sixth Refractory Composites Working Group Meeting, Dayton, Ohio, June 1962.

25. V. L. Hill and J. J. Rausch, "Protective Coatings for Tantalum Base Alloys," AFML-TR-64-354, Part II, January 1966.

26. J. M. Criscione, et al., "High Temperature Protective Coatings for Graphite," AFML-TDR-64-173, Part II, Contract AF-33(657)-11253, October 1964.

27. V. L. Hill, "Protective Coatings for Refractory Metals in Rocket Engines," Contract NAS7-431 (Interim Report), March 1968.

IIT RESEARCH INSTITUTE

IITRI-B6102-13
(Final Report)

REFERENCES (cont.)

28. P. N. Walsh, "Research on Physical and Chemical Principles Affecting High-Temperature Materials for Rocket Nozzles," Contract DA-30-069-ORD-2787, Vol. I (Final Report), August 1965.

29. A. K. Kuriakose and J. L. Margrave, "Kinetics of the Reactions of Elemental Fluorine With Zirconium Carbide and Zirconium Diboride at High Temperatures," J. Phys. Chem., 68, (2), February 1964.

30. A. K. Kuriakose and J. L. Margrave, "Kinetics of Reaction of Elemental Fluorine II. The Fluorination of Hafnium Carbide and Hafnium Boride," J. Phys. Chem., 68, (8), August 1964.

31. G. H. Miller and G. C. Robinson, Jr., "Investigation of Fiber Systems of Ablative Materials," NASA-CR-54722, Contract NAS3-4196 (Final Report), September 1965.

32. S. R. Aspinall, "Principles Governing the Behavior of Solid Materials in Severe High Temperature Environments," Contract DA-01-021-AMC-11926(Z) (Final Report), May 1966.

33. M. Ebner, "Stability of Refractories in Hydrogen-Fluorine Flames," J. Amer. Cer. Soc., 44, (1), January 1961.

34. J. D. Batchelor and E. L. Olcott, "Behavior of Nozzle Materials Under Extreme Rocket Motor Environments," Contract NOw 64-0393-c (Final Technical Report), June 1965.

35. H. M. Blaes, et al., "Application of Materials to Advanced Rocket Nozzle and Hot Gas Control Systems," AFML-TR-67-106, Vol. I, Contract AF 33(657)-11217, March 1967.

36. H. M. Blaes, et al., "Application of Materials to Advanced Nozzle and Hot Gas Control Systems," AFML-TR-65-125, Vol. I, Contract AF 33(657)-11217, April 1965.

37. E. G. Parks, Jr., "Design, Test and Evaluation of a Hybrid Nozzle," NASA-CR-66566, Contract NAS1-6555 (Final Report).

38. C. G. Ruderer, et al., "Development of a Protective Coating System for Regeneratively Cooled Thrust Chambers," NASA-CR-72596, May 1969.

39. W. J. Lewis, "Coatings for Advanced Thrust Chambers," NASA-CR-72604, Contract NAS3-11185 (Final Report).

REFERENCES (cont.)

40. D. N. Crump et al., "Improved Throat Inserts for Ablative Thrust Chambers," NASA-CR-54984, Contract NAS3-6280 (Final Report), September 1967.

41. K. I. Portnoi and V. M. Romashov, "Phase Diagram of the Rhenium-Boron System," Sov. Powder Met., No. 2, pp. 112-114, 1968.

42. P. L. Faust, "Oxidation of Tungsten and Other Refractory Metals," ML-TR-64-162, April 1965.

43. W. J. Moore, Physical Chemistry, 2nd ed., Prentice-Hall, Inc., Englewood Cliffs, New Jersey, 1955, p. 166.

44. T. R. Wright et al., "The Fabrication of Iridium and Iridium-Alloy Coatings on Graphite by Plasma Arc Deposition and Gas-Pressure Bonding," AFML-TR-68-6, Contract No. AF 33(615)-3706, February 1968.

APPENDIX A

OXIDATION-CORROSION DATA TABLES

TABLE A-I

CORROSION RATE OF REFRACTORY MATERIALS
IN ARGON-6.5 v/o FLUORINE

Alloy Composition, w/o	Exposure[a] Temperature, °F	Weight Loss, gm	Specific Weight Loss, mg/cm^2	Calculated Surface Recession Rate, mil/min
W-15Re-10Ir	3500	1.158	88.5	1.75
	4000	1.084	92.3	1.83
	4500	1.102	88.0	1.75
	4800	0.516	54.0	1.10
W-15Re-15Ir	3500	1.126	83.5	1.64
	3500	1.096	87.0	1.71
	4000	1.091	73.6	1.45
	4500	1.076	73.8	1.45
	4800	0.510	43.0	0.88
W-15Re-20Ir	3500	1.092	70.9	1.39
	4000	1.088	67.5	1.32
	4500	1.070	65.0	1.27
W-25Re-10Ir	3500	1.127	74.0	1.45
	4000	1.183	79.2	1.55
	4000	1.081	81.2	1.59
	4500	1.001	66.5	1.30
	4700	0.499	37.8	0.77
W-25Re-15Ir	3500	0.978	73.5	1.43
	4000	1.026	72.2	1.40
	4500	0.918	59.2	1.15
	4700	0.423	35.4	0.72
W-25Re-20Ir	3500	1.053	62.6	1.21
	4000	1.022	62.1	1.20
	4500	0.782	49.0	0.99
Re-25Ir	3000	1.043	68.6	1.26
	4000	0.825	51.5	0.95
	4500	0.526	34.0	0.65
Re-35Ir	3000	1.277	79.5	1.46
	4000	0.818	51.0	0.93
	4500	0.359	23.4	0.43

IITRI-B6102-13
(Final Report)

Alloy Composition, w/o	Exposure[a] Temperature, °F	Weight Loss, gm	Specific Weight Loss, mg/cm^2	Calculated Surface Recession Rate, mil/min
Ir-23Hf	3000	0.930	61.0	1.25
	3500	0.415	24.8	0.51
	3500	0.559	34.4	0.70
	4000	0.595	37.1	0.76
Ir-23.9Ta	3000	1.208	78.0	1.58
	3500	0.279	19.7	0.40
	3500	0.286	18.7	0.38
	4000	0.506	32.8	0.67

[a] Exposure time - 5 min

TABLE A-II

CORROSION RATE OF REFRACTORY METALS
IN FLOWING ARGON-10 v/o HYDROGEN FLUORIDE

Alloy Composition, w/o	Exposure[a] Temperature, °F	Weight Loss, g	Specific Weight Loss, mg/cm^2	Calculated Surface Recession Rate, mil/min
W-15Re-10Ir	3500	0.031	1.91	0.04
	4000	0.047	2.94	0.06
	4500	0.048	3.09	0.06
W-15Re-15Ir	3500	0.035	2.14	0.04
	4000	0.033	1.94	0.04
	4500	0.036	2.14	0.04
	4500	0.037	2.20	0.04
W-15Re-20Ir	3500	0.027	1.67	0.03
	4000	0.032	1.62	0.03
	4500	0.029	1.87	0.04
W-25Re-10Ir	3500	0.077	4.92	0.10
	4000	0.092	5.57	0.11
	4500	0.053	3.40	0.07
	4500	0.063	4.18	0.08
W-25Re-15Ir	3500	0.034	2.18	0.04
	4000	0.027	1.96	0.04
	4500	0.051	3.01	0.06
W-25Re-20Ir	3500	0.007	0.42	0.01
	4000	0.021	1.26	0.03
	4500	0.035	2.19	0.04
Re-25Ir	3000	0.005	0.34	0.006
	4000	0.041	2.61	0.50
	4500	0.034	2.76	0.05
Re-35Ir	3000	0.011	0.73	0.01
	4000	0.009	0.41	0.007
	4500	0.007	0.59	0.01
Ir-23Hf	3000	0.113	7.8	0.16
	3500	0.126	8.8	0.25
	4500	0.265	16.7	0.35
Ir-23.9Ta	3000	0.007	0.49	0.001
	3500	0.021	1.5	0.03
	4500	0.103	7.6	0.15

[a]Exposure time 5 min.

TABLE A-III

CORROSION RATE OF REFRACTORY MATERIALS
IN FLOWING ARGON-6.5 v/o FLUORINE-5.4 v/o OXYGEN

Alloy Composition, w/o	Exposure[a] Temperature, °F	Weight Loss, g	Specific Weight Loss, mg/cm^2	Calculated Surface Recession Rate, mil/min
W-15Re-10Ir	3500	1.445	148.0	2.93
	4000	1.554	169.5	3.36
	4500	1.976	203.0	4.01
W-15Re-15Ir	3500	1.469	150.0	2.95
	4000	1.446	149.0	2.94
	4500	1.519	164.8	3.24
W-15Re-20Ir	3500	1.627	109.0	2.13
	4000	1.872	123.0	2.40
	4500	1.961	135.0	2.64
W-25Re-10Ir	3500	1.184	161.2	3.15
	3500	1.432	163.5	3.20
	4000	1.519	153.0	3.01
	4500	1.410	160.0	3.12
W-25Re-15Ir	3500	1.340	138.8	2.70
	4000	1.470	155.2	3.02
	4500	1.393	153.1	2.98
W-25Re-20Ir	3500[b]	1.739	111.0	2.15
	4000	1.158	139.5	2.70
	4000	1.108	147.0	2.85
	4500	1.110	134.0	2.60
Re-25Ir	3000	1.141	125.0	2.30
	4000	1.213	146.0	2.69
	4500	1.315	162.0	2.98
Re-35Ir	3000	1.008	110.0	2.01
	4000	0.935	108.5	2.00
	4500	0.881	111.5	2.02
Ir-23Hf	3000	2.088	136.0	2.78
	3500	0.641	71.6	1.46
	4500	0.357	48.3	0.99
Ir-23.9Ta	3000	0.578	80.2	1.63
	3500	0.240	27.7	0.56
	4500	0.486	57.2	1.16

[a] Exposure time 5 min unless noted otherwise.

[b] Exposure time 3 min.

TABLE IV

CORROSION RATE OF REFRACTORY MATERIALS
IN FLOWING ARGON-10 v/o HYDROGEN FLUORIDE-2.3 v/o OXYGEN

Alloy Composition, w/o	Exposure[a] Temperature, °F	Weight Loss, gm	Specific Weight Loss, mg/cm^2	Calculated Surface Recession Rate, mil/min
W-15Re-10Ir	3500	0.824	55.0	1.09
	4000	0.802	58.0	1.15
	4000	0.753	55.7	1.10
	4500	0.826	60.0	1.19
	4500	0.716	62.4	1.24
W-15Re-15Ir	3500	0.685	53.1	1.05
	4000	0.779	54.0	1.06
	4500	0.777	60.6	1.19
W-15Re-20Ir	3500	0.672	53.0	1.03
	4000	0.634	54.2	1.06
	4500	0.749	66.2	1.29
W-25Re-10Ir	3500	0.482	46.4	0.91
	3500	0.728	52.7	1.03
	4000	0.823	68.0	1.34
	4000	0.826	68.6	1.35
	4500	0.859	63.5	1.25
	4500	0.747	59.5	1.17
W-25Re-15Ir	3500	0.870	52.8	1.03
	4000	0.641	50.5	0.99
	4500	0.788	58.8	1.14
W-25Re-20Ir	3500	0.558	42.3	0.82
	4000	0.499	40.0	0.77
	4500	0.496	38.2	0.74
Ir-23Hf	3000	0.048	3.4	0.07
	3500	0.002	0.14	0.003
	4400	+0.008[b]	0.66	--
Ir-23.9Ta	3000	+0.002[b]	+0.12[b]	--
	3500	0.022	1.75	0.04
	4400	0.066	4.35	0.09
Re-25Ir	3000	0.622	49.0	0.90
	4000	0.849	61.0	1.12
	4500	0.978	72.7	1.34
Re-35Ir	3000	0.187	14.8	0.27
	4000	0.317	26.0	0.48
	4500	0.472	35.6	0.65

[a] Exposure time 5 min.

[b] Sample gained weight.

112

IITRI-B6102-13
(Final Report)

TABLE A-V

CORROSION RATES OF REFRACTORY MATERIALS
IN FLOWING ARGON-10 v/o BORON TRIFLUORIDE

Material	Exposure[a] Temperature, °F	Weight Loss, g	Specific Weight Loss, mg/cm²/min	Calculated Surface Recession Rate, mils/min
Tungsten	3500	0.019	1.51	0.03
	4000	0.019	1.41	0.03
	4500	0.27	1.95	0.04
ATJ graphite	3500	0.005	0.32	0.07
	4000	0.006	0.42	0.09
	4000	0.005	0.37	0.08
	4500	0.007	0.44	0.10
	4500	0.009	0.74	0.16
	4500	0.007	0.50	0.11
	4800	0.013	0.86	0.19
Iridium	3000	0.000	-	-
	3500	0.000	-	-
	4000	0.004	0.36	0.01
Re-25Ir	4000	0.045	3.81	0.07
Re-35Ir	4000	0.023	1.89	0.03

$\underline{4.3BF_3}$

Tungsten	3500	0.012	1.02	0.02
	4000	0.022	1.56	0.03
	5500	0.024	1.82	0.04

[a] Exposure time, 5 min.

TABLE A-VI

CORROSION RATE OF ATJ GRAPHITE AND TUNGSTEN
IN FLOWING ARGON-4.32 v/o BF_3-4.0 v/o O_2

Material	Exposure[a] Temperature, °F	Weight Loss, g	Specific Weight Loss, mg/cm^2	Calculated Surface Recession Rate, mil/min
ATJ Graphite	3000	0.133	15.3	3.34
	3500	0.159	18.5	4.05
	4000	0.184	19.7	4.32
	4500	0.167	18.3	4.00
	4500	0.171	18.8	4.12
Tungsten	3500	0.563	74.5	1.51
	4000	0.802	99.9	2.01
	4500	0.863	114.5	2.33
	5000	0.960	120.0	2.45

[a] Exposure time, 5 min.

CORROSION RATE OF REFRACTORY MATERIALS

IN FLOWING ARGON-10 v/o HYDROGEN-10 v/o BORON TRIFLUORIDE

Material	Exposure Temp., °F [a]	Weight Loss, g	Specific Weight Loss, $mg/cm^2/min$	Calculated Surface Recession Rate, mils/min
Tungsten	3500	0.032	3.40	0.07
	3500	0.040	3.08	0.06
	4000 [a]	+0.003	+0.28	--
	4000 [a]	+0.008	+0.32	--
	4500	0.018	1.47	0.03
	4500	0.020	1.50	0.03
ATJ Graphite	3500	0.006	0.40	0.09
	4000	0.005	0.35	0.07
	4500	0.010	0.72	0.16
	4800	0.019	1.38	0.30
Iridium	3000	-- [b]	--	5 [c]
	3500	-- [b]	--	15 [c]
	4000	-- [b]	--	30 [c]
Re-25Ir	4000	0.003	0.26	0.005
Re-35Ir	4000	-- [a]	--	5 [c]

[a] Exposure time 10 min.

[b] Samples brazed to W support rod.

[c] Estimated % melting of the sample.

TABLE A-VIII

CORROSION RATE OF ATJ GRAPHITE

IN FLOWING ARGON-HYDROGEN

Exposure Temp., °F	Weight Loss, g	Specific Weight Loss, mg/cm^2	Calculated Surface Recession Rate, mils/min
		Argon	
4500	0.004	.313	0.068
4500	0.007	.510	0.112
		Argon-2.2 v/o H$_2$	
3500	0.004	0.31	0.07
3500	0.009	0.68	0.151
4000	0.005	0.32	0.071
4500	0.008	0.47	0.102
		Argon-10 v/o H$_2$	
3000	0.004	0.30	0.07
3000	0.011	0.74	0.16
3500	0.010	0.69	0.15
3500	0.012	0.785	0.17
4000	0.006	0.44	0.10
4000	0.006	0.42	0.09
4500	0.009	0.59	0.13
4900	0.028	1.84	0.40
4900	0.050	3.90	0.85

TIME DEPENDENCE OF THE CORROSION RATE
OF W-Re-Ir ALLOYS IN FLOWING ARGON-6.5 v/o FLUORINE

| Alloy Composition, w/o | Exposure Conditions | | Weight Loss, gm | Specific Weight Loss, mg/cm^2 | Calculated Surface Recession Rate, mil/min |
	Temp, °F	Time, [a] min			
W-15Re-10Ir	4000	0.5	0.126	92.5	1.81
		1	0.119	89.4	1.72
		2	0.207	76.2	1.50
		4	0.391	71.8	1.41
	4500	0.5	0.117	109.0	2.14
		1	0.096	89.8	1.78
		2	0.201	93.8	1.86
		4	0.395	92.3	1.83
W-15Re-15Ir	4000	0.5	0.144	99.0	1.95
		1	0.136	93.3	1.85
		2	0.257	88.3	1.75
		4	0.482	82.8	1.64
	4500	0.5	0.124	102.0	2.00
		1	0.105	86.0	1.69
		2	0.201	82.4	1.62
		4	0.362	74.2	1.46
W-15Re-20Ir	4000	1	0.231	73.5	1.44
		2	0.209	66.5	1.30
		4	0.424	66.5	1.30
	4500	1	0.185	70.0	1.37
		2	0.187	71.0	1.39
		4	0.325	61.6	1.21
W-25Re-10Ir	4000	0.5	0.134	70.5	1.38
		1	0.143	76.8	1.51
		2	0.242	65.0	1.27
		4	0.467	63.2	1.24
	4500	0.5	0.117	90.0	1.76
		1	0.105	80.6	1.58
		2	0.202	77.7	1.52
		4	0.360	69.3	1.36

117

Alloy Composition, w/o	Exposure Conditions		Weight Loss, gm	Specific Weight Loss, mg/cm²	Calculated Surface Recession Rate, mil/min
	Temp, °F	Time, min [a]			
W-25Re-15Ir	4000	0.5	0.101	72.1	1.40
		1	0.096	68.5	1.33
		2	0.194	69.3	1.34
		4	0.313	56.0	1.09
	4500	0.5	0.083	68.9	1.34
		1	0.090	74.6	1.45
		2	0.160	66.4	1.29
		4	0.310	64.2	1.25
W-25Re-20Ir	4000	1	0.224	69.0	1.34
		2	0.189	58.2	1.13
		4	0.384	59.4	1.15
	4500	1	0.160	53.4	1.03
		2	0.181	60.1	1.16
		4	0.312	51.8	1.00

[a] Cumulative exposure on single sample.

TABLE A-X

CORROSION RATE OF ATJ GRAPHITE
IN FLOWING ARGON-6.5 v/o FLUORINE

Temp., °F	Impingement Angle, deg [a]	Weight Loss, g	Specific Weight Loss, mg/cm^2	Calculated Surface Recession Rate, mils/min
3500	30	0.106	6.7	1.5
4000	30	0.101	6.2	1.4
4500	30	0.147	8.0	1.8
4750+	30 [b]	0.104	10.9	2.0
3500 [c]	45	0.116	8.3	1.8
4000 [c]	45	0.093	6.5	1.4
4000 [c]	45	0.068	7.4	1.6
4500 [c]	45	0.070	8.7	1.9
4500 [c]	45	0.086	10.9	2.3
4800 [c]	45	0.078	9.2	2.1
3500	90	0.120	10.1	2.2
4000	90	0.119	9.4	2.1
4500	90	0.126	9.8	2.2
4800	90 [b]	0.160	13.2	2.9

[a] Angle of gas impingement measured from horizontal.

[b] 3 min run; remainder 5 min.

[c] Previous data for standard test parameters. [1]

TABLE A-XI

CORROSION RATE OF TUNGSTEN IN FLOWING ARGON-6.5 v/o FLUORINE

Temp., °F	Impingement Angle, deg [a]	Weight Loss, g	Specific Weight Loss, mg/cm^2	Calculated Surface Recession Rate, mils/min	Utilization Factor, UF
3500	30	1.110	87.2	1.8	0.3 [b]
4000	30	1.208	92.1	1.9	
4500	30	1.168	91.6	1.9	
5000	30	1.172	88.0	1.8	
5500	30 [c]	0.410	48.0	1.0	
3500 [d]	45	1.718	126.4	2.6	0.4 [b]
4000 [d]	45	1.787	128.8	2.6	
4580 [d]	45	1.747	124.8	2.5	
5100 [d]	45	1.21	92.0	1.9	
5500 [d]	45 [c]	0.460	55.2	1.1	
3500	90 [c]	1.212	151.0	3.1	0.5 [b]
4000	90	2.292	161.5	3.6	
4000	90	2.164	162.0	3.3	
4500	90	2.451	153.0	3.1	
5000	90	1.916	146.0	3.0	
5500	90	1.077	78.2	1.8	

[a] Angle of gas impingement measured from horizontal.

[b] Average value for the range 3500°-5000°F.

[c] 3 min run; remainder 5 min.

[d] Previous data for standard test parameters.

IITRI-B6102-13
(Final Report)

CORROSION RATE OF ATJ GRAPHITE AND W-15Re-20Ir IN FLOWING FLUORINE

Material Composition	Test Temp., °F	Fluorine Concentration v/o	Weight Loss, g	Specific Weight Loss, mg/cm²/min	Recession Rate, mils/min
ATJ Graphite	3000	6.5 [b]	0.135	10.0	2.2
	3500	6.5	0.116	8.3	1.8
	4000	6.5	0.093	6.5	1.4
	3000 [a]	100 [c]	0.200	13.9	3.0
	4000	100	0.212	15.2	3.3
W-15Re-20Ir	3000	6.5	--	--	2.5 [d]
	3500	6.5 [b]	1.092	70.9	1.4
	4000	6.5	1.088	67.5	1.3
	3000 [a]	100 [c]	2.750	280.0	5.4
	4000	100	1.420	145.5	2.8

[a] Temperature rise ~300°F during 5 min run.

[b] Total flow rate 10 cfh.

[c] Total flow rate 0.65 cfh.

[d] Estimated.

COMPARISON OF CALCULATED AND MEASURED RECESSION RATES

OF TUNGSTEN IN FLOWING FLUORINE-OXYGEN ATMOSPHERES AT 4000°F

Fluorine Flow Rate, cfh	Oxygen Flow Rate, cfh	Recession Rate, mils/min		Average Utilization Factor [b]
		Experimental [a]	Calculated, UF = 0.4	
0	0.108	0.92	0.76	0.48
-	0.163	1.04	1.17	0.36
-	0.325	2.32	2.48	0.37
-	0.40	2.66	2.93	0.36
-	0.54	3.13	3.93	0.32
0.65	0.108	2.72	2.92	0.37
0.65	0.163	2.76	3.29	0.34
0.65	0.325	3.85	4.50	0.34
0.65	0.40	4.38	5.05	0.34
0.65	0.54	5.62	6.32	0.35

[a] From reference 1.

[b] Calculated from experimental recession rate, quation

TABLE A-XIV

COMPARISON OF CALCULATED AND MEASURED RECESSION RATES

OF RHENIUM IN FLOWING FLUORINE-OXYGEN

| Test Temperature, °F | Utilization Factor [a] | | Recession Rate, mils/min | |
	F_2	O_2	Experimental[b]	Calculated
	6.5 v/o F_2-4.0 v/o O_2			
3500	0.4	0.35	4.22	4.64
4500	0.18	0.4	4.37	3.50
5200	0.09	0.4	3.39	2.89
	6.5 v/o F_2-5.4 v/o O_2			
3500	0.4	0.35	5.02	5.37
4500	0.18	0.4	4.38	4.27
5200	0.09	0.4	3.94	3.78

[a]UF calculated from data in individual environments.

[b]From reference 1.

IITRI-B6102-13
(Final Report)

DISTRIBUTION LIST FOR FINAL REPORT
"INVESTIGATION OF REFRACTORY COMPOSITES
FOR LIQUID ROCKET ENGINES"
Contract NAS7-758

NASA Headquarters
Washington, D.C. 20546
Attn: Frank Compitello   (1)
       Patent Office   (1)

NASA Lewis Research Center
21000 Brookpark Rd.
Cleveland, Ohio 44135
Attn: Office of Technical
         Information   (1)
       Contracting Officer   (1)
       Patent Office   (1)

NASA Manned Spacecraft Center
Houston, Texas 77058
Attn: Office of Technical
         Information   (1)
       Contracting Officer   (1)
       Patent Office   (1)

NASA Marshall Space Flight Center
Huntsville, Alabama 35812
Attn: Office of Technical
         Information, MS-IP   (2)
       Technical Library   (1)
       Purchasing Office, PR-EC   (1)
       Patent Office, M-PAT   (1)
       Dale Burrows S+E-ASTN-PJ   (1)
       Technology Utilization
         Office, MS-T   (1)

NASA Ames Research Center
Moffett Field, California   94035
Attn: Patents and Contracts
         Management   (1)

Jet Propulsion Laboratory
4800 Oak Grove Drive
Pasadena, California   91102
Attn: Gary Heidenreich   (2)

Manager, Liquid Rocket Pro-
  pulsion Tech., Code RPL
Office of Advanced Research
  and Technology
NASA Headquarters
Washington, D.C. 20546   (3)

Director, Technology Utilization
  Division
Office of Technology Utilization
NASA Headquarters
Washington, D.C. 20546   (1)

NASA Scientific and Technical
  Information Facility
P. O. Box 33   (25)
College Park, Maryland 20740

Director, Launch Vehicles and
  Propulsion, SV
Office of Space Science and
  Applications
NASA Headquarters
Washington, D.C. 20546   (1)

Director, Advanced Manned
  Missions, MT
Office of Manned Space Flight
NASA Headquarters
Washington, D.C. 20546   (1)

Mission Analysis Division
NASA Ames Research Center (1)
Moffett Field, Calif. 24035

Ames Research Center
Moffett Field, California
Attn: Hans M. Mark   (2)

Goddard Space Flight Center
Greenbelt, Maryland 20771
Attn: Merland L. Moseson
         Code 620   (1)

IIT RESEARCH INSTITUTE

124

IITRI-B6102-13
(Final Report)

Jet Propulsion Laboratory
California Institute of
  Technology
4800 Oak Grove Drive
Pasadena, California 91103
Attn: Henry Burlage, Jr.
       Propulsion Div. 38   (2)

John F. Kennedy Space Center,
NASA
Cocoa Beach, Florida 32931
Attn: Dr. Kurt H. Debus   (1)

Langley Research Center
Langley Station
Hampton, Virginia 23365
Attn: Ed Cortwright
       Director   (1)

Lewis Research Center
21000 Brookpark Road
Cleveland, Ohio 44135
Attn: Bruce Lundin
       Director   (1)

Marshall Space Flight Center
Huntsville, Alabama 35812
Attn: Hans G. Paul
       Code R-P+VED   (2)

Manned Spacecraft Center
Houston, Texas 77058
Attn: J.G. Thibodaux, Jr.
       Chief, Prop. + Power
         Div.
       H. Pohl   (2)

Headquarters, U.S. Air Force
Washington 25, D.C. 20546
Attn: Col. C. K. Stambaugh
       AFRST   (1)

Arnold Engineering Development
  Center
Arnold Air Force Station
Tullahoma, Tennessee 37388
Attn: Dr. H. K. Doetsch   (1)

Air Force Rocket Propulsion
  Laboratory
Research and Technology Div.
Air Force Systems Command
Edwards, California 93523
Attn: Mr. H. Main, RPRPD   (1)

Air Force Missile Test Center
Holloman Air Force Base,
  New Mexico 45433
Attn: Library   (1)

Air Force Missile Test Center
Patrick Air Force Base, Florida
Attn: L. J. Ullian   (1)

Aeronautical Systems Division
Air Force Systems Command
Wright-Patterson Air Force Base
Dayton, Ohio 45433
Attn: D. L. Schmidt
       Code ASRCNC-2   (1)

Space and Missile Systems
  Organization
Air Force Unit Post Office
Los Angeles 45, California 90045
Attn: Col. Clark
       Technical Data Center (1)

Defense Documentation Center
  Headquarters
Cameron Station, Building 5
5010 Duke Street
Alexandria, Virginia 22314
Attn: TISIA   (1)

Bureau of Naval Weapons
Department of the Navy
Washington, D.C. 20546
Attn: J. Kay
       RTMS-41   (1)

U.S. Naval Ordnance Test Station
China Lake, California 93557
Attn: Code 4562
       Chief, Missile Propulsion
         Division   (1)

Picatinny Arsenal
Dover, New Jersey 07801
Attn: I. Forsten, Chief
       Liquid Propulsion Lab. (1)

U. S. Army Missile Command
Redstone Arsenal
Alabama 35809
Attn: Mr. Walter Wharton   (1)

Chemical Propulsion Information
  Agency
Applied Physics Laboratory
8621 Georgia Avenue
Silver Spring, Maryland 20910
Attn: Tom Reedy   (1)

A erojet-General Corp.
P. O. Box 296
Azusa, California 91703
Attn: W. L. Rogers   (1)

Aerojet Liquid Rocket Company
P. O. Box 13222
Technical Library, Bldg 2015,
  Dept. 2410
Sacramento, California 95813
Attn: R. Stiff   (1)

Aerojet-General Corporation
Space Division
9200 East Flair Drive
El Monte, California 91734
Attn: S. Machlawski   (1)

Aerospace Corporation
2400 East El Segundo Blvd.
P. O. Box 95085
Los Angeles, Calif. 90045
Attn: John G. Wilder
       MS-2293   (1)

Avco Systems Division
Wilmington, Massachusetts
Attn: Howard B. Winkler   (1)

Beech Aircraft Corporation
Boulder Division
Box 631
Boulder, Colorado
Attn: J. H. Rodgers   (1)

Bell Aerosystems Company
P. O. Box 1
Buffalo, New York 14240
Attn: W. M. Smith   (1)

Bellcomm
955 L-Enfant Plaza, S.W.
Washington, D.C.
Attn: H. S. London   (1)

Bendix Systems Division
Bendix Corporation
3300 Plymouth Road
Ann Arbor, Michigan 48105
Attn: John M. Brueger   (1)

Boeing Company
P. O. Box 3999
Seattle, Washington 98124
Attn: J. D. Alexander   (1)

Boeing Company
1625 K Street, N.W.
Washington, D.C. 20006
Attn: Library   (1)

Boeing Company
P. O. Box 1680
Huntsville, Alabama 35801
Attn: Ted Snow   (1)

Missile Division
Chrysler Corporation
P. O. Box 2628
Detroit, Michigan 48231
Attn: Mr. John Gates   (1)

Wright Aeronautical Division
Curtiss-Wright Corporation
Wood-Ridge, New Jersey 07075
Attn: G. Kelley   (1)

Research Center
Fairchild Hiller Corporation
Germantown, Maryland
Attn: Ralph Hall   (1)

Republic Aviation Corporation
Fairchild Hiller Corporation
Farmingdale, Long Island, New York
Attn: Library   (1)

General Dynamics, Convair Div.
P. O. Box 1128
San Diego, California
Attn: Library   (1)

Missile and Space Systems Center
General Electric Company
Valley Forge Space Technology Center
P. O. Box 8555
Philadelphia, Pennsylvania
Attn: F. Mezger
       F. E. Schultz   (1)

Grumman Aircraft Engineering
  Corporation
Bethpage, Long Island
New York   11714
Attn: Joseph Gavin   (1)

Honeywell, Inc.
Aerospace Division
2600 Ridgway Rd.
Minneapolis, Minn.
Attn: Mr. Gordon Harms   (1)

Hughes Aircraft Co.
Aerospace Group
Centinela and Teale Streets
Culver City, Calif.   90230
Attn: E. H. Meier
       V.P. and Div. Mgr.,
       Research + Dev. Div. (1)

Walter Kidde and Company, Inc.
Aerospace Operations
567 Main Street
Belleville, New Jersey
Attn: R. J. Hanville   (1)
       Dir. of Research Engr.

Ling-Temco-Vought Corporation
P. O. Box 5907
Dallas, Texas   75222
Attn: Library   (1)

Arthur D. Little, Inc.
20 Acorn Park
Cambridge, Massachusetts 02140
Attn: Library   (1)

Lockheed Missiles and Space Co.
P. O. Box 504
Sunnyvale, California   94088
Attn: Technical Information
         Center
       J. Guill   (1)

Lockheed Propulsion Company
P. O. Box 111
Redlands, California   92374
Attn: Library   (1)

The Marquardt Corporation
16555 Saticoy Street
Van Nuys, Calif.   91409
Attn: Library   (1)

Baltimore Division
Martin Marietta Corporation
Baltimore, Maryland   21203
Attn: Mr. J. Calathes (3214) (1)

Denver Division
Martin Marietta Corporation
P. O. Box 179
Denver, Colorado 80201
Attn: Dr. Morganthaler
       A. J. Kullas   (1)

Orlando Division
Martin Marietta Corp.
Box 5837
Orlando, Florida
Attn: J. Ferm   (1)

McDonnell-Douglas Astronautics Co.
5301 Bolsa Ave.
Huntington Beach, Calif.   92647
Attn: J. L. Waisman   (1)

McDonnell-Douglas Corp.
P. O. Box 516
Municipal Airport
St. Louis, Missouri   63166
Attn: R. A. Herzmark   (1)

Space + Information Systems Div.
North American Rockwell
12214 Lakewood Boulevard
Downey, California   90241
Attn: Library   (1)

Rocketdyne (Library 586-306)
6633 Canoga Avenue
Canoga Park, Calif.   91304
Attn: Dr. R. J. Thompson
       S. F. Iacobellis   (1)

Northrop Space Laboratories
3401 West Broadway
Hawthorne, California   90250
Attn: Dr. William Howard   (1)

Aeroneutronic Corporation
Philco Corporation
Ford Road
Newport Beach, California   92663
Attn: Library   (1)

127

Astro-Electronics Division
Radio Corporation of American
Princeton, New Jersey 08540
Attn: Y. Brill   (1)

Rocket Research
York Center
Redmond, Washington 98052
Attn: F. McCullough, Jr.   (1)

Scientific Service Bureau Inc.
P. O. Box 375
Morrisplains, New Jersey 07950
Attn: T. F. Seamans   (1)

Stanford Research Institute
333 Ravenswood Avenue
Menlo Park, California 94025
Attn: Dr. Gerald Marksman   (1)

Sunstrand Aviation
4747 Harrison Ave.
Rockford, Illinois 61101
Attn: R. W. Reynolds   (1)

TRW Systems Group
TRW Incorporated
One Space Park
Redondo Beach, Calif. 90278
Attn: G. W. Elverum   (1)

Tapco Division
TRW, Incorporated
23555 Euclid Avenue
Cleveland, Ohio 44117
Attn: P. T. Angell   (1)

Thiokol Chemical Corp.
 Aerospace Services
Elkton Division
Bristol, Pennsylvania
Attn: Library   (1)

Thiokol Chemical Corporation
Huntsville Division
Huntsville, Alabama 35807
Attn: John Goodloe   (1)

Research Laboratories
United Aircraft Corp.
400 Main St.
East Hartford, Conn. 06108
Attn: Erle Martin   (1)

Hamilton Standard Division
United Aircraft Corp.
Windsor Locks, Conn. 06096
Attn: Mr. R. Hatch   (1)

United Technology Center
587 Methilda Avenue
P. O. Box 358
Sunnyvale, California 94088
Attn: Dr. David Altman   (1)

Florida Research And Development
Pratt and Whitney Aircraft
United Aircraft Corporation
P. O. Box 2691
West Palm Beach, Florida 33402
Attn: R. J. Coar   (1)

Vickers, Inc.
Box 302
Troy, Michigan
Attn: Library   (1)

Ames Laboratory USAEC
Iowa State University
Ames, Iowa 50010
Attn: M. S. Rashid   (1)